Intermolecular Exchange, Solvent Microenvironment, and Catalysis in Nanoparticulate Complexes of Nucleic Acids and Polycationic Polymers

by

Anisha Shakya

A dissertation submitted in partial fulfillment
of the requirements for the degree of
Doctor of Philosophy
(Chemistry)
in The University of Michigan
2016

Doctoral Committee:

Professor Hashim Al-Hashimi, Co-Chair
Professor Mark Banaszak Holl, Co-Chair
Professor Anna Mapp
Professor Ayyalusamy Ramamoorthy

DEDICATION

To my Grandmother, who was self-motivated to teach herself how to read and write, and to my Mother and Father, who sacrificed everything in their capacity to make me capable of getting my desired level of education.

ACKNOWLEDGEMENTS

I want to start by thanking my advisors, Professor Hashim Al-Hashimi and Professor Mark Banaszak Holl for their patience, support, and encouragement in this venture. Not only have I learned significantly from their scientific expertise, but also their unique individual styles have helped foster creative and independent thinking. I am deeply indebted to past group members Dr. Janghyun Lee (Kevin) and Dr. Yi Xue that have helped me greatly through the years. Kevin's unconditional mentorship sets the standards of an ideal senior lab member. There was never a question too big or too small for him to find time to help. Yi was ever so willing to teach me his amazing computational skills as well as providing a critical ear to hear my thoughts and experiments. I thank Professor Ayyalusamy Ramamoorthy and Professor Anna Mapp for serving in my thesis committee and providing their valuable insights. Finally, there are no words big enough to fully express my gratitude towards my family for their dedication, trust, and unconditional love towards me.

TABLE OF CONTENTS

LIST OF FIGURES

LIST OF SCHEMES

LIST OF TABLES

LIST OF APPENDICES

LIST OF ABBREVIATIONS

1D	one dimensional
2D	two dimensional
AFM	Atomic Force Microscopy
bp	basepairs
bPEI	branched PEI
CD	Circular Dichroism
CPMG	Carr-Purcell-Meiboom-Gill
DLS	Dynamic Light Scattering
DNA	Deoxyribonucleic acid
ds	double stranded
EM	Electron Microscopy
EMSA	Electromobility Shift Assay
FI	Fluorescence Intensity
FL	Fluorescein
G3	Generation 3
G4	Generation 4
G5	Generation 5
HIV-1	Human Immunodeficiency Virus type -1
HSQC	Heteronuclear Single Quantum Coherence
IR	Infrared spectroscopy
lPEI	linear PEI
MD	Molecular Dynamics
MW	Molecular Weight
N:P	Nitrogen:Phosphate
NMR	Nuclear Magnetic Resonance
PAMAM	poly(amidoamine)
PEC	polyelectrolyte complex
PEG	poly(ethyleneglycol)
PEI	poly(ethyleneimine)
PLL	poly-L-Lysine
POCP	polycationic polymer

RNA	Ribonucleic Acid
RNAi	RNA interference
SAXS	Small Angle X-ray Scattering
siRNA	small interfering RNA
ss	single stranded
TAR	Transactivation Response Element
TOPRNA	TOPological modeling of RNA

ABSTRACT

Owing to their polyelectrolyte-like character, nucleic acids are known to form nanoparticulate structures/aggregates (polyplexes) with polycationic polymers (POCPs), which are of particular interest in biology due to their ability to deliver therapeutic nucleic acids. However, very little knowledge exists on the structure and dynamics of these complex particles at the molecular/atomic level. In addition, experimental descriptions of solvent environment close to interacting surfaces that can arise due to the heterogeneity of counterion distributions is also lacking in the field. Such details of structure and dynamics of polyplex components can significantly affect polyplex structural organization as well as its response to endogenous molecules in the intracellular environment.

Leveraging solution NMR techniques, we obtain information on the site-specific structure and dynamics of polyplex components. Results on a model polyplex of a short hairpin RNA, the 29-nucleotide transactivation response element (TAR) from the human immunodeficiency virus type 1 (HIV-1) and PEGylated G5-PAMAM (G5-PEG) show that while the RNA exit, in rapid intermolecular exchange between free and bound forms, no significant change in its structure or fast dynamics is observed upon polyplex formation at low N:P ratios. However, structural perturbations at N:P ratios > 1 cannot not be ruled out owing to low signal from RNA. DLS measurements reveal polydisperse polyplexes with the majority of polyplexes having small average size consistent with the size measured using NMR relaxation parameters. In addition, using fluorescently tagged and untagged RNA, it was demonstrated that the RNA in the complexes can be competitively exchanged rapidly in solution over a wide range of N:P ratios. Combining these studies we provide a picture of polyplexes as dynamic assemblies in which the bound nucleic acid are capable of intermolecular exchange. Such a dynamic

exchange could potentially provide mechanisms for intracellular release of delivered therapeutic nucleic acids.

We use prototropic/solvatochromic fluorescein dye to characterize the local solvent environments in these complexes. It is observed that the nucleic acid-POCP interactions gives rise to unique microenvironments with solvent properties like local pH being significantly different than that of bulk solution. The magnitude of local changes is highly dependent on the polymer type, with branched polymers displaying more acidic microenvironments compared to linear polymers. This data demonstrates that polymer structural details play a key role in defining the heterogeneity in local solvent environments in polyplexes.

We also show that the polyplex environment does not disrupt the functional structure and thus the catalytic activity of nucleic acids. Moreover, the product yields are enhanced at higher N:P ratios with POCPs that favor exchange of bound RNA under ribozyme excess conditions. The enhancement of observed rates, however, is observed only for mutants (sequentially elongated at one of the helices) that are less active than the wild type. This suggests that the POCP environment can help overcome the rate limiting conditions imposed by the mutation. While the rate limiting steps in the RNA catalysis with and without POCP are yet to be elucidated, it is clear from our results that the structural details of the nucleic acid and POCP can determine the structural organization of polyplexes, local microenvironment, and exchange dynamics in a way that can affect the function of catalytic RNA.

CHAPTER 1 INTRODUCTION

Complexes of polycationic polymers (POCP) and nucleic acids (polyplexes) have long been of interest to several areas of physics, chemistry, and biology. Nucleic acid themselves being highly charged polymer chains, polyplexes present a special case of the classic polymer physics problem of *polyelectrolyte complexation*.[1-3] Despite having a long history of almost three centuries, understanding the precise nature of interactions in such polyelectrolyte complexes (PEC) remains a challenge. The complexity arises due to the presence of interactions at different length scales; short-range excluded volume, long-range columbic, and counterion screening induced intermediate length scale interactions.[4] Moreover, the local structure and dynamics of the constituent polymers, as well as those of solvent molecules (water and ions) adds complexity to understanding PECs.[5,6] Even the main driving force of association, whether it is entropic or electrostatic, is still actively tested, both theoretically and experimentally.[7] In addition, since the highly charged surfaces of POCPs and nucleic acids in aqueous environments are associated with counterions, large effects on the local solvent and ions is expected upon complex formation ultimately affecting the chemical properties such as changes in pH, pKa, and local counterion concentrations.[8-10] With respect to biology, polyplexes have been used as model systems to understand how thousands of base-pair long genomic DNA molecules are effectively packaged inside seemingly small cellular compartment.[6,11] Packaging of long RNA chains is also essential for viruses that use RNA as their genome. A second thrust of biological application that spurred interest in study of these complex systems is the delivery of therapeutic nucleic acids like plasmid DNA (pDNA) and oligonucleotides such as siRNA, antisense RNA/DNA, miRNA, ribozymes and deoxyribozymes to target cells.[12-14] While there is significant literature on the biological application of a variety of different polyplex systems, the mechanistic pathways are not yet elucidated.[15,16] Studies have shown correlations of knockdown/transfection efficiencies of therapeutic RNA polyplexes with modulations of POCP

properties.[17-21] However, a molecular-level understanding of these correlations continues to elude the field resulting in poor understanding of the relationship between polyplex structure/dynamics and function.[22,23]

1.1 The Interaction between Oppositely Charged Polymers: Historical Perspective

The realization of "electrostatic" nature of interaction between two oppositely charged polymers has been credited to Kossel,[24] who, after his discovery of complexes of nucleic acids with the then empirically termed substance "histone" in 1884, described the interaction as "salt-like" linkages. Histone was later confirmed to be a charged protein (a polymer of amino acids). In 1934 Willstatter in his studies of complexes of polyionic synthetic and natural polymers termed the complexes as "simplexes" as they could form under simple mixing conditions. Bungenberg de Jong and Kyut[25] are often credited for carrying out more conclusive studies of ionic interactions between naturally occurring polymers during the 1930s and 1940s. They proposed the term "coacervation" to describe the observed phase separation of the complexes. After the observation by Fuoss and Sadek[26] in 1949 of precipitates of oppositely charged strongly acidic/basic synthetic polymers and by Michaels[27] in 1961 on preparation of well defined 1:1 stoichiometric complexes, there was a surge of interest in understanding the phenomenon of polyelectrolyte complexation and the structure and composition of resulting complexes. Industrial application of multilayer thin-films of PECs further fuelled the studies. Systematic studies by Tuschida *et al.*[28] and Kabanov *et al.*[1] in the 1970s and 1980s showed that soluble PECs could be formed between oppositely charged polyions with weak ionic groups that differed in the degree of polymerization (molecular weights). Although the realization that the interaction with natural polyamines could lead to a compact state of DNA was much older, the interest in understanding the physical origin of the interaction sparked around late 1970s when it was shown that very long DNA molecules could be packed by such polyamines into nanometer sized, often toroidal particles in vitro.[29-32] Formation of similar structures was also observed for cationic polypeptides such as poly(lysine)[33] and histone H1.[34] In the late 1980s, it was demonstrated that DNA in the form of PECs with linear polycations, could be delivered and expressed in cells.[35-37] As the field of therapeutic nucleic acids grew, in particular after

discovery of antisense oligonucleotides and RNAi nucleic acids in the 1990s,[38] and more recent Crisper/Cas9, POCPs has garnered more attention as delivery vehicles. Several POCPs have even been tested in clinical trials (Table 1) as delivery vectors either stand alone or in combination with lipids, proteins, and inactivated viruses. Consequently, such prospective applications of POCPs have generated a huge amount of interest in understanding their complexes with nucleic acids and their mechanism of action.

Table 1 Polyplexes in human clinical trials

Polymer vector	Nucleic Acid	Disease
Transferrin-PLL	IL-2 pDNA	Melanoma
PEG-PLL	CFTR pDNA	Cystic fibrosis
PEI	DT-A pDNA	Bladder cancer
PEG-PEI-cholesterol	IL-12 pDNA	Ovarian cancer
Transferrin-cyclodextrin-oligocation	RRM2 siRNA	Solid tumors
PEI-mannose-dextrose	HIV antigen coding pDNA	HIV
Tri-NAG-oligoamide conjugate	TTR siRNA	TTR amyloidosis
Biodegradable polymer (LODER)	KRAS siRNA	Pancreatic Cancer

1.2 Interplay of Nucleic Acid Structure, Electrostatics, and Counterion Distribution

The building block of nucleic acids (Figure 1.1), termed nucleotide, comprises a phosphate group, a sugar moiety (ribose or deoxyribose), and a nitrogenous base (purine or pyrimidine). Owing to very low pKa (~1.5), the phosphate group in the sugar-phosphate backbone is readily deprotonated in solution resulting into a negative charge per nucleotide. Although the nitrogenous bases can also be ionized under extreme pH or unique local structural environments,[39,40] major contribution to the net charge on the nucleic acid chain is due to the phosphate and hence the polyelectrolyte character. The charges in any polyelectrolyte chain in solution, however, are surrounded by counterions and depending upon the amount of added salt, charges are "screened" to different extents. The electrostatic interaction between

charged residues reduces due to "screening" and with the "screening" effect decreasing exponentially with distance.[41] Although it has been difficult to quantitatively describe the nature of the counterion distribution around polyelectrolyte chains, it is expected that the structure of the chains dictate the counterion distribution. On the reverse, their counterion environment is expected to have large effects on structural aspects such as chain stiffness and conformation. Therefore, while a large electrostatic energy barrier due to repulsive interactions needs to be overcome when nucleic acids chains come together in space either during annealing of two base-complementary polynucleotide chains to form double stranded helices, tertiary folding, or compaction by proteins or polycations, these processes still occur as a result of the interaction of the nucleic acid with its ion atmosphere.[42-44]

Besides existing in nature as two distinct chemical forms (DNA and RNA), nucleic acids also occur in a variety of different architectures. The genomic DNA is double stranded (base paired) and thousands of base pairs long. RNA on the other hand is shorter and exist as single strands more frequently, for e.g., either as very short single stranded molecules or longer RNA with base-paired and unpaired sequences folded into complex three-dimensional architectures resulting in regions of distinct electrostatic potential.[45] Theoretical predictions[46] as well as emerging new experimental studies[47,48] show that the electrostatic interactions of nucleic acids with small counterions or polycations significantly depend on their details of their molecular architecture.

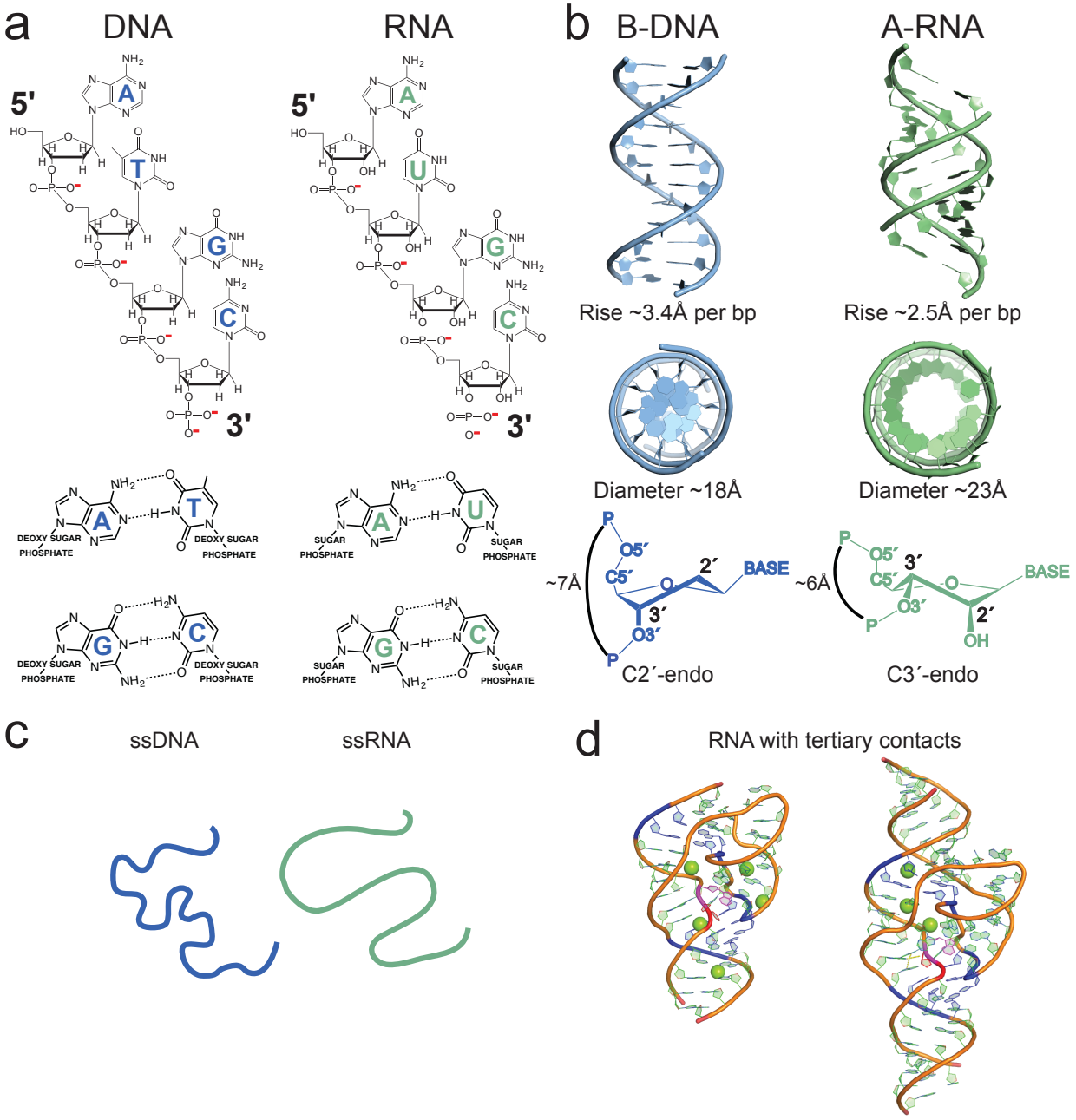

Figure 1.1 Structure of nucleic acids. (a) **Chemical representation of DNA and RNA. Polynucleotide chains with deprotonated phosphate groups (top). Watson-Crick pairing between nucleotide bases (bottom)** (b) **Structural differences between B-form DNA and A-form RNA.** (c) **Topology of nucleic acid chains. Single stranded DNA and RNA modeled as WLC highlighting, difference in the contour lengths.** (d) **Crystal structures of two RNA molecules that form tertiary contacts. PDB ID 4OJI (left) 4QJH (right)**

1.2.1 Double Helical DNA and RNA

A double stranded helical structure of nucleic acid is formed upon hydrogen bond pairing of the nitrogenous bases of two polynucleotide chains. Double helical nucleic acids are known to exist in different forms classified as A-form, B-form, and Z-form; B-form and A-form being the most common for double stranded DNA (dsDNA) and double stranded RNA (dsRNA) respectively. The A-form RNA is shorter and wider compared to B-form DNA of the same base pair length. Its major grove is deeper and narrower and the minor groove is shallower. The bases are displaced to a greater degree from their helical axis compared to the B-form DNA. The A-form RNA is more rigid and has been shown to have longer persistent length (60 nm).[49] Even though there is same number of negative charges per base pair, due to shorter rise per base pair (~2.8 Å vs. ~3.4 Å), the A-form RNA has increased linear charged density compared to B-form DNA. Owing to the charge density differences, theories based on simple electrostatics predict that the counterion distribution will be different between the A-form and B-form. Pabit *et al.*, based on SAXS and ASAXS measurements, showed that counterions screen the charges of dsRNA at much lower ionic strength due to closer proximity of the counterions to the helical axis compared to dsDNA.[48] Therefore, purely based on electrostatic differences arising due to the details of the helix geometry, differences in the recognition of A-form RNA vs. B-form DNA by binding ligands or charged polyions can be expected.

1.2.1.1 Plasmid DNA

The pDNA molecule naturally occurs in bacteria and some eukaryotes and is used by those cells to export certain genes. It is circular, double stranded, and much smaller than the genomic DNA. Naturally occurring pDNA are supercoiled, however more relaxed forms such as nicked (cut at one of the strands), or linearized (both strands cut) are also used for gene delivery. It has been observed that binding affinity with POCPs, polyplex size, and exchange reactions are dependent on pDNA topology.[47] Higher binding affinities and smaller average sizes have been observed for supercoiled pDNA polyplexes compared to linear and nicked. Nuclease resistance and uptake has also been found to be greater for polyplexes of supercoiled pDNA.[50,51] It has been argued that higher charge density of supercoiled DNA and thus

increased number of condensed monovalent counterions should result in more favorable interaction with POCPs.[47]

1.2.1.2 siRNA

siRNA molecules are naturally produced in cells by enzymatic cleavage of longer double stranded RNA molecules as a part of the RNA interference (RNAi) mechanism that leads to destruction of certain mRNA (process termed gene silencing). These are small double stranded nucleic acids with typically 19 base pairs and symmetric 2-nt overhangs at the 3' end and a phosphate at the 5' end of the target complementary strand (antisense strand). The double stranded region takes the A-form geometry[52,53] while the terminal base pairs show lower duplex stability[54] that could be sequence dependent. While sequence dependence of siRNA and POCP interactions is not known, it was found that when 5 to 8-nt long complementary overhangs at the 3' ends of both strands were introduced, enhanced silencing activity was observed when delivered using PEI. This was conjectured to be due to increased stability of the polyplexes due to increased interaction resulting from formation of siRNA concatemers[55] thus suggesting that the structure of siRNA can play a role in determining interaction with POCP.

1.2.2 Single Stranded DNA and RNA Oligonucleotides

Although single stranded nucleic acids having sequential adenine residues (A-tract) tend to be structured (helical) due to the highly favorable stacking interaction of adjacent adenines, unstructured single stranded nucleic acids are more flexible compared to dsDNA or dsRNA of same length.[40] The single stranded forms have a lower linear charge density than the double helical forms, therefore from the viewpoint of electrostatics, the free energy of binding of single stranded vs double stranded nucleic acids to counter ions are expected to be significantly different. Further more differences exist between single stranded RNA (ssRNA) and single stranded DNA (ssDNA) oligonucleotides with respect to flexibility. Using SAXS and single molecule FRET based experiments and assuming the WLC model, it was found that even for the most unstructured ssRNA, poly(uridine), longer persistence length and shorter contour length compared to the single ssDNA counterpart, poly(thymidine).[56]

1.2.2.1 Antisense Oligos

Antisense oligonucleotides (asOligos) are short single stranded DNA/RNA about 13-25 nt long with sequences complementary to target mRNA. While homopolymeric oligonucleotides do not have intra strand base pairing asOligos can fold into hairpin structures if the sequence permits intra strand base pairs. Surveys[57] of asOligo based antisense experiments have shown that the asOligos that are more efficient have greater thermodynamic preference for forming duplexes with target mRNA compared to self-interaction. However, asOligo structure based interaction with POCP can also be a contributing factor to the apparent antisense activity reported in cell-based assays. It has been reported that even when there are only few base pairs, hairpin asOligos have significantly higher binding affinity with POCP and lower release rates form polyplexes compared to asOligo of same nucleotide length.[58]

1.2.3 Complex Tertiary Folded RNA

Several naturally occurring RNA molecules are known have single stranded and double stranded helical regions folded into complex tertiary conformations. While the topological constraints imposed by secondary structure of the RNA can restrict the conformational ensemble to a predisposed subset of folded structures,[59] folding per se is energetically unfavorable due to the dominant repulsive interactions of the phosphate groups. For e.g. the electrostatic repulsion energy of a ~400 nt RNA is calculated to be ~600 kcal/mol[44] which is substantially larger than the energy gained by base pairing and base stacking interactions. Presence of simple salts, however, favors the folded structures mostly attributed to, in simple terms, "screening" of the repulsive interactions. For example, it was observed that at very low monovalent salt concentrations the P4-P6 domain of tetrahymena ribozyme existed in an extended conformation while at ~100 mM salt the structure was more relaxed and disordered.[60] At much higher (ten fold) concentration, the RNA structure could fold into near-native structures forming tertiary contacts.

It is generally accepted that metal ions are located within few angstroms of the nucleic acid surface and that they are capable of exchanging to the bulk, although precisely describing the ion atmosphere around intricately folded nucleic acids is challenging both experimentally and theoretically. Nonetheless,

it has been clear that the local atomic details are important in defining the interaction with the surrounding ions and consequently affect interactions with binding ligands.[61] Calculation of electrostatic potentials of folded RNA structures have shown that regions of distinct electrostatic potentials exist which could provide specificity in interactions of nucleic acids with divalent metal ions and binding ligands.[45] As discussed in earlier sections, even apparently small differences in charge density arising due to differences the nucleic acid structure can affects its interaction with POCPs. However, there are only few systematic studies on how the structure of nucleic acids with complex three-dimensional architectures influences the interaction with POCPs. Such studies would be of interest not only from the fundamental point of view, but can be informative from the design point of view for delivery of catalytic nucleic acids for therapy.

1.3 Common Nucleic Acid Delivery Polymers and the Role of Structure in their Protonation Behaviour

Figure 1.2 shows the chemical structures of a variety of POCP platforms used in nucleic acid delivery. The first generation polycations used in delivery of viral genomes and pDNA (process termed as transfection) were diethylaminoethyl (DEAE) dextran,[62,63] PLL,[64] poly (L-Ornithine) (PLO), poly (L-Arginine) (PLR).[65] These POCPs were pendant-type (i.e. cationic groups on the side chains) with all cationic groups protonated at physiological pH. Later much of the attention shifted to integral-type (i.e. cationic groups on the backbone) weak polyelectrolyte POCPs that had significant buffering capacity; i.e only partially protonated at neutral pH, but at levels enough to bind nucleic acid, while increasing protonation levels at lower pH. One such example is the lPEI,[66-68] which is a very efficient transfection agent. The high transfection efficiency of lPEI led Boussif *et al.* [69] to propose that the delivered pDNA is released from lysosomes due to their buffering capacity, the so called "proton sponge" hypothesis. The validity of "proton sponge" hypothesis is still debated;[68] nonetheless the discovery of high transfection ability of PEI led to significant amount of research on polyplexes of amine-based polyelectrolytes having significant buffer capacity. Branched PEI and PAMAM dendrimers are the other two commonly studied POCPs. Branched and dendrimeric polymers have gained attention do to the high density of functional

groups that can be readily functionalized to achieve multifunctionality.[70,71] Cyclodextrins [72] are another class of naturally occurring polymers that have been modified to contain different cationic and functional groups.

As encountered in section 1.2, the structure of a polyelectrolyte and the counterion distribution in polyelectrolyte chains are intimately related which in turn influence the recognition and binding interaction with oppositely charged polyions. Besides the chemical nature of the ionizable groups, structural aspects such as the distance between the repeating ionizable units, whether they are located on the backbone or the side chain, and whether the overall polymer topology is linear or branched influence the protonation behavior of POCPs. The section describes in greater detail more widely employed POCPs; poly-L-Lysine (PLL), poly(ethylenimine) (PEI), and poly(amidoamine) (PAMAM) dendrimers (Figure 1.2) and with respect to their structure and protonation behavior. All these polymers have amine groups that can be protonated at physiological pH allowing for polyvalent electrostatic interactions with the negatively charged nucleic acids.

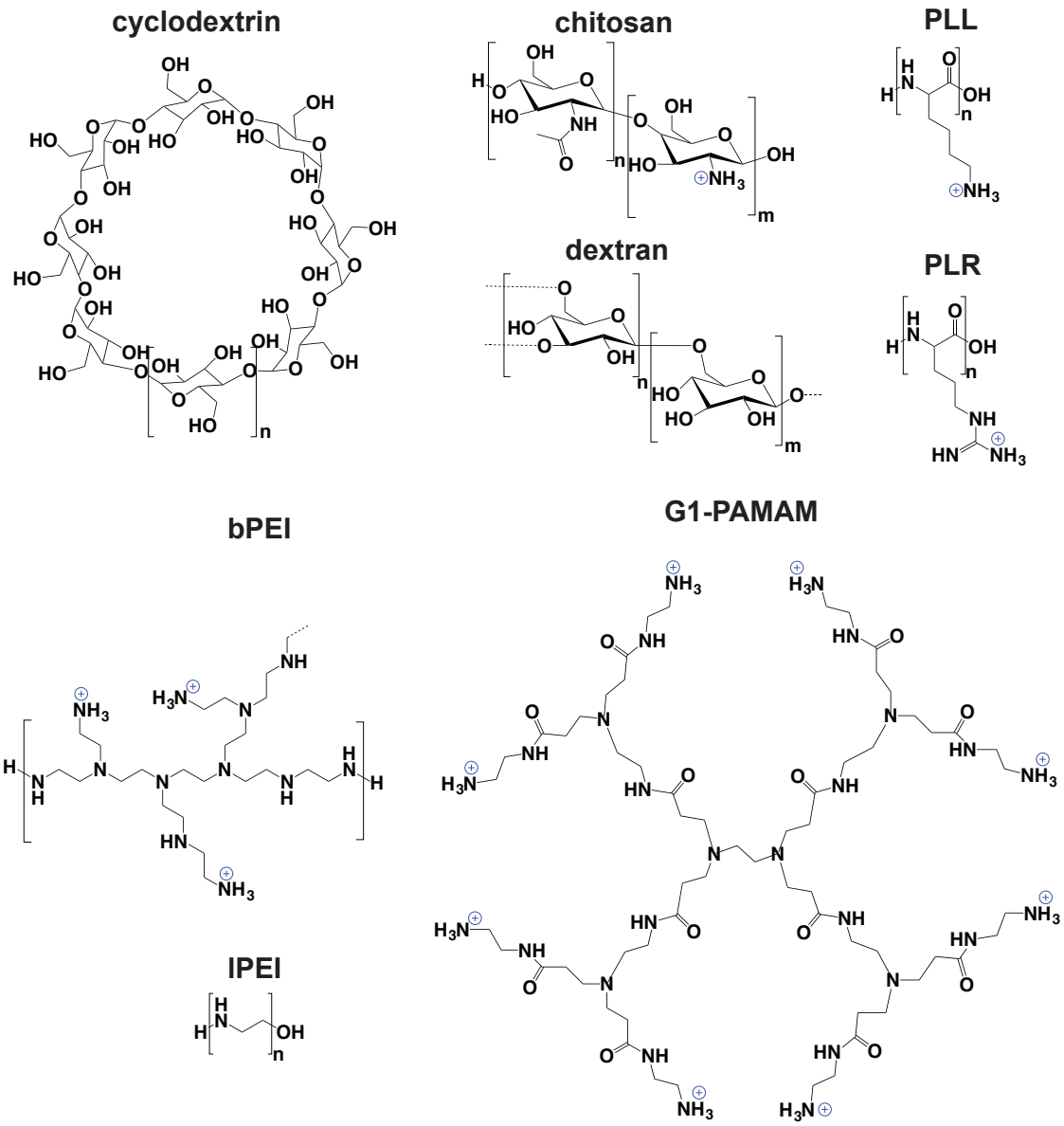

Figure 1.2 Chemical structure of common polycationc polymers for therapeutic nucleic acid delivery. Cyclodextrin, dextran, and chitosan are naturally occurring polymers. PLL, PLR, PEI, and PAMAM dendrimers are synthetic polymers. The primary amine groups that are readily protonated at physiological pH are shown as having positive charge.

1.3.1 Poly-L-Lysine

PLL polymers were one of the first polycationic polymers demonstrating the ability to deliver nucleic acids into cells.[35] PLL is synthesized using a ring-opening polymerization of *N*-carboxy-(*N*-

benzyloxycarbonyl)-L-lysine anhydride using a primary amine initiator, with the ratio of L-lysine monomer to initiator determining the molecular weight of the PLL chain. The anhydride is obtained from conversion of ξ-amine protected L-lysine.[73] Each repeating unit of PLL contains L-lysine side chain, which has a primary amine in the ξ position (Figure 1.2). The pKa of the primary amines in aqueous solution is 9.85[74,75] hence at physiological pH each residue of PLL is capable of being protonated and interacting with nucleic acid phosphates.

While the charge per length of PLL is higher compared to lPEI, another most commonly employed linear POCP (described in the section below), computational studies[76,77] have shown that the charge compensation upon interacting with the nucleic acid chain is not as effective thus resulting into overall weaker binding. This is a result of charges being located on the side chain instead of the backbone as in lPEI. The primary amine in PLL is separated from the backbone by four methylene units that provide a steric limit to interaction with DNA/RNA phosphates. Thus simply accounting for the total charges in a POCP is not sufficient to understand its interaction with nucleic acids. Moreover, it is also fairly well established PLL adopts various secondary structures depending on solution conditions.[74,75,78-80] Due to the repulsive interactions of protonated primary amines, at pH < 7 PLL mostly assumes extended secondary structures. At pH 2 the ratio of PII helix conformation to extended β−helix was reported to be 60:40. Increase of pH stabilizes α-helical (at pH ~11.6 the conformation is mostly α-helical).[80] Therefore, the interaction of PLL with nucleic acids can be expected to depend on its protonated state, both due to amount of total charge as well as differences in the secondary structures.

1.3.2 Poly(ethyleneimine)

PEI polymers can be synthesized as linear or branched chains. The branched forms are synthesized via an acid-catalyzed polymerization scheme of aziridine, whereas the linear forms are synthesized using ring-opening polymerization of 2-ethyl-2-oxazoline followed by hydrolysis.[73] Comparing the two forms of PEI, chemically they are very similar with every third atom being protonable (monomer unit -CH_2-CH_2-NH-). However, they differ significantly in the arrangement of protonated sites along the main chain. The hyperbranched architecture of bPEI results in primary, secondary, and tertiary amines in an

estimated ratio 1:2:1. lPEI only has secondary amines except at the chain end which is terminated by primary amine. Under physiological pH and salt, the protonated sites in lPEI alternate with un-protonated sites along the chain.[81] In bPEI, there is an additional energetic penalty to protonate the already acidic tertiary amines due electrostatic effects from three easily protonable neighboring primary or secondary nitrogen atoms.[82] Secondly, the branched topology makes bPEI more rigid compared to lPEI.[83] Differences in the arrangement of protonated sites along with differences in chain flexibility have been often attributed to different modes of binding[83] with nucleic acid molecules subsequently leading to differences in the hierarchical assembly. However, due to large variations in molecular weight distribution, accurate quantification of protonable amines in each PEI polymer chain by ensemble techniques becomes difficult.

1.3.3 Poly(amidoamine) dendrimers

The interest in dendrimers, in general, is due to the ability to achieve superior molecular weight homogeneity and thus control the surface charge density and functional group modifications. The dendrimer structure can be distinguished into three regions; a core, an interior, and the surface the functionality each of which determines the dendrimer 3D structure. The surface groups are important in determining the solubility of the dendrimers. Both the ionic groups terminating the surface and covalently attached hydrophilic groups can be used to impart solubility.

PAMAM dendrimers are one of the first dendrimeric polymers synthesized and have been extensively studied for applications in drug and nucleic acid delivery and are commercially available. The synthesis involves Michael addition of an amine initiator core with methyl acrylate and amidation of resulting esters. The steps are repeated multiple times depending on the desired number of successive (generation, Gn) layers.[84] The theoretical[84] molecular mass, number of surface groups, and size for G0-G9 using an ethylenediamine core are given in Table 2 (*Dendritech, Inc.).* Although studies have shown that defects and synthesis failures can lead to deviations from theoretically predicted values, dendrimers are nonetheless well-defined at the molecular level as compared to most polymers.

Table 2 Generation dependent theoretical molecular weight, number of surface groups, and diameters of PAMAM dendrimers

Generation	Molecular Weight	Number of Surface Groups	Diameter (Å)
0	517	4	15
1	1430	8	22
2	3,256	16	29
3	6,909	32	36
4	14,215	64	45
5	28,826	128	54
6	58,048	256	67
7	116,493	512	81
8	233,383	1024	97
9	467,162	2048	114

Several simulations and theory reveal generation dependent properties of PAMAM dendrimers.[85] For e.g, low generation (G0-G3) mostly behave like small molecules in solution while the higher generation PAMAM tend to behave like colloidal/nanoparticles. PAMAM dendrimers are sometimes also referred to as synthetic proteins owing to the network of amide bonds (Figure 1.2). The tertiary amines provide branching points while the surface terminates with primary amines. These amines can be protonated to different extent depending on solution pH imparting polyelectrolyte character. The primary amines have higher pKa than the tertiary amines. Due to the high pKa of primary amines they are easily protonated at physiological pH while the tertiary amines do not protonate until very low pH (<4) is reached.[84,86] In general, due to large number of charged units polyelectrolytes are expected to show pH dependent conformational changes.[87] Several computational and theoretical and some experimental studies have reported pH dependent conformation behavior of PAMAM dendrimers.[88,89]

While some discrepancies exist between computation and experiments,[90] computational studies have suggested conformational transition from a "dense core" to a "dense shell" upon decreasing pH.[88] Such particular interest in pH behavior of PAMAM is fueled by the possible implications in pH dependent release of bound small molecule drugs and nucleic acids.

1.4 Polyelectrolyte Complexes of Nucleic Acid/ POCPs

In the field of therapeutic nucleic acid delivery, it is more common to use the term polyplex for complexes of nucleic acids and POCPs.[91] While the nucleic acid displays a strong polyelectrolyte character owing to the fully charged phosphate backbone, the POCPs employed in delivery of nucleic acids (Figure 1.2) often carry weakly dissociating functional groups such as amines and carboxyl groups. Polyplexes therefore share several general physicochemical properties of synthetic PECs involving weak polyelectrolytes. Moreover, several theoretical and experimental concepts from polyelectrolyte complexation can be applied to understand the physical origins of the observed physicochemical properties of polyplexes, principles of supramolecular assembly, role of counterions, kinetics and thermodynamics of intramolecular exchange reactions, and role of structure and dynamics of constituents.

1.4.1 Physicochemical Properties

The physicochemical properties of polyplexes depend on the concentrations of the components, concentrations of simple metal salts, pH, and presence of uncharged hydrophilic groups. The simplest parameter commonly used to describe the polyplexes is the mixing ratio of POCP to nucleic acid, expressed as the total cationic charge to anionic charge molar ratio. This mixing ratio is often represented as N:P for polyplexes involving protonable nitrogen containing POCPs. Indeed how well-defined the N:P ratio is depends to how precisely the molar charges can be estimated which is a challenge for polymers with molecular weight inhomogeneity. Several studies report a window of mixing ratios around a critical mixing ratio where the solution appears turbid or visible precipitate is observed compared to very high or very low mixing ratios. Early on Kabanov *et al.*, based on their extensive studies of non-stoichiometric synthetic PECs mostly using methods such as light scattering, analytical

ultracentrifugation and fluorescence provided the following general explanation of the dependence of the on mixing ratios. A) Under conditions where the DNA (or the larger polyion) is in excess, non-stoichiometric complexes are formed and due to the uncompensated charges of excess polyion the complexes remain soluble. B) The complex attains a critical non-stoichiometric composition up to a certain concentration of the polycation. Beyond this critical concentration, *disproportionation* occurs, i.e. stoichiometric complexes (complexes where the DNA charge is fully neutralized and hence hydrophobic) are formed *in addition to* the non-stoichiometric complexes of the critical composition. C) As the polycation concentration further increases, the population of stoichiometric complexes grows and thus the turbidity or precipitation while the population of non-stoichiometric complexes finally becomes *null* when mixing ratios attaining total charge neutrality is reached. D) Beyond a second critical composition, the stoichiometric complexes undergo *reorganization* forming non-stoichiometric complexes with excess of polycation, which help them to stay soluble in the solution.[1,92] Since large numbers of charges are involved the physiochemical properties of such polyplexes significantly depend salt concentration, type of the metal salt, and factors such as pH and presence of hydrophilic groups that alter the charge density on the POCP as exemplified in the sections below.

1.4.1.1 Effect of Salt

The prediction of salt effects on PEC behavior is difficult due to several factors involved, such as chemical nature of the ionic groups and structure of the polymer and the type of salt. In general, for a giving mixing ratio (charge ratio), PECs are often prone to aggregation in absence and at very high concentrations of monovalent salts, while under small amounts of salts are more colloidally stable.[93,94] For polyplexes of pDNA and PAMAM dendrimers was observed using cryo TEM that aggregate size and morphology highly depends on salt concentration.[95] At low salt (10 mM NaBr) polyplex size was independent of dendrimer generation whereas at high salt (150 mM NaBr) the size increases in a dendrimer generation dependent manner. Similarly, it has been observed via AFM and TEM, that sizes of siRNA/PAMAM polyplexes are much higher at 150 mM NaCl (800 nm –several μM) compared with those prepared in absence of salt (30-130 nm).[96] From a theoretical standpoint it is generally postulated

that even when (primary) complexes have a net surface charge, they tend to aggregate at high salt concentrations due to "screening" leading to overcoming of the electrostatic repulsive interactions by short-range attractive forces.[97] Effect of salt is important from the viewpoint of delivery to cells because due to aggregation in the extracellular environment polyplex uptake by cells is hindered.

1.4.1.2 Effect of pH

The pH of bulk solution is important especially for PECs involving polyions with weak ionic groups. Most of the second-generation POCPs for nucleic acid delivery weak ionic groups: for example PEI and PAMAM dendrimers. The protonation behavior of these polymers is discussed in the section 1.3. Several theoretical[98,99] and experimental studies[100-102] show that the strength of interaction depends on the charge density of the POCPs, which varies with the bulk solution pH. For e.g. the binding affinity of DNA-PEI at lower pH was found to be strong with the average polyplex size being larger. At basic pH, the binding was weaker; polyplex size is smaller with more uniform population.[102]

1.4.1.3 Effect of Hydrophilic groups

Due to the tendency of polyplexes to aggregate and precipitate, especially at high concentration and high salt environments,[103-106] often POCPs or the polyplexes as a whole are conjugated to hydrophilic uncharged moieties. PEG is one of the most commonly employed hydrophilic polymer chain employed for this purpose.[73,107] The general strategy is to PEGylate only a fraction of positively charged groups so that nucleic acids can still be complexed. Another strategy is to use block co-polymers with hydrophilic uncharged and charged units.[19] The average sizes and polydispersity of such polyplexes are often reported to be much smaller.[108,109] However, evidence exists in literature showing that the activity is highly dependent on the chemical nature[110,111] and degree of polymerization[19,109] of the hydrophilic moieties.

1.4.2 Insights from DNA Condensation Theories

Much of our understanding of polyplexes is based on the studies of polyplexes of DNA molecules much longer than the complexing POPCs. For e.g. the most common model DNA that have been used in

experimental studies are pDNA, calf thymus DNA (ctDNA), salmon sperm DNA having sizes > 2000 bp. However, as discussed in section 1.2, the local electrostatic properties and counterion distribution in nucleic acids are intimately linked to their local as well as global structure. Although expected to be important, it is not clearly understood to what extent such local details contribute to the assembly, structure and dynamics of polyplexes as the complex nature of the interactions makes polyplexes difficult systems to study both theoretically and experimentally. There are relatively fewer experimental studies[23,112-123] focusing on the effect of the molecular/atomic and structural details of the nucleic acid and POCPs as opposed to a vast literature on use of polyplexes as delivery agents. Existing theories have mostly focused on understanding how long DNA molecules that behave as a random coil or worm-like chains in dilute solutions gets tightly packed in small volumes. This section summarizes the theoretical approaches developed to understand condensation DNA.

Besides the description of the intrinsic polymer physics of the polyelectrolyte chains, much of the theoretical difficulty arises from accurately describing the role of counterions within a common theoretical framework. Very early on mean-field approaches such as Poisson-Boltzmann (PB) equation and Debye-Huckel (DH) approximations were popularly used to understand the interaction of small ions with polyelectrolytes modeled as charged cylinders in solution.[5] Solutions to the former predict a continuous distribution of counterions around polyelectrolyte chain. Using the latter framework Manning pioneered the concept of "counterion condensation"[124] which implies binding of counterions to polyelectrolyte chains even at infinite dilution. Presence of this "bound layer/cloud" of counterions then implies that the effective charge on a polyelectrolyte chain is lowered hence reducing the intrinsic electrostatic repulsive interactions between two like-charged polyelectrolyte chains. However, neither the PB nor the Manning theory directly predicts the attraction between two like-charged polyelectrolytes, as the mean-field force between two like charges is always repulsive.[5] Theoretical conditions have been worked out under which two like-charged polyelectrolytes can be attracted to each other due to density fluctuations in their counterion "cloud" or due to correlations between counterions themselves. The condensed counterions are treated as being mobile rather than frozen at the

polyelectrolyte surface thus giving rise to thermal fluctuations.[4,125,126] The correlated thermal fluctuations of condensed counterions when two like charged polyelectrolyte chains approach each other can lead to attractive interactions in a manner similar to Van der Waals attraction between polarizable molecules.[4]

By treating the ions as "liquid-like" instead of randomly oriented, correlations between ions themselves can mediate attraction between like charged chains in presence of multivalent screening counterions. This concept was elegantly used by Shklovskii *et al*. to explain "charge inversion", i.e. reversal of the sign of the net charge on a polyelectrolyte when an excess of counterions are bound.[127] An application of this concept is the explanation of the phenomenon of reversal of direction of migration in observed in electrophoretic experiments on polyelectrolyte complexes.[128] Such a reversal of electrophoretic migrations is observed for all polyelectrolyte complexes in aqueous solutions after a certain critical composition (positive to negative charge ratio) is reached, regardless of the structure, chemical nature, or size of polyelectrolytes involved. Another implication of "charge inversion" is the resolubilization of polyelectrolyte complexes that precipitate at charge ratios close to neutrality.[128] Charge inversion plays an important role in designing polyplexes for gene delivery as positively charged polyplex surface helps nucleic acids cross the negatively charged membrane barriers.

Other theories to explain attractive forces between oppositely charged polyelectrolyte chains are the hydration force theory[129] and electrostatic zipper.[130] The so-called hydration force arises due to structuring of water by the charged units on the polyelectrolyte chain and the oppositely charged ions. The electrostatic zipper model treats the polyelectrolyte chains as inhomogenously charged rods rather than homogenously charged rods assumed in most other electrostatic models. This allows accounting for the correlations between the counterions themselves, the like charged units between two like charged chains as well as the charge on the chain and the screening counterion. However, the underlying theoretical principles behind the attractive interactions of oppositely charged helices are still debated due to several underlying assumptions and lack of sufficient experiments that definitively prove or disprove the theories.

1.4.3 Condensation/Aggregation of Small Nucleic Acids Molecules

Most POCPs that condense/compact large DNA are also capable of forming nanoparticulate complexes with small DNA or RNA molecules and have been explored as delivery agents. While the physical forces behind packing of nucleic acids much smaller than the persistence length into nanoscopic dimensions may be similar to that of large DNA molecules, the effect of huge differences in sizes cannot be ignored. Moreover, several reports have shown that POCPs that are effective for delivery of pDNA are not as effective for delivery and/or function of small nucleic acids under similar conditions.[131] pDNA condensed with PEI (both branched and linear forms) have been shown to be effectively delivered and show activity (expression), with lPEI usually exhibiting higher efficiency.[132] However, while both linear and branched form of PEI could deliver siRNA, activity was achieved only for bPEI under relatively high (0.2 μM) siRNA concentrations.[133] Similarly, a 20-nt asDNA could be successfully delivered with 25KDa bPEI however no antisense activity was obtained. While the differences in fate of the nucleic acid: whether they need to reach the cytosol (siRNA, asOligo, ribozymes), find the mRNA on their own (asOligo, ribozymes), or get transported into the nucleus (pDNA) is one of the limiting factors, differences in the chemical environment, structure and dynamics of the polyplexes cannot be ignored. In case of asOligos, using a systems modeling approach, Roth suggested that their ultimate activity depends more heavily on factors such as intracellular trafficking, rate of hybridization with target mRNA, and rate of nuclease degradation rather than transfection efficiency (crossing the cell membrane barrier).[134] The latter, on the other hand, is critical for pDNA delivery as only one or few pDNA molecules are condensed in particle size capable of being transported through the cell membrane, whereas a single small nucleic acid/POCP particle will have several nucleic acid molecules, although it is difficult to estimate the exact stoichiometry. The uptake efficiency has been regarded to be mostly dependent on the effective charge on the polyplexes, size, and aggregation behavior in the extracellular fluid. However, factors such as hybridization with mRNA,[57,135] rate of nuclease degradation are more intimately linked with the structure and dynamics of the nucleic acid their immediate chemical environment as well as exchange dynamics and sustained release. Therefore, a

more fundamental understanding of the complex interplay of chemistry, size and structure/dynamics of the constituent polyions and resulting polyplexes is necessary in addition to the physicochemical properties such as dependence of size and stability on charge ratios.

While the term "condensation" is loosely used to refer formation of nanoparticles with POCP, in a strict sense the term "condensation" was applied in the pioneering studies to refer to the reduction in the fractional volume occupancy of long DNA chain (sometimes also referred to as "compaction").[136] Moreover, dsDNA molecules condensed in presence of polycations are observed via electron microscopy as nanosized toroids and interestingly the dimensions of the toroids are similar regardless of the size of the DNA above its persistence length. However, for nucleic acids smaller than their persistence length Bloomfield maintained that such condensation couldn't be achieved as they behave as rigid rods, and therefore formation of particles with POCPs is more of an "aggregation" phenomenon.[136,137] Polyplexes of small nucleic acid/POCP polyplexes are more often observed as spherical particles or randomly aggregated structures[138-141] as opposed to the more often observed toroidal structures for large DNA polyplexes, although toroidal structures have also been reported for short nicked and gapped duplexes and some single stranded oligonucleotides.[139]

1.4.4 Multivalent Ionic Interactions of Nucleic Acids: DNA vs RNA

The study of polyplexes of therapeutic RNA with POCPs borrows several ideas from pDNA condensation studies. However, besides the differences in the size of small therapeutic RNA vs pDNA, the local structural differences of a dsRNA vs dsDNA helix can affect their interactions with POCPs. Even for short ssDNA and ssRNA differences in flexibility and chain conformations have been observed.[56] It has been reported that the A-form vs B-form helix topology gives rise to differences in the spatial distribution of counterions, with the A-form RNA helix being more effectively screened compared to dsDNA.[48] It was also recently reported that dsRNA helices resisted condensation (defined as the tendency to precipitate in their experiments) by the trivalent cation cobalt hexamine ($Co[NH_3]_6^{3+}$), which is well known to condense DNA.[142,143] This was a surprising result as the A-form RNA helix has greater linear charge density compared to the B-form DNA helix and thus expected to

have stronger interaction with cobalt hexamine. Using atomistic MD simulations, it was shown that the A-form vs B-form helices had different modes of binding. The cobalt hexamine ions preferred to bind deeply into the major groove of the A-form helices owing to its strong electrostatic potential and hence not capable of mediating the ion-bridge between the helices compared to the B-form.[144]

1.5 Kinetics of Complex Formation and Intermolecular Exchange in Polyelectrolyte Complexes/Polyplexes

Kinetic studies of complex formation of polyplexes of large DNA molecules and polycationic polymers indicate that multiple steps are involved during polyplex formation.[145,146] Stopped-flow fluorescence studies by Braun *et al.* on the polyplexes of 4.9 kbp supercoiled pDNA and PAMAM dendrimers suggested two kinetic processes; a very fast (<100 ms) step and a slower step. The fast step was attributed to binding, the activation energy for which was higher for lower generation dendrimers. The slower step, attributed to DNA condensation, showed greater activation for higher generation dendrimers. Dey *et al.* in their studies of polyplexes of calf thymus DNA with PAMAM dendrimers,[146] PEGylated linear block co-polymers,[147] and bottle-brush copolymers[148] have also reported presence of at least two kinetic steps. However, the absolute values of the observed rate constants were dependent on the intercalating dye probes used.

Very early on from their studies[149] on PECs of double stranded DNA (calf thymus) and poly-4-vinylpyridine (PVP) Miller and Bach suggested that polyelectrolyte chains could undergo dynamic rearrangements in the PECs of DNA. More comprehensive studies[1] on the kinetics and mechanism of intermolecular exchange in synthetic PECs was done by Kabanov *et al.* by monitoring exchange reactions upon adding polyelectrolytes of either same or different chemical nature and/or degree of polymerization. Using stopped flow measurements on fluorescently labeled polymer, they obtained typical rate constant of coupling (i.e formation of PEC) on the order of rate constant of diffusion collisions (~10^9 M^{-1} sec^{-1}). However, the rate constant of exchange i.e, transfer of shorter chain "guest" from in complex with a longer chain "host" to another "host" chain was in order of 10^4 to 10^7 M^{-1} sec^{-1}, 3-5 orders of magnitude smaller than the rate constant of diffusion collisions, leading them to propose

that such exchange reactions occur via an intermediate ternary complex. The exchange reactions were highly dependent on concentrations (and type) of simple salts (such as Na^+, K^+, Li^+), and in absence of salt no exchange reactions occurred. It was also observed, based on competitive exchange reaction with poly(methacrylate) (PMA), that the exchange of large DNA molecules in PECs with poly(N-ethyl-4-vinly-pyridinium) (PEVP) were completely reversible, i.e. equilibrium was achieved whether the DNA was added to preformed PMA-PEVP complexes or vice versa.[150]

1.5.1 Importance of Dynamics Intermolecular Exchange between Polyplex Constituents for Therapeutic Nucleic Acid Delivery

Understanding intermolecular exchange in polyplexes is particularly important for therapeutic nucleic acid delivery because polyplexes are in constant interaction with other charged macromolecules in the intracellular and extracellular environment, for example the membrane lipids, proteins, polyamines as well as cellular nucleic acids. Most of the polyplex literature has focused on aspects such as size and stability as these aspects are important with respect to transport across membranes and stability against nucleases. However, intracellular release of the nucleic acid cargo a crucial step for function,[151-154] thus making the studies of intramolecular exchange relevant. Although early studies indicated the presence of intermolecular exchange in DNA polyplexes and suggested role of the structural aspects of the polycations,[155] this area is studied infrequently. More recently studies on DNA release from polyplex using Atomic Force Microscopy (AFM)[156] suggests a time scale of tens of minutes. While emerging studies using MD simulations[157] have revealed exchange dynamics at fast times scales, only few experimental techniques like 2D-IR and NMR are capable of measuring fast dynamics. Considering the variety of POCPs being developed for nucleic acid delivery, detailed and systematic investigation of the role of POCPs chemistry and architecture in intermolecular exchange is crucial.

1.6 Techniques Employed to Characterize Polyplexes

The most common techniques for routine characterization of polyplexes are gel electrophoresis to measure degree of complexation as a function of N:P ratio and DLS to measure hydrodynamic diameter.[158] In addition, electron microscopy (TEM, SEM)[95,103,159-165] and AFM[96,119,120] have been

applied to access shape and size distribution. Synchroton X-ray diffraction,[166] small angle X-ray scattering (SAXS)[167-172] cross polarized microscopy[166] have been used to study phase transition and to access size and structure of ordered phases. Optical tweezing force-pull experiments were used by Ritort *et al.*[173] to study condensation-decondensation of long DNA molecules complexed with POCPs. Circular dichroism(CD)[23,119,120,147] and linear dichroism(LD)[174] have been useful to access changes in the secondary structure of nucleic acids. Some extent of information in changes in structure of nucleic acids as well as changes in polymer structure in polyplexes has been obtained using FTIR.[23,119-121] Nucleic acid melting studies using UV absorption[147,175,176] and Differential Scanning Calorimetry (DSC)[23] have been used to assess thermal stability of nucleic acids in the polyplex forms. Isothermal Calorimetry (ITC)[23,169] has been used to access thermodynamic parameters such as enthalpy, entropy, and absolute charge ratios. Zeta potential measurements are also commonly used to measure net charge on the electrostatic double layer as net positive charge is considered to be desirable for enhanced delivery through the cellular membrane.[158] However, owing to the sensitivity of the physicochemical properties of polyplexes (and polyelectrolyte complexes in general) to the absolute concentration of the constituents it is challenging to study these complexes using solution-based techniques.

Fluorescence (polarization, fluorescence intensity, fluorescence quenching) has been employed to a greater extent to study binding and competitive exchange as the high of fluorescence sensitivity enables use of low concentrations that prevent large-scale aggregation and precipitation.[158] While fluorescence based methods are very useful to study binding, composition and stoichiometry, thermodynamics and kinetics of assembly, they lack structural resolution unless single molecule techniques are used. Fluorescence based techniques have used both fluorescently tagged POCP/nucleic acids as well as intercalating dyes such as ethidium bromide, picogreen, YOYO, while ethidium bromide being most commonly used dye for routine characterization of extent of binding.[158] Although equilibrium measurements are reported more often, kinetics studies are relatively fewer as the kinetic profiles are typically non-trivial to interpret. Some of the studies using stopped flow florescence[145,146,148] and stopped flow circular dichroism[145] are discussed in section 1.5.

Although studies involving size, shape, size distribution and binding are more commonly reported, detailed studies to access local environment, dynamics at different timescales, in addition to overall rotational correlation as measured by light scattering, such as intermolecular exchange, dynamics of local sites both on the polymer and the nucleic acid are rare. Such aspects in biomolecules and their interactions have been widely studied using NMR. However, advantages of NMR have not been fully recognized for studying polyplexes. Few studies have implemented NMR to obtain polyplex stoichiometry[116,177] and rotational correlation based sizes.[112] Indeed solution NMR based techniques suffers from limitations such as solubility, however these can be overcome for polymers with hydrophilic groups such as PEG and dextran, working at N:P ratios far from charge neutrality where soluble complexes can be obtained, or working at relatively lower concentrations using site-specifically isotope labeled samples.

In this thesis, a combination of a variety of 1D and 2D solution NMR, fluorescence spectroscopy, DLS, and gel electrophoresis have been applied to understand the size, structure, dynamics, local solvent environment, and activity of catalytic RNA upon polyplex formation with POCPs.

1.7 Dissertation Outline

The remainder of this thesis focuses on the studies of intermolecular exchange of polyplexes of different POCPs and small nucleic acids by NMR and fluorescence, characterizing their local solvent microenvironment using fluorescence spectroscopy, effect of polyplex interaction on the structure and activity of a catalytic RNA (twister ribozyme) and its topological mutants as well as NMR characterization of this ribozyme.

Chapter 2 describes our initial work on characterizing, in site-specific detail using NMR, the effect of polyplex formation on the structure and dynamics of a short hairpin RNA, the 29-nucleotide transactivation response element (TAR) from the human immunodeficiency virus type 1 (HIV-1) and PEGylated G5-PAMAM (G5-PEG). It was observed that while the RNA is in rapid intermolecular exchange between free and bound forms, no significant change in its structure or ps-ns dynamics was observed upon polyplex formation at low N:P ratios. At N:P ratios > 1 signals from the RNA was

unobservable via NMR. However, monitoring the G5-PAMAM signals suggested that while no significant perturbations of the polymer structure is observed at low N:P ratios, at N:P ratios > 1 structural reorganization of the polyplex could occur. DLS measurements revealed polydisperse polyplexes of with the majority of polyplexes having small average size consistent with the size measured using NMR relaxation parameters. Using fluorescently tagged and untagged RNA, it was demonstrated that the RNA in the complexes could be competitively exchanged rapidly in solution in a wide range of N:P ratios. Using similar fluorescence assays, the effect of the POCP structure and oligonucleotide structure on the degree of complexation and exchange was studied. It was observed that even for the same average molecular weights, the degree of complexation was different for branched vs linear POCPs and hairpin vs unstructured oligonucleotides. The amount of the oligonucleotide exchanged was also dependent on the POCP type. Using fluorescently tagged and untagged G5-PAMAM it was demonstrated that the polymer could also be competitively exchanged rapidly into the solution.

Chapter 3 presents a fluorescence spectroscopy based approach to probe the local solvent environment of polyplexes. Using the spectroscopic properties of the solvatochromic and prototropic dye fluorescein different microenviroment in polyplexes were revealed that differed in the local pH and was a function of the N:P ratio. The magnitude of changes was dependent on the type of POCP, thus providing a new observable parameter for characterizing a variety of different polyplexes.

Chapter 4 describes our studies on the interactions of the env22 twister ribozyme (twister, in short) and its helical mutants with POCPs that demonstrate the role of structure and intermolecular exchange on activity. NMR titrations showed that the base pairing interactions and tertiary structure are not perturbed upon POCP binding at low N:P ratios suggesting the ribozyme should function in presence of the POCP. Activity assays using gel electrophoresis showed that preformed twister remained active at low N:P ratios. Using a competitive exchange scheme, it was observed that under multiple turnover conditions the activity of the wild type twister was significantly enhanced for polyplexes formed at N:P ratios > 1 and that the activity depended on the type of POCP. POCPs that were observed to favor exchange of bound RNA showed enhancement in activity, suggesting the role of exchange for the

availability of the RNA for activity. While the role of tested POCPs in enhancing activity was predictable, it was surprising that even small changes in base pairing of the RNA could lead to drastically different results in presence of POCP, highlighting the importance of structural details on polyplex function.

Chapter 5 summarizes the NMR studies of the wild type and mutants of twister and chemical shift predictions of the tertiary structure. As the twister class of ribozymes was discovered only recently, only one NMR study had been published during the course of our studies. Our goal was to obtain the chemical shift signature of twister in absence and in presence of Mg^{2+} in order to assess the secondary structure and tertiary folding of the ribozyme as well as obtain assignments of key residues at the active site for dynamics studies. Formation of folded structure of a bimolecular twister construct in presence of sufficient concentrations of Mg^{2+} was evident from imino proton spectra and comparison of aromatic spectra with LARMOR^{D} predicted spectra. However, significant spectral overlap precluded unambiguous assignment of residues. Therefore, the RNA synthesized with site(atom) specific isotope labels using solid phase synthesis which enabled assignment of the carbon chemical shifts of the key residues in the active site. Comparison with the imino proton spectra of the full-length (single stranded) twister suggested that the secondary structure base pairs in hybridized form of bimolecular construct are less stable. It was also shown that elongation of helix3 of twister does not significantly affect the overall secondary structure.

Chapter 6 summarizes the studies and presents a future outlook on the importance of the local structure based understanding of the interaction between nucleic acid and gene delivery POCPs.

1.8 References

1. Kabanov, V. A. Polyelectrolyte Complexes in Solution and in the Condensed Phase. *Usp. Khim.* 2005, *74*, 5-23.
2. van der Gucht, J.; Spruijt, E.; Lemmers, M.; Cohen Stuart, M. A. Polyelectrolyte Complexes: Bulk Phases and Colloidal Systems. *J. Colloid Interface Sci.* 2011, *361*, 407-422.
3. Sing, C. E. Development of the Modern Theory of Polymeric Complex Coacervation. *Adv. Colloid Interface Sci.* 2016.
4. Barrat, J.-L.; Joanny, F. Theory of Polyelectrolyte Solutions. In *Advances in Chemical Physics*, John Wiley & Sons, Inc.: 2007; pp 1-66.

5. Kornyshev, A. A.; Lee, D. J.; Leikin, S.; Wynveen, A. Structure and Interactions of Biological Helices. *Rev. Mod. Phys.* 2007, *79*, 943-996.
6. Ran, S. Y.; Jia, J. L. A Multi-Field Approach to DNA Condensation. *Chinese. Phys. B.* 2015, *24*, 128702.
7. Fu, J.; Schlenoff, J. B. Driving Forces for Oppositely Charged Polyion Association in Aqueous Solutions: Enthalpic, Entropic, but Not Electrostatic. *J. Am. Chem. Soc.* 2016, *138*, 980-990.
8. Hartvig, R. A.; van de Weert, M.; Ostergaard, J.; Jorgensen, L.; Jensen, H. Protein Adsorption at Charged Surfaces: The Role of Electrostatic Interactions and Interfacial Charge Regulation. *Langmuir* 2011, *27*, 2634-2643.
9. Trefalt, G.; Behrens, S. H.; Borkovec, M. Charge Regulation in the Electrical Double Layer: Ion Adsorption and Surface Interactions. *Langmuir* 2016, *32*, 380-400.
10. Lund, M.; Jonsson, B. Charge Regulation in Biomolecular Solution. *Q. Rev. Biophys.* 2013, *46*, 265-281.
11. Teif, V. B.; Bohinc, K. Condensed DNA: Condensing the Concepts. *Prog. Biophys. Mol. Bio.* 2011, *105*, 208-222.
12. Kanasty, R.; Dorkin, J. R.; Vegas, A.; Anderson, D. Delivery Materials for siRNA Therapeutics. *Nat. Mater.* 2013, *12*, 967-977.
13. Lachelt, U.; Wagner, E. Nucleic Acid Therapeutics Using Polyplexes: A Journey of 50 Years (and Beyond). *Chem. Rev.* 2015, *115*, 11043-11078.
14. Draghici, B.; Ilies, M. A. Synthetic Nucleic Acid Delivery Systems: Present and Perspectives. *J. Med. Chem.* 2015, *58*, 4091-4130.
15. Yue, Y.; Wu, C. Progress and Perspectives in Developing Polymeric Vectors for in Vitro Gene Delivery. *Biomater. Sci.* 2013, *1*, 152-170.
16. Merkel, O. M.; Kissel, T. Quo Vadis Polyplex? *J. Control. Release* 2014, *190*, 415-423.
17. Wong, S. Y.; Pelet, J. M.; Putnam, D. Polymer Systems for Gene Delivery—Past, Present, and Future. *Prog. Polym. Sci.* 2007, *32*, 799-837.
18. Namvar, A.; Bolhassani, A.; Khairkhah, N.; Motevalli, F. Physicochemical Properties of Polymers: An Important System to Overcome the Cell Barriers in Gene Transfection. *Biopolymers* 2015, *103*, 363-375.
19. Mao, S.; Neu, M.; Germershaus, O.; Merkel, O.; Sitterberg, J.; Bakowsky, U.; Kissel, T. Influence of Polyethylene Glycol Chain Length on the Physicochemical and Biological Properties of Poly(Ethyleneimine)-Graft-Poly(Ethyleneglycol) Block Copolymer/siRNA Polyplexes. *Bioconjug. Chem.* 2006, *17*, 1209-1218.
20. Waite, C. L.; Sparks, S. M.; Uhrich, K. E.; Roth, C. M. Acetylation of PAMAM Dendrimers for Cellular Delivery of siRNA. *BMC Biotechnol.* 2009, *9*.
21. Uchida, H.; Itaka, K.; Nomoto, T.; Ishii, T.; Suma, T.; Ikegami, M.; Miyata, K.; Oba, M.; Nishiyama, N.; Kataoka, K. Modulated Protonation of Side Chain Aminoethylene Repeats in N-Substituted Poly(aspartamides) Promotes mRNA Transfection. *J. Am. Chem. Soc.* 2014, *136*, 12396-12405.

22. Chen, D. J.; Majors, B. S.; Zelikin, A.; Putnam, D. Structure-Function Relationships of Gene Delivery Vectors in a Limited Polycation Library. *J. Control. Release* 2005, *103*, 273-283.
23. Braun, C. S.; Vetro, J. A.; Tomalia, D. A.; Koe, G. S.; Koe, J. G.; Middaugh, C. R. Structure/Function Relationships of Polyamidoamine/DNA Dendrimers as Gene Delivery Vehicles. *J. Pharm. Sci.* 2005, *94*, 423-436.
24. Kossel, A. Longmans, Green and Co.: London, New York, 1928.
25. Kruyt, H. R. Elsevier Pub. Co.: New York, 1949.
26. Fuoss, R. M.; Sadek, H. Mutual Interaction of Polyelectrolytes. *Science* 1949, *110*, 552-554.
27. Michaels, A. S.; Miekka, R. G. Polycation-Polyanion Complexes: Preparation and Properties of Poly(Vinylbenzyltrimethylammonium) Poly(Styrenesulfonate). *J. of Phys. Chem.* 1961, *65*, 1765-1773.
28. Tsuchida, E.; Abe, K. Interactions between Macromolecules in Solution and Intermacromolecular Complexes. *Adv. Polym. Sci.* 1982, *45*, 1-119.
29. Gosule, L. C.; Schellman, J. A. Compact Form of DNA Induced by Spermidine. *Nature* 1976, *259*, 333-335.
30. Gosule, L. C.; Schellman, J. A. DNA Condensation with Polyamines I. Spectroscopic Studies. *J. Mol. Biol.* 1978, *121*, 311-326.
31. Chattoraj, D. K.; Gosule, L. C.; Schellman, A. DNA Condensation with Polyamines. II. Electron Microscopic Studies. *J. Mol. Biol.* 1978, *121*, 327-337.
32. Widom, J.; Baldwin, R. L. Cation-Induced Toroidal Condensation of DNA Studies with $Co^{3+}(NH_3)_6$. *J. Mol. Biol.* 1980, *144*, 431-453.
33. Laemmli, U. K. Characterization of DNA Condensates Induced by Poly(Ethyleneoxide) and Polylysine. *Proc. Natl. Acad. Sci. USA* 1975, *72*, 4288-4292.
34. Hsiang, M. W.; Cole, R. D. Structure of Histone H1-DNA Complex: Effect of Histone H1 on DNA Condensation. *Proc. Natl. Acad. Sci. USA* 1977, *74*, 4852-4856.
35. Wu, G. Y.; Wu, C. H. Receptor-Mediated in Vitro Gene Transformation by a Soluble DNA Carrier System. *J. Biol. Chem.* 1987, *262*, 4429-4432.
36. Kabanov, A. V.; Kiselev, V. I.; Chikindas, M. L.; Astaf'eva, I. V.; Glukhov, A. I. Increase in the Transforming Activity of Plasmid DNA by Means of Its Inclusion in the Interpolyelectrolytic Complex with a Carbon-Chain Cation. *Dokl. Akad. Nauk. SSSR* 1989, *306*, 226-229.
37. Behr, J. P.; Demeneix, B.; Loeffler, J. P.; Perez-Mutul, J. Efficient Gene Transfer into Mammalian Primary Endocrine Cells with Lipopolyamine-Coated DNA. *Proc. Natl. Acad. Sci. USA* 1989, *86*, 6982-6986.
38. Sen, G. L.; Blau, H. M. A Brief History of RNAi: The Silence of the Genes. *FASEB J.* 2006, *20*, 1293-1299.
39. Saenger, W. Springer-Verlag: New York, 1984.
40. Bloomfield, V. A.; Crothers, D. M.; Tinoco, I. University Science Books: Sausalito, Calif., 2000.
41. Dobrynin, A. V.; Rubinstein, M. Theory of Polyelectrolytes in Solutions and at Surfaces. *Prog. Polym. Sci.* 2005, *30*, 1049-1118.

42. Draper, D. E.; Grilley, D.; Soto, A. M. Ions and RNA Folding. *Annu. Rev. Biophys. Biomol. Struct.* 2005, *34*, 221-243.
43. Wong, G. C.; Pollack, L. Electrostatics of Strongly Charged Biological Polymers: Ion-Mediated Interactions and Self-Organization in Nucleic Acids and Proteins. *Annu. Rev. Phys. Chem.* 2010, *61*, 171-189.
44. Lipfert, J.; Doniach, S.; Das, R.; Herschlag, D. Understanding Nucleic Acid-Ion Interactions. *Annu. Rev. Biochem.* 2014, *83*, 813-841.
45. Chin, K.; Sharp, K. A.; Honig, B.; Pyle, A. M. Calculating the Electrostatic Properties of RNA Provides New Insights into Molecular Interactions and Function. *Nat. Struct. Biol.* 1999, *6*, 1055-1061.
46. Kornyshev, A. A.; Leikin, S. Helical Structure Determines Different Susceptibilities of dsDNA, dsRNA, and tsDNA to Counterion-Induced Condensation. *Biophys. J.* 2013, *104*, 2031-2041.
47. Bronich, T. K.; Nguyen, H. K.; Eisenberg, A.; Kabanov, A. V. Recognition of DNA Topology in Reactions between Plasmid DNA and Cationic Copolymers. *J. Am. Chem. Soc.* 2000, *122*, 8339-8343.
48. Pabit, S. A.; Qiu, X.; Lamb, J. S.; Li, L.; Meisburger, S. P.; Pollack, L. Both Helix Topology and Counterion Distribution Contribute to the More Effective Charge Screening in dsRNA Compared with dsDNA. *Nucleic Acids Res.* 2009, *37*, 3887-3896.
49. Abels, J. A.; Moreno-Herrero, F.; van der Heijden, T.; Dekker, C.; Dekker, N. H. Single-Molecule Measurements of the Persistence Length of Double-Stranded RNA. *Biophys. J.* 2005, *88*, 2737-2744.
50. Dhanoya, A.; Chain, B. M.; Keshavarz-Moore, E. The Impact of DNA Topology on Polyplex Uptake and Transfection Efficiency in Mammalian Cells. *J. Biotechnol.* 2011, *155*, 377-386.
51. Dhanoya, A.; Chain, B. M.; Keshavarz-Moore, E. Role of DNA Topology in Uptake of Polyplex Molecules by Dendritic Cells. *Vaccine* 2012, *30*, 1675-1681.
52. Ma, J. B.; Yuan, Y. R.; Meister, G.; Pei, Y.; Tuschl, T.; Patel, D. J. Structural Basis for 5'-End-Specific Recognition of Guide RNA by the A. Fulgidus Piwi Protein. *Nature* 2005, *434*, 666-670.
53. Parker, J. S.; Roe, S. M.; Barford, D. Structural Insights into mRNA Recognition from a Piwi Domain-siRNA Guide Complex. *Nature* 2005, *434*, 663-666.
54. Podbevsek, P.; Allerson, C. R.; Bhat, B.; Plavec, J. Solution-State Structure of a Fully Alternately 2'-F/2'-Ome Modified 42-Nt Dimeric siRNA Construct. *Nucleic Acids Res.* 2010, *38*, 7298-7307.
55. Bolcato-Bellemin, A. L.; Bonnet, M. E.; Creusat, G.; Erbacher, P.; Behr, J. P. Sticky Overhangs Enhance siRNA-Mediated Gene Silencing. *Proc. Natl. Acad. Sci. USA* 2007, *104*, 16050-16055.
56. Chen, H.; Meisburger, S. P.; Pabit, S. A.; Sutton, J. L.; Webb, W. W.; Pollack, L. Ionic Strength-Dependent Persistence Lengths of Single-Stranded RNA and DNA. *Proc. Natl. Acad. Sci. USA* 2012, *109*, 799-804.
57. Matveeva, O. V.; Mathews, D. H.; Tsodikov, A. D.; Shabalina, S. A.; Gesteland, R. F.; Atkins, J. F.; Freier, S. M. Thermodynamic Criteria for High Hit Rate Antisense Oligonucleotide Design. *Nucleic Acids Res.* 2003, *31*, 4989-4994.

58. Sundaram, S.; Viriyapthakorn, S.; Roth, C. M. Oligonucleotide Structure Influences the Interactions between Cationic Polymers and Oligonucleotides. *Biomacromolecules* 2005, *6*, 2961-2968.
59. Bailor, M. H.; Mustoe, A. M.; Brooks, C. L., 3rd; Al-Hashimi, H. M. Topological Constraints: Using RNA Secondary Structure to Model 3D Conformation, Folding Pathways, and Dynamic Adaptation. *Curr. Opin. Struct. Biol.* 2011, *21*, 296-305.
60. Takamoto, K.; Das, R.; He, Q.; Doniach, S.; Brenowitz, M.; Herschlag, D.; Chance, M. R. Principles of RNA Compaction: Insights from the Equilibrium Folding Pathway of the P4-P6 RNA Domain in Monovalent Cations. *J. Mol. Biol.* 2004, *343*, 1195-1206.
61. Marcia, M.; Pyle, A. M. Principles of Ion Recognition in RNA: Insights from the Group Ii Intron Structures. *RNA* 2014, *20*, 516-527.
62. Vaheri, A. Infectious Poliovirus RNA: A Sensitive Method of Assay. 1965; Vol. 27, p 434.
63. McCutchan, J. H. Enchancement of the Infectivity of Simian Virus 40 Deoxyribonucleic Acid with Diethylaminoethyl-Dextran. *J. Natl. Cancer Inst.* 1968, *41*, 351.
64. Wagner, E.; Ogris, M.; Zauner, W. Polylysine-Based Transfection Systems Utilizing Receptor-Mediated Delivery. *Adv. Drug Deliv. Rev.* 1998, *30*, 97-113.
65. Farber, F. E.; Melnick, J. L.; Butel, J. S. Optimal Conditions for Uptake of Exogenous DNA by Chinese Hamster Lung Cells Deficient in Hypoxanthine-Guanine Phosphoribosyltransferase. *Biochim. Biophys. Acta.* 1975, *390*, 298-311.
66. Godbey, W. T.; Wu, K. K.; Mikos, A. G. Poly(Ethylenimine) and Its Role in Gene Delivery. *J. Control. Release* 1999, *60*, 149-160.
67. Neu, M.; Fischer, D.; Kissel, T. Recent Advances in Rational Gene Transfer Vector Design Based on Poly(Ethyleneimine) and Its Derivatives. *J. Gene Med.* 2005, *7*, 992-1009.
68. Neuberg, P.; Kichler, A. Recent Developments in Nucleic Acid Delivery with Polyethylenimines. *Adv. Genet.* 2014, *88*, 263-288.
69. Boussif, O.; Lezoualc'h, F.; Zanta, M. A.; Mergny, M. D.; Scherman, D.; Demeneix, B.; Behr, J. P. A Versatile Vector for Gene and Oligonucleotide Transfer into Cells in Culture and in Vivo: Polyethylenimine. *Proc. Natl. Acad. Sci. USA* 1995, *92*, 7297-7301.
70. Wang, D.; Zhao, T.; Zhu, X.; Yan, D.; Wang, W. Bioapplications of Hyperbranched Polymers. *Chem. Soc. Rev.* 2015, *44*, 4023-4071.
71. Dehshahri, A.; Sadeghpour, H. Surface Decorations of Poly(Amidoamine) Dendrimer by Various Pendant Moieties for Improved Delivery of Nucleic Acid Materials. *Colloids Surf. B Biointerfaces* 2015, *132*, 85-102.
72. Lai, W. F. Cyclodextrins in Non-Viral Gene Delivery. *Biomaterials* 2014, *35*, 401-411.
73. Mintzer, M. A.; Simanek, E. E. Nonviral Vectors for Gene Delivery. *Chem. Rev.* 2009, *109*, 259-302.
74. Hull, W. E.; Kricheldorf, H. R.; Fehrle, M. ^{15}N-NMR Spectroscopy. IV. Comparison of Poly(L-Lysine) and Isopoly(L-Lysine). *Biopolymers* 1978, *17*, 2427-2443.

75. Dos, A.; Schimming, V.; Tosoni, S.; Limbach, H. H. Acid-Base Interactions and Secondary Structures of Poly(L-Lysine) Probed by ^{15}N and ^{13}C Solid State NMR and Ab Initio Model Calculations. *J. Phys. Chem. B* 2008, *112*, 15604-15615.
76. Antila, H. S.; Harkonen, M.; Sammalkorpi, M. Chemistry Specificity of DNA-Polycation Complex Salt Response: A Simulation Study of DNA, Polylysine and Polyethyleneimine. *Phys. Chem. Chem. Phys.* 2015, *17*, 5279-5289.
77. Ziebarth, J.; Wang, Y. Molecular Dynamics Simulations of DNA-Polycation Complex Formation. *Biophys. J.* 2009, *97*, 1971-1983.
78. Davidson, B.; Fasman, G. D. The Conformational Transitions of Uncharged Poly(L-Lysine). α Helix-Random Coil- β Structure. *Biochemistry* 1967, *6*, 1616-1629.
79. Perly, B.; Chevalier, Y.; Chachaty, C. NMR and ESR Study of the Conformations and Dynamical Properties of Poly(L-Lysine) in Aqueous Solutions. *Macromolecules* 1981, *14*, 969-975.
80. Mirtic, A.; Grdadolnik, J. The Structure of Poly(L-Lysine) in Different Solvents. *Biophys. Chem.* 2013, *175-176*, 47-53.
81. Ziebarth, J. D.; Wang, Y. M. Understanding the Protonation Behavior of Linear Polyethylenimine in Solutions through Monte Carlo Simulations. *Biomacromolecules* 2010, *11*, 29-38.
82. Borkovec, M.; Koper, G. J. M. Proton Binding Characteristics of Branched Polyelectrolytes. *Macromolecules* 1997, *30*, 2151-2158.
83. Sun, C. B.; Tang, T.; Uludag, H. Molecular Dynamics Simulations for Complexation of DNA with 2 kDa PEI Reveal Profound Effect of PEI Architecture on Complexation. *J. Phys. Chem. B* 2012, *116*, 2405-2413.
84. Tomalia, D. A.; Baker, H.; Dewald, J.; Hall, M.; Kallos, G.; Martin, S.; Roeck, J.; Ryder, J.; Smith, P. A New Class of Polymers: Starburst-Dendritic Macromolecules. *Polym. J.* 1985, *17*, 117-132.
85. Tian, W.-d.; Ma, Y.-q. Theoretical and Computational Studies of Dendrimers as Delivery Vectors. *Chem. Soc. Rev.* 2013, *42*, 705-727.
86. Chen, W.; Tomalia, D. A.; Thomas, J. L. Unusual pH-Dependent Polarity Changes in PAMAM Dendrimers: Evidence for pH-Responsive Conformational Changes. *Macromolecules* 2000, *33*, 9169-9172.
87. Rangarajan, B.; Coons, L. S.; Scranton, A. B. Characterization of Hydrogels Using Luminescence Spectroscopy. *Biomaterials* 1996, *17*, 649-661.
88. Liu, Y.; Bryantsev, V. S.; Diallo, M. S.; Goddard Iii, W. A. PAMAM Dendrimers Undergo pH Responsive Conformational Changes without Swelling. *J. Am. Chem. Soc.* 2009, *131*, 2798-2799.
89. Lee, I.; Athey, B. D.; Wetzel, A. W.; Meixner, W.; Baker, J. R. Structural Molecular Dynamics Studies on Polyamidoamine Dendrimers for a Therapeutic Application: Effects of pH and Generation. *Macromolecules* 2002, *35*, 4510-4520.
90. Maiti, P. K.; Goddard, W. A. Solvent Quality Changes the Structure of G8 PAMAM Dendrimer, a Disagreement with Some Experimental Interpretations. *J. of Phys. Chem. B* 2006, *110*, 25628-25632.

91. Felgner, P. L.; Barenholz, Y.; Behr, J. P.; Cheng, S. H.; Cullis, P.; Huang, L.; Jessee, J. A.; Seymour, L.; Szoka, F.; Thierry, A. R.; Wagner, E.; Wu, G. Nomenclature for Synthetic Gene Delivery Systems. *Hum. Gene Ther.* 1997, *8*, 511-512.
92. Kabanov, A. V.; Kabanov, V. A. DNA Complexes with Polycations for the Delivery of Genetic Material into Cells. *Bioconj. Chem.* 1995, *6*, 7-20.
93. Dautzenberg, H. Polyelectrolyte Complex Formation in Highly Aggregating Systems. 1. Effect of Salt: Polyelectrolyte Complex Formation in the Presence of NaCl. *Macromolecules* 1997, *30*, 7810-7815.
94. Dautzenberg, H.; Karibyants, N. Polyelectrolyte Complex Formation in Highly Aggregating Systems. Effect of Salt: Response to Subsequent Addition of NaCl. *Macromol. Chem. Phys.* 1999, *200*, 118-125.
95. Carnerup, A. M.; Ainalem, M.-L.; Alfredsson, V.; Nylander, T. Condensation of DNA Using Poly(Amidoamine) Dendrimers: Effect of Salt Concentration on Aggregate Morphology. *Soft Matter* 2011, *7*, 760-768.
96. Perez, A. P.; Romero, E. L.; Morilla, M. J. Ethylendiamine Core PAMAM Dendrimers/siRNA Complexes as in Vitro Silencing Agents. *Inter. J. of Pharm.* 2009, *380*, 189-200.
97. Müller, M.; SpringerLink. Springer Berlin Heidelberg : Imprint: Springer: Berlin, Heidelberg, 2014.
98. Jorge, A. F.; Sarraguca, J. M. G.; Dias, R. S.; Pais, A. A. C. C. Polyelectrolyte Compaction by pH-Responsive Agents. *Phys. Chem. Chem. Phys.* 2009, *11*, 10890-10898.
99. DeRouchey, J.; Parsegian, V. A.; Rau, D. C. Cation Charge Dependence of the Forces Driving DNA Assembly. *Biophys. J.* 2010, *99*, 2608-2615.
100. Zelikin, A. N.; Trukhanova, E. S.; Putnam, D.; Izumrudov, V. A.; Litmanovich, A. A. Competitive Reactions in Solutions of Poly-L-Histidine, Calf Thymus DNA, and Synthetic Polyanions: Determining the Binding Constants of Polyelectrolytes. *J. Am. Chem. Soc.* 2003, *125*, 13693-13699.
101. Rungsardthong, U.; Ehtezazi, T.; Bailey, L.; Armes, S. P.; Garnett, M. C.; Stolnik, S. Effect of Polymer Ionization on the Interaction with DNA in Nonviral Gene Delivery Systems. *Biomacromolecules* 2003, *4*, 683-690.
102. Jorge, A. F.; Dias, R. S.; Pereira, J. C.; Pais, A. A. C. C. DNA Condensation by pH-Responsive Polycations. *Biomacromolecules* 2010, *11*, 2399-2406.
103. Tang, M. X.; Szoka, F. C. The Influence of Polymer Structure on the Interactions of Cationic Polymers with DNA and Morphology of the Resulting Complexes. *Gene Ther.* 1997, *4*, 823-832.
104. Kwoh, D. Y.; Coffin, C. C.; Lollo, C. P.; Jovenal, J.; Banaszczyk, M. G.; Mullen, P.; Phillips, A.; Amini, A.; Fabrycki, J.; Bartholomew, R. M.; Brostoff, S. W.; Carlo, D. J. Stabilization of Poly(L-Lysine)/DNA Polyplexes for in Vivo Gene Delivery to the Liver. *Biochim. Biophys. Acta.* 1999, *1444*, 171-190.
105. Anchordoquy, T. J.; Koe, G. S. Physical Stability of Nonviral Plasmid-Based Therapeutics. *J. Pharm. Sci.* 2000, *89*, 289-296.

106. Jones, N. A.; Hill, I. R.; Stolnik, S.; Bignotti, F.; Davis, S. S.; Garnett, M. C. Polymer Chemical Structure Is a Key Determinant of Physicochemical and Colloidal Properties of Polymer-DNA Complexes for Gene Delivery. *Biochim. Biophys. Acta.* 2000, *1517*, 1-18.
107. Thakur, S.; Kesharwani, P.; Tekade, R. K.; Jain, N. K. Impact of Pegylation on Biopharmaceutical Properties of Dendrimers. *Polymer* 2015, *59*, 67-92.
108. Millili, P. G.; Selekman, J. A.; Blocker, K. M.; Johnson, D. A.; Naik, U. P.; Sullivan, M. O. Structural and Functional Consequences of Poly(Ethylene Glycol) Inclusion on DNA Condensation for Gene Delivery. *Microsc. Res. Tech.* 2010, *73*, 866-877.
109. Debus, H.; Baumhof, P.; Probst, J.; Kissel, T. Delivery of Messenger RNA Using Poly(Ethyleneimine)-Poly(Ethyleneglycol)-Copolymer Blends for Polyplex Formation: Biophysical Characterization and in Vitro Transfection Properties. *J. Control. Release* 2010, *148*, 334-343.
110. Nguyen, H. K.; Lemieux, P.; Vinogradov, S. V.; Gebhart, C. L.; Guerin, N.; Paradis, G.; Bronich, T. K.; Alakhov, V. Y.; Kabanov, A. V. Evaluation of Polyether-Polyethyleneimine Graft Copolymers as Gene Transfer Agents. *Gene Ther.* 2000, *7*, 126-138.
111. Zheng, M.; Zhong, Z.; Zhou, L.; Meng, F.; Peng, R.; Zhong, Z. Poly(Ethyleneoxide) Grafted with Short Polyethylenimine Gives DNA Polyplexes with Superior Colloidal Stability, Low Cytotoxicity, and Potent in Vitro Gene Transfection under Serum Conditions. *Biomacromolecules* 2012, *13*, 881-888.
112. Pavan, G. M.; Posocco, P.; Tagliabue, A.; Maly, M.; Malek, A.; Danani, A.; Ragg, E.; Catapano, C. V.; Pricl, S. PAMAM Dendrimers for siRNA Delivery: Computational and Experimental Insights. *Chem. Euro. J.* 2010, *16*, 7781-7795.
113. Miyoshi, D.; Ueda, Y. M.; Shimada, N.; Nakano, S.; Sugimoto, N.; Maruyama, A. Drastic Stabilization of Parallel DNA Hybridizations by a Polylysine Comb-Type Copolymer with Hydrophilic Graft Chain. *ChemMedChem* 2014, *9*, 2156-2163.
114. Sato, Y.; Kim, W. J.; Saito, M.; Kano, A.; Akaike, T.; Maruyama, A. Cationic Comb-Type Copolymers as an Artificial Nucleic Acid-Chaperone: Spectroscopic Analyses for DNA/Copolymer Interaction. *Nucleic Acids Res. Suppl.* 2003, 129-130.
115. Sato, Y.; Moriyama, R.; Choi, S. W.; Kano, A.; Maruyama, A. Spectroscopic Investigation of Cationic Comb-Type Copolymers/DNA Interaction: Interpolyelectrolyte Complex Enhancement Synchronized with DNA Hybridization. *Langmuir* 2007, *23*, 65-69.
116. Snoussi, K.; Bulte, J. W.; Gueron, M.; van Zijl, P. C. Sensitive Cest Agents Based on Nucleic Acid Imino Proton Exchange: Detection of Poly(Ru) and of a Dendrimer-Poly(Ru) Model for Nucleic Acid Delivery and Pharmacology. *Magn. Reson. Med.* 2003, *49*, 998-1005.
117. Shakya, A.; Dougherty, C. A.; Xue, Y.; Al-Hashimi, H. M.; Holl, M. M. B. Rapid Exchange between Free and Bound States in RNA-Dendrimer Polyplexes: Implications on the Mechanism of Delivery and Release. *Biomacromolecules* 2016, *17*, 154-164.
118. Prevette, L. E.; Nikolova, E. N.; Al-Hashimi, H. M.; Holl, M. M. B. Intrinsic Dynamics of DNA-Polymer Complexes: A Mechanism for DNA Release. *Mol. Pharm.* 2012, *9*, 2743-2749.

119. Froehlich, E.; Mandeville, J. S.; Kreplak, L.; Tajmir-Riahi, H. A. Aggregation and Particle Formation of tRNA by Dendrimers. *Biomacromolecules* 2011, *12*, 2780-2787.
120. Reyes-Reveles, J.; Sedaghat-Herati, R.; Gilley, D. R.; Schaeffer, A. M.; Ghosh, K. C.; Greene, T. D.; Gann, H. E.; Dowler, W. A.; Kramer, S.; Dean, J. M.; Delong, R. K. mPEG-PAMAM-G4 Nucleic Acid Nanocomplexes: Enhanced Stability, RNase Protection, and Activity of Splice Switching Oligomer and Poly I:C RNA. *Biomacromolecules* 2013, *14*, 4108-4115.
121. Lucotti, A.; Tommasini, M.; Pezzoli, D.; Candiani, G. Molecular Interactions of DNA with Transfectants: A Study Based on Infrared Spectroscopy and Quantum Chemistry as Aids to Fluorescence Spectroscopy and Dynamic Light Scattering Analyses. *RSC Adv.* 2014, *4*, 49620-49627.
122. Choosakoonkriang, S.; Lobo, B. A.; Koe, G. S.; Koe, J. G.; Middaugh, C. R. Biophysical Characterization of PEI/DNA Complexes. *J. Pharm. Sci.* 2003, *92*, 1710-1722.
123. Alajangi, H. K.; Santhiya, D. Fluorescence and Forster Resonance Energy Transfer Investigations on DNA Oligonucleotide and PAMAM Dendrimer Packing Interactions in Dendriplexes. *Phys. Chem. Chem. Phys.* 2015, *17*, 8680-8691.
124. Manning, G. S. The Molecular Theory of Polyelectrolyte Solutions with Applications to the Electrostatic Properties of Polynucleotides. *Q. Rev. Biophys.* 1978, *11*, 179-246.
125. Arenzon, J. J.; Stilck, J. F.; Levin, Y. Simple Model for Attraction between Like-Charged Polyions. *Euro. Phys. J. B* 1999, *12*, 79-82.
126. Ha, B. Y.; Liu, A. J. Counterion-Mediated, Non-Pairwise-Additive Attractions in Bundles of Like-Charged Rods. *Phys. Rev. E.* 1999, *60*, 803-813.
127. Grosberg, A. Y.; Nguyen, T. T.; Shklovskii, B. I. Colloquium: The Physics of Charge Inversion in Chemical and Biological Systems. *Rev. Mod. Phys.* 2002, *74*, 329-345.
128. Mengarelli, V.; Auvray, L.; Pastre, D.; Zeghal, M. Charge Inversion, Condensation and Decondensation of DNA and Polystyrene Sulfonate by Polyethylenimine. *Eur. Phys. J. E Soft Matter* 2011, *34*, 127.
129. Leikin, S.; Parsegian, V. A.; Rau, D. C.; Rand, R. P. Hydration Forces. *Annu. Rev. Phys. Chem.* 1993, *44*, 369-395.
130. Kornyshev, A. A.; Leikin, S. Electrostatic Zipper Motif for DNA Aggregation. *Phys. Rev. Lett.* 1999, *82*, 4138-4141.
131. Scholz, C.; Wagner, E. Therapeutic Plasmid DNA Versus siRNA Delivery: Common and Different Tasks for Synthetic Carriers. *J. Control. Release* 2012, *161*, 554-565.
132. Kwok, A.; Hart, S. L. Comparative Structural and Functional Studies of Nanoparticle Formulations for DNA and siRNA Delivery. *Nanomedicine* 2011, *7*, 210-219.
133. Grayson, A. C.; Doody, A. M.; Putnam, D. Biophysical and Structural Characterization of Polyethylenimine-Mediated siRNA Delivery in Vitro. *Pharm. Res.* 2006, *23*, 1868-1876.
134. Roth, C. M. Molecular and Cellular Barriers Limiting the Effectiveness of Antisense Oligonucleotides. *Biophys. J.* 2005, *89*, 2286-2295.

135. Forster, Y.; Schwenzer, B. Efficient Suppression of Tissue Factor Synthesis Using Antisense Oligonucleotides Selected by an Enhanced Strategy for Evaluation of Structural Characteristics. *Oligonucleotides* 2008, *18*, 355-364.
136. Bloomfield, V. A. Condensation of DNA by Multivalent Cations: Considerations on Mechanism. *Biopolymers* 1991, *31*, 1471-1481.
137. Bloomfield, V. A. DNA Condensation by Multivalent Cations. *Biopolymers* 1997, *44*, 269-282.
138. Junghans, M.; Kreuter, J.; Zimmer, A. Phosphodiester and Phosphorothioate Oligonucleotide Condensation and Preparation of Antisense Nanoparticles. *Biochim. Biophys. Acta.* 2001, *1544*, 177-188.
139. Sarkar, T.; Conwell, C. C.; Harvey, L. C.; Santai, C. T.; Hud, N. V. Condensation of Oligonucleotides Assembled into Nicked and Gapped Duplexes: Potential Structures for Oligonucleotide Delivery. *Nucleic Acids Res.* 2005, *33*, 143-151.
140. Zhou, J.; Wu, J.; Hafdi, N.; Behr, J. P.; Erbacher, P.; Peng, L. PAMAM Dendrimers for Efficient siRNA Delivery and Potent Gene Silencing. *Chem. Commun. (Camb)* 2006, 2362-2364.
141. Dauty, E.; Behr, J. P.; Remy, J. S. Development of Plasmid and Oligonucleotide Nanometric Particles. *Gene Ther.* 2002, *9*, 743-748.
142. Li, L.; Pabit, S. A.; Meisburger, S. P.; Pollack, L. Double-Stranded RNA Resists Condensation. *Phys. Rev. Lett.* 2011, *106*.
143. Tolokh, I. S.; Pabit, S. A.; Katz, A. M.; Chen, Y.; Drozdetski, A.; Baker, N.; Pollack, L.; Onufriev, A. V. Why Double-Stranded RNA Resists Condensation. *Nucleic Acids Res.* 2014, *42*, 10823-10831.
144. Wu, Y. Y.; Zhang, Z. L.; Zhang, J. S.; Zhu, X. L.; Tan, Z. J. Multivalent Ion-Mediated Nucleic Acid Helix-Helix Interactions: RNA Versus DNA. *Nucleic Acids Res.* 2015, *43*, 6156-6165.
145. Braun, C. S.; Fisher, M. T.; Tomalia, D. A.; Koe, G. S.; Koe, J. G.; Middaugh, C. R. A Stopped-Flow Kinetic Study of the Assembly of Nonviral Gene Delivery Complexes. *Biophys. J.* 2005, *88*, 4146-4158.
146. Dey, D.; Kumar, S.; Maiti, S.; Dhara, D. Stopped-Flow Kinetic Studies of Poly(amidoamine) Dendrimer-Calf Thymus DNA to Form Dendriplexes. *J. Phys. Chem. B* 2013, *117*, 13767-13774.
147. Dey, D.; Kumar, S.; Banerjee, R.; Maiti, S.; Dhara, D. Polyplex Formation between Pegylated Linear Cationic Block Copolymers and DNA: Equilibrium and Kinetic Studies. *J. Phys. Chem. B* 2014, *118*, 7012-7025.
148. Dey, D.; Maiti, C.; Maiti, S.; Dhara, D. Interaction between Calf Thymus DNA and Cationic Bottle-Brush Copolymers: Equilibrium and Stopped-Flow Kinetic Studies. *Phys. Chem. Chem. Phys.* 2015, *17*, 2366-2377.
149. Miller, I. R.; Bach, D. Interaction of DNA with Heavy Metal Ions and Polybases: Cooperative Phenomena. *Biopolymers* 1968, *6*, 169-179.
150. Izumrudov, V. A.; Kargov, S. I.; Zhiryakova, M. V.; Zezin, A. B.; Kabanov, V. A. Competitive Reactions in Solutions of DNA and Water-Soluble Interpolyelectrolyte Complexes. *Biopolymers* 1995, *35*, 523-531.

151. Chen, H. H.; Ho, Y.-P.; Jiang, X.; Mao, H.-Q.; Wang, T.-H.; Leong, K. W. Quantitative Comparison of Intracellular Unpacking Kinetics of Polyplexes by a Model Constructed from Quantum Dot-Fret. *Mol. Ther.* 2008, *16*, 324-332.
152. Thibault, M.; Nimesh, S.; Lavertu, M.; Buschmann, M. D. Intracellular Trafficking and Decondensation Kinetics of Chitosan-pDNA Polyplexes. *Mol. Ther.* 2010, *18*, 1787-1795.
153. Schaffer, D. V.; Fidelman, N. A.; Dan, N.; Lauffenburger, D. A. Vector Unpacking as a Potential Barrier for Receptor-Mediated Polyplex Gene Delivery. *Biotechnol. Bioeng.* 2000, *67*, 598-606.
154. Gabrielson, N. P.; Pack, D. W. Acetylation of Polyethylenimine Enhances Gene Delivery Via Weakened Polymer/DNA Interactions. *Biomacromolecules* 2006, *7*, 2427-2435.
155. Kabanov, V. A.; Zhiryakova, M. V.; Kargov, S. I.; Zezin, A. B.; Izumrudov, V. A. Degree of Polymerization of Polyions Can Determine a Direction of the Competitive Reaction in Solutions of the Nonstoichiometric Inter Polyelectrolyte Complexes and DNA. *Dokl. Akad. Nauk.* 1993, *332*, 722-726.
156. Wan, L.; Manickam, D. S.; Oupicky, D.; Mao, G. DNA Release Dynamics from Reducible Polyplexes by Atomic Force Microscopy. *Langmuir* 2008, *24*, 12474-12482.
157. Ouyang, D.; Zhang, H.; Parekh, H. S.; Smith, S. C. Structure and Dynamics of Multiple Cationic Vectors-siRNA Complexation by All-Atomic Molecular Dynamics Simulations. *J. Phys. Chem. B* 2010, *114*, 9231-9237.
158. Shcharbin, D.; Pedziwiatr, E.; Bryszewska, M. How to Study Dendriplexes I: Characterization. *J. Control. Release* 2009, *135*, 186-197.
159. Ainalem, M. L.; Nylander, T. DNA Condensation Using Cationic Dendrimers-Morphology and Supramolecular Structure of Formed Aggregates. *Soft Matter* 2011, *7*, 4577-4594.
160. Ainalem, M. L.; Bartles, A.; Muck, J.; Dias, R. S.; Carnerup, A. M.; Zink, D.; Nylander, T. DNA Compaction Induced by a Cationic Polymer or Surfactant Impact Gene Expression and DNA Degradation. *PLOS One* 2014, *9*, e92692.
161. Mannisto, M.; Vanderkerken, S.; Toncheva, V.; Elomaa, M.; Ruponen, M.; Schacht, E.; Urtti, A. Structure-Activity Relationships of Poly(L-Lysines): Effects of Pegylation and Molecular Shape on Physicochemical and Biological Properties in Gene Delivery. *J. Control. Release* 2002, *83*, 169-182.
162. Wood, K. C.; Little, S. R.; Langer, R.; Hammond, P. T. A Family of Hierarchically Self-Assembling Linear-Dendritic Hybrid Polymers for Highly Efficient Targeted Gene Delivery. *Angew. Chem. Int. Ed. Engl.* 2005, *44*, 6704-6708.
163. Kukowska-Latallo, J. F.; Bielinska, A. U.; Johnson, J.; Spindler, R.; Tomalia, D. A.; Baker, J. R., Jr. Efficient Transfer of Genetic Material into Mammalian Cells Using Starburst Polyamidoamine Dendrimers. *Proc. Natl. Acad. Sci. USA* 1996, *93*, 4897-4902.
164. Ramaswamy, C.; Sakthivel, T.; Wilderspin, A. F.; Florence, A. T. Dendriplexes and Their Characterisation. *Int. J. Pharm.* 2003, *254*, 17-21.
165. Bielinska, A. U.; Kukowska-Latallo, J. F.; Baker, J. R., Jr. The Interaction of Plasmid DNA with Polyamidoamine Dendrimers: Mechanism of Complex Formation and Analysis of Alterations

Induced in Nuclease Sensitivity and Transcriptional Activity of the Complexed DNA. *Biochim. Biophys. Acta.* 1997, *1353*, 180-190.

166. Evans, H. M.; Ahmad, A.; Ewert, K.; Pfohl, T.; Martin-Herranz, A.; Bruinsma, R. F.; Safinya, C. R. Structural Polymorphism of DNA-Dendrimer Complexes. *Phys. Rev. Lett.* 2003, *91*, 075501.
167. Su, C. J.; Chen, H. L.; Wei, M. C.; Peng, S. F.; Sung, H. W.; Ivanov, V. A. Columnar Mesophases of the Complexes of DNA with Low-Generation Poly(amidoamine) Dendrimers. *Biomacromolecules* 2009, *10*, 773-783.
168. Peng, S.-F.; Su, C.-J.; Wei, M.-C.; Chen, C.-Y.; Liao, Z.-X.; Lee, P.-W.; Chen, H.-L.; Sung, H.-W. Effects of the Nanostructure of Dendrimer/DNA Complexes on Their Endocytosis and Gene Expression. *Biomaterials* 2010, *31*, 5660-5670.
169. Jensen, L. B.; Mortensen, K.; Pavan, G. M.; Kasimova, M. R.; Jensen, D. K.; Gadzhyeva, V.; Nielsen, H. M.; Foged, C. Molecular Characterization of the Interaction between siRNA and PAMAM G7 Dendrimers by SAXS, ITC, and Molecular Dynamics Simulations. *Biomacromolecules* 2010, *11*, 3571-3577.
170. Dootz, R.; Toma, A. C.; Pfohl, T. Pamam6 Dendrimers and DNA: pH Dependent "Beads-on-a-String" Behavior Revealed by Small Angle X-Ray Scattering. *Soft Matter* 2011, *7*, 8343-8351.
171. Prevost, S.; Riemer, S.; Fischer, W.; Haag, R.; Bottcher, C.; Gummel, J.; Grillo, I.; Appavou, M. S.; Gradzielski, M. Colloidal Structure and Stability of DNA/Polycations Polyplexes Investigated by Small Angle Scattering. *Biomacromolecules* 2011, *12*, 4272-4282.
172. Yang, C.-C.; Huang, Y.-C.; Chen, C.-Y.; Su, C.-J.; Chen, H.-L.; Ivanov, V. A. Structure of the Electrostatic Complex of DNA with Cationic Dendrimer of Intermediate Generation: The Role of Counterion Entropy. *Macromolecules* 2014, *47*, 3117-3127.
173. Ritort, F.; Mihardja, S.; Smith, S. B.; Bustamante, C. Condensation Transition in DNA-Polyaminoamide Dendrimer Fibers Studied Using Optical Tweezers. *Phys. Rev. Lett.* 2006, *96*, 118301.
174. Choi, Y. S.; Cho, T.-S.; Kim, J. M.; Han, S. W.; Kim, S. K. Amine Terminated G-6 PAMAM Dendrimer and Its Interaction with DNA Probed by Hoechst 33258. *Biophys. Chem.* 2006, *121*, 142-149.
175. Maruyama, A.; Watanabe, H.; Ferdous, A.; Katoh, M.; Ishihara, T.; Akaike, T. Characterization of Interpolyelectrolyte Complexes between Double-Stranded DNA and Polylysine Comb-Type Copolymers Having Hydrophilic Side Chains. *Bioconjug. Chem.* 1998, *9*, 292-299.
176. Ottaviani, M. F.; Furini, F.; Casini, A.; Turro, N. J.; Jockusch, S.; Tomalia, D. A.; Messori, L. Formation of Supramolecular Structures between DNA and Starburst Dendrimers Studied by Epr, Cd, Uv, and Melting Profiles. *Macromolecules* 2000, *33*, 7842-7851.
177. Wang, X.; Kelkar, S. S.; Hudson, A. G.; Moore, R. B.; Reineke, T. M.; Madsen, L. A. Quantitation of Complexed Versus Free Polymers in Interpolyelectrolyte Polyplex Formulations. *ACS Macro Lett.* 2013, *2*, 1038-1041.

CHAPTER 2 INTERMOLECULAR EXCHANGE IN POLYPLEX SYSTEMS

The work presented in section 2.1 of this chapter has been published in the following paper:

Shakya, A.; Dougherty, C. A.; Xue, Y.; Al-Hashimi, H. M.; Holl, M. M. B. "Rapid Exchange between Free and Bound States in RNA-Dendrimer Polyplexes: Implications on the Mechanism of Delivery and Release" *Biomacromolecules* **2016**, *17*, 154-164.

2.1 Structure and Exchange Dynamics of RNA-Dendrimer Polyplexes

Despite being studied for decades as delivery agents for therapeutic nucleic acids, it has been difficult to achieve detailed atomic/molecular picture of the polyplex structure and dynamics and how these properties vary as a function of key vector properties such as molecular weight, hydrophobicity, and charge density as well as the type of nucleic acid.[1] Most of experimental studies employed to understand polyplex structure have been based on techniques such as electron microscopy (EM),[2] atomic force microscopy (AFM) imaging,[3,4] circular diochroism (CD),[5-7] infrared (IR) spectroscopy,[8] and small angle X-ray scattering studies (SAXS).[9,10] On the dynamics front, molecular dynamics (MD) simulations[11-14] have been employed to some extent. However, studies on polyplexes based on NMR spectroscopy, which is a powerful experimental tool to study both structure and dynamics of macromolecules, are scant in literature.

Using 1D ^{1}H NMR spectroscopy, a previous study by our group recently provided evidence that a 20-bp DNA duplex rapidly exchanges (exchange times < ms) between free and bound forms of polyplexes formed with generation 5 poly(amidoamine) (G5 PAMAM) dendrimer with 10% of its primary amines functionalized with 5000 molecular weight poly(ethyleneglycol) (PEG), (G5-PEG).[15] The G5 PAMAM scaffold was PEGylated to increase polyplex solubility and this form has been shown to be effective for *in vivo* knockdown of protein expression.[16] Based on the ^{1}H NMR chemical shifts, there

was no evidence for changes in the DNA duplex structure or dynamics upon binding to the dendrimer. This study immediately raised the question of whether a similar exchange mechanism might apply for RNA/polymer polyplexes, as despite having an overall similar structure, DNA and RNA differ significantly in their local structure and dynamics (Figure 1.1). A double stranded DNA helix typically adopts a B-form whereas a double stranded RNA helix adopts A-form configuration. Not only these two forms have different strctural parameters, they also differ in inherent flexibility and base-pair dynamics. DNA B-form helix is more locally flexible than RNA A-form helices. In addition, naturally occuring RNA molecules can form alternative secondary structures that contain A-form helices as well as non-canonical motifs such as bulges and apical loops. RNA and DNA also have distinct dynamic properties. Such motifs in RNA can give rise to complex dynamics, including local motions in junctions such as bulges and collective motions of helical domains across these junctions.[17,18]

We use 2D NMR spectroscopy to characterize the interaction between a $^{13}C/^{15}N$ isotopically enriched model RNA system, the 29-nucleotide transactivation response element (TAR) from the human immunodeficiency virus type 1 (HIV-1)[19] and G5-PEG.[15] TAR is one of the key regulatory RNA elements in the HIV-1 viral genome which plays essential roles in viral replication. Although there has been interest in studying TAR/PAMAM dendrimer interactions in the context of Tat-TAR inhibition,[20,21] here we focus on using TAR as a model flexible RNA system[22-25] that contains non-canonical secondary structural elements, including a 3-nucleotide bulge and 6-nucleotide apical loop. G5-PEG has several advantages for NMR-based studies of polyplex. The G5 PAMAM scaffold is structurally well-defined, has a fairly narrow molecular weight distribution, and is well characterized in terms of NMR spectral properties.[26-31] The 10% PEGylation gives G5 PAMAM excellent biological properties. The structure of PEG-modified poly(ethylene imines) influences biodistribution and pharmacokinetics of their complexes. Moreover, it provides convenient aqueous solubility properties for NMR experiments.[15]

We report exchange and dynamic properties of HIV-1 TAR/G5-PEG polyplexes formed across a range of N:P ratios. Using a combination of solution state 1D and 2D NMR spectroscopy, including ^{13}C

spin relaxation based dynamics measurements, DLS, and fluorescence spectroscopy, we show that the free RNA exists in rapid exchange with polyplex particles in the smaller size range ~12-40 nm that are detectable by NMR and larger particles in the size range ~140-200 nm that are NMR 'invisible'. Interestingly, we find that interactions with the dendrimer results in negligible changes in the structure and dynamics of RNA that is in rapid exchange with smaller polyplex particles, although we cannot rule out changes that might occur in larger particles not observed in the NMR experiments.

2.1.1 Experimental

2.1.1.1 Materials

Sodium chloride (NaCl), sodium dihydrogen phosphate (NaH_2PO_4), ethylenediamine tetraacetic acid (EDTA), 0.1 N hydrochloric acid (HCl), tris (hydroxymethyl)-aminomethane, Triton-X, and methoxypoly(ethyleneglycol) tresylate (5000 MW; PEG 5000) were purchased from Sigma, St. Louis, MO. 99.96% deuterium oxide (D2O) was purchased from Cambridge Isotope Laboratories, Inc.. G5 PAMAM dendrimer was purchased from Dendritech Inc. (Midland, MI) and purified using published protocols.[30] HPLC purified TAR tagged with fluorescein at the 3' end was purchased from Dharmacon (Lafayette, CO).

2.1.1.2 RNA Synthesis and Purification

Unlabeled and uniformly $^{13}C/^{15}N$ labeled TAR was prepared by *in vitro* transcription using a dsDNA (Integrated DNA Technologies) template containing T7 promoter at 5'-end. T7 RNA polymerase (Takara Mirus Bio, Inc.) was used to transcribe the dsDNA sequence in the presence of unlabeled (SILANTES, ISOTEC, Inc.) or $^{13}C/^{15}N$ labeled (Cambridge Isotope Laboratories, Inc.) ribonucleotide triphosphates. The RNA was purified using 20% (w/v) denaturing polyacrylamide gel electrophoresis (PAGE) in 8 M urea and 1X TBE buffer followed by electroelution in 20 mM Tris (pH 8) buffer and ethanol precipitation. The purified RNA pellet was redissolved in Tris buffer and exchanged into NMR buffer (15 mM sodium phosphate, 25 mM sodium chloride, 0.1 mM EDTA, pH 7.4) using a centricon

ultracell YM-3 concentrator (Millipore Corp.). The concentration of RNA was measured by optical absorption using Nanodrop 2000 (Thermo Scientific) assuming an extinction coefficient of 268900 L/M.

2.1.1.3 PEGylation of G5 PAMAM Dendrimer

G5 PAMAM dendrimer (0.0624 g, 2.22 x 10^{-6} mol, 1 equiv.) was dissolved in 4.0 mL of 1X PBS in a 50 mL round bottom flask. In a vial, 5,000 MW PEG tresylate (0.128 g, 2.6x10^{-5} mol, 12 equiv.) was dissolved in 2.0 mL of 1X PBS. PEG solution was added to dendrimer solution dropwise and stirred for 4 days at room temperature. The resulting conjugate was purified by 8 rounds of dialysis (first 2 rounds 2 hours each, the rest 4 hours each) in 4 L of water using 30,000-MW cutoff dialysis tubing. Solvent was removed using lyophilization yielding a puffy white solid. The yield was 0.169 g. The purified and lyophilized product was analyzed by MALDI, which gave average molecular weight of 85239 g/mol corresponding to an average of 12 PEG-5000 per dendrimer. From potentiometric titration, the number of primary amines was determined to be 101 per dendrimer.

2.1.1.4 Dynamic Light Scattering

Polyplexes of TAR/G5-PEG were prepared at the same concentration, buffer, and salt conditions as NMR experiments at N:P ratios 0, 0.25, 1, and 5 (at TAR concentration of 200 μM) and incubated for at least 30 min before measurements were recorded. The hydrodynamic diameter was measured at room temperature using Malvern Zetasizer Nano ZS (Worchestershire, United Kingdom). Three rounds of measurements were performed for each sample, with the diameter obtained in each round being an average of at least 6-10 measurements with duration of 40 s. Standard deviation was obtained by averaging the width of each peak obtained from the three rounds of measurements. The dispersant viscosity and refractive index were assumed to be that of water (cP 0.8872 and 1.33, respectively) whereas the material refractive index was assumed to be that of a standard protein sample (1.59). Since the intensity distribution showed multiple peaks (polydisperse sample, polydispersity index (PDI) > 0.1), we report intensity average and number average diameters separately instead of the commonly used Z-average size.

2.1.1.5 NMR Experiments

All NMR experiments were carried out on a 600 MHz Bruker instrument equipped with a 5 mm triple-resonance cryogenic probe at a temperature of 37°C. The buffer used was pH 7.4 NMR buffer (15 mM sodium phosphate, 25 mM NaCl, 0.01% EDTA). The spectra were processed and analyzed using NMRpipe software,[32] unless mentioned otherwise.

2.1.1.6 1D ^{1}H NMR Titrations.

200 μM TAR (^{13}C/^{15}N labeled or unlabeled) in NMR buffer was lyophilized and suspended in D_2O twice to minimize ^{1}H-based signals, including those from exchangeable amide protons that overlap in chemical shift with aromatic RNA signals of interest. Increasing volumes of 4 mM G5-PEG (NMR buffer, lyophilized and resuspended in D_2O twice) was added to the TAR sample resulting in increasing N:P ratios (0, 0.17, 0.25, 0.5, 1.0, and 5.0). 1D ^{1}H NMR spectra were acquired with or without ^{13}C/^{15}N decoupling during acquisition for labeled or unlabeled RNA respectively following each G5-PEG addition. The spectra were collected using excitation sculpting water suppression schemes. For 1D ^{1}H NMR titration of TAR into G5-PEG, 5 μM G5-PEG was titrated to decreasing N:P ratios (4, 3, 2, 0.5, and 0.25) by adding increasing volumes of 1 mM TAR in NMR buffer.

2.1.1.7 ^{1}H CPMG Relaxation Dispersion.

^{1}H NMR titration of G5-PEG into 200 μM unlabeled TAR to increasing N:P ratios (0, 0.25, 0.5, and 1.0) was performed as mentioned above. For each titration point, effective "transverse" relaxation rates ($R_{2,effective}$) were measured using 1D Carr-Purcell-Meiboom-Gill (CPMG) experiments.[15,33,34] CPMG relaxation dispersion experiments can be used to access the contribution of chemical exchange to $R_{2,effective}$ in the ms-μs timescale. In this experiment a series of 180° pulses that refocus the observed spins are applied with variable time interval between two 180° pulses. While longer time interval (low CPMG field strength) allows for observation of chemical exchange in the $R_{2,effective}$ values, short time interval (high CPMG field strength) suppress contribution to $R_{2,effective}$ from chemical exchange. How the chemical exchange contribution to $R_{2,effective}$ varies with the CPMG field strength, is termed relaxation dispersion. For the dispersion experiments herewith, three CPMG field strengths, ν_{CPMG} ($\nu_{CPMG} = 1/2\tau_{cp}$

in Hz, where τ_{cp} is the interval between two 180° proton pulses during the CPMG element); 625 Hz (τ_{cp} = 0.8 ms), 250 Hz (τ_{cp} = 2.0 ms), and 125 Hz (τ_{cp} = 4.0 ms) were used. For each CPMG field strength, the $R_{2,effective}$ rates were obtained from monoexponential fitting of integrated areas of resonances obtained at each of the following 14 delay series with two duplicate measurements for error estimation; [1, 10, 20 (x2), 30, 40, 60, 80, 100, 120, 140, 160 (x2), 200 ms] at 625 Hz, [1, 6, 12, 18, 24, 30 (x2), 42, 48, 54, 60, 70 (x2), 80 ms] at 250 Hz, [1, 2, 4 (x2), 6, 8, 12, 16, 20, 24, 28, 32 (x2), 40 ms] at 125 Hz for N:P 0; [1, 8 (x2), 16, 24, 32, 40, 60, 80, 100, 120, 140 (x2), 160 ms] at 625 Hz, [1, 6 (x2), 12, 18, 24, 30, 36, 42, 48, 54, 60 (x2), 64 ms] at 250 Hz, [1, 4 (x2), 6, 8, 10, 12, 14, 16, 18, 20, 26 (x2), 32 ms] at 125 Hz for N:P 0.25; [1, 6 (x2), 12, 18, 24, 30, 36, 40, 50, 60 (x2), 70, 80 ms] at 625 Hz, [1, 4 (x2), 6, 8, 10, 12, 14, 16, 18, 20, 26 (x2), 32 ms] at 250 Hz, [1, 2, 4 (x2), 5, 7, 6, 8, 9, 10, 12 (x2), 14, 16 ms] at 125 Hz for N:P 0.5; [1 (x2), 2, 4, 6, 8, 10, 12, 14, 16, 18 (x2), 24, 30 ms] at 625 Hz, [1, 2 (x2), 3, 4, 5, 6, 7, 8, 9, 10 (x2), 11, 12 ms] at 250 Hz, [1 (x2), 2 (x3), 3 (x2), 4 (x3), 5 (x2), 6 (x2) ms] at 125 Hz for N:P 1. Spectra were processed and analyzed using mNova software (Mestrelab research) to obtain integrated area. The regions 6.6-9.0 ppm (for H2/H6/H8) and 5.1-6.3 ppm (for H5/H1') were integrated separately. The integrated area versus relaxation delay times were fitted to a monoexponential decay using Origin Software (Origin Corporation) to obtain $R_{2,effective}$. To estimate $R_{2,polyplex}$ values, the $R_{2,effective}$ values measured at the highest field strength (ν_{CPMG} = 625 Hz) for different N:P ratios were globally fit to eq. 1[15] employing a nonlinear regression algorithm using an in house python script. The fits were obtained using random initial values of each parameter using the constraints $0 \leq f_{ree} \leq 1$; $0 \leq R_{2,polyplex} \leq 500$.

2.1.1.8 2D ^{1}H-^{13}C HSQC

2D ^{1}H-^{13}C spectra were obtained for the same samples used in ^{1}H NMR titrations at N:P of 0, 0.17, 0.25, 0.5, and 1.0. Spectra were processed using NMRpipe[32] and Sparky 3 NMR Assignment and Integration Software (University of California, San Francisco).

2.1.1.9 Measurement of ^{13}C R_1 and R_2 Relaxation Rates

^{13}C "longitudinal" relaxation rate constant (R_1) and "transverse" relaxation rate constant (R_2) were measured for the same samples used in ^{1}H NMR and HSQC titrations at N:P of 0 and 0.25 using 2D R_1

and $R_{1\rho}$ relaxation experiments[23] for base C2, C6, and C8 and sugar C1' carbons. To maintain adequate signal to noise ratio, we carried out ^{13}C R_2/R_1 relaxation at low dendrimer concentration (N:P of 0.25). The $R_{1\rho}$ relaxation experiment was carried out using a 3.5 kHz spin-lock field strength and a spin-lock carrier centered at aromatic C6 (for C2, C6, and C8) or sugar C1' resonances. The spin-lock power was sufficiently high to suppress undesired chemical exchange (R_{ex}) contributions. For N:P 0, relaxation data were collected using the delay series [10, 55, 140, 250 (x3) ms] for R_1 and [4, 16, 32, 48 (x3) ms] for $R_{1\rho}$, with triplicate measurements for error estimation for aromatic (C2, C6, and C8) carbons and [20, 140 (x2), 280, and 580 (x2) ms] for R_1 and [0.4, 8.4, 24.4 (x2), and 48.4 (x2) ms] for $R_{1\rho}$, with two duplicate measurements for error estimation for sugar C1' carbons. For N:P 0.25, the delay series [10, 140 (x2), 280, and 480 (x2) ms] for R_1 and [0.4, 8.4 (x2), 16.4, and 28.4 (x2) ms] for $R_{1\rho}$, with two duplicate measurements for error estimation, was used for both aromatic (C2,C6,C8) and sugar (C1') carbons. The spectra were processed with NMRPipe[32] and relaxation rate constants determined by fitting the resonance intensities to monoexponential decays using Mathematica 6.0 (Wolfram Research, Inc.). The R_2 values were calculated from the relationship $R_{1\rho} = R_1 \cos^2\theta + R_2 \sin^2\theta$ where θ = arctan (spinlock power/ resonance offset).

2.1.1.10 Calculation of Observed Polyplex Hydrodynamic Diameter using ^{1}H NMR Relaxation Data

^{1}H $R_{2,polyplex}$ values were used to calculate the rotational correlation time (τ_m) of the polyplex. For a X-H group, R_2 relaxation rates are dependent on a linear combination of spectral density functions evaluated at five frequencies, J(0), J(ω_H), J(ω_X), J($\omega_X + \omega_H$), and J($\omega_X - \omega_H$), where ω_H and ω_X are the frequencies of H and X nuclei respectively at a given spectrometer field.[35] Assuming that dipole-dipole coupling dominates ^{1}H R_2 relaxation due to directly bonded carbon as well as neighboring protons within 4 Å, $R_{2,polyplex}$ was expressed as a sum of R_2 relaxation rates[15,23,36]

$$R_{2,polyplex}{}^{H} = \sum \frac{1}{8} d^2 [4J(0) + 3J(\omega_H) + J(\omega_X - \omega_H) + 6J(\omega_X) + 6J(\omega_X + \omega_H)] \quad (2.1)$$

where d is the dipolar coupling constant given by

$$d = \frac{\mu_0 \gamma_H \gamma_X h}{8\pi^2 \langle r^3{}_{HX} \rangle} \quad (2.2)$$

μ_0 is the permittivity of free space, γ_H and γ_C are the magnetogyric ratios of ^{1}H and ^{13}C respectively and h is the Plank's constant. r_{HC} is the distance of the aromatic and sugar protons to their directly bonded carbon (1.104 Å and 1.115 Å for base C-H bond and sugar C1'-H1' bond respectively) and r_{HH} are the distances to neighboring protons within 4 Å. These distances were obtained from the solution NMR structure of free TAR (protein structure database ID: 1ANR).[37] J(ω) as defined by the "simplified" model-free formalism for isotropic overall tumbling.[35]

$$J(\omega) = \frac{2}{5}\left(\frac{S^2 \tau_m}{1 + (\omega\tau_m)^2}\right) \quad (2.3)$$

where S^2 is the generalized order parameter. An average of residue specific S^2 values (0.763 and 0.809 for H2/H6/H8 and H5/H1' respectively) previously published[23] for elongated UUCG-TAR based on ^{13}C relaxation data was used. Assuming spherical shape, polyplex hydrodynamic diameter (D) was computed using Stokes-Einstein equation for the range of τ_m values obtained from ^{1}H relaxation data.

$$R = \left(\frac{3k_B T \tau_m}{4\pi\eta}\right)^{1/3} \quad (2.4)$$

where R = D/2 is the radius of a sphere. k_B is the Boltzman's constant, T is temperature, η is the viscosity of the solvent at temperature T.

2.1.1.11 Calculation of Observed Polyplex Hydrodynamic Diameter using ^{13}C Relaxation Data

Residue specific ^{13}C $R_{2,polyplex}$ were obtained using ^{13}C R_2 values in eq. 1 where p_{free} and p_{bound} values were obtained from analysis of ^{1}H relaxation at N:P of 0.25 (Table 1). Since chemical shift anisotropy (CSA) also significantly contributes to carbon relaxation, $R_{2,polyplex}$ was obtained as a sum of contribution due to dipole-dipole coupling and CSA as given by[23,36]

$$R_{2,polyplex}{}^{C} = \frac{1}{8} d^2 [4J(0) + 3J(\omega_C) + J(\omega_H - \omega_C) + 6J(\omega_H) + 6J(\omega_H + \omega_C)] + \frac{1}{18}(CSA \times 10^{-6} \times \omega_C)^2 (4J(0) + 3J(\omega_C)) \quad (2.5)$$

where *d* and J(ω) are as defined earlier and CSA = 134.3 ppm, 178.8 ppm, 149.9 ppm, 40 ppm for C8, C6, C2, and C1' respectively.[36,38] Residue specific S^2 values (ranging from 0.43 to 0.93) were used in the J(ω) expression.[23] Assuming spherical shape, polyplex hydrodynamic diameter was obtained using the Stokes-Einstein equation as mentioned above.

2.1.1.12 Fluorescence Quenching Based Competition Assay

TAR with 3' end tagged with fluorescein was employed for the fluorescence quenching based assay. The RNA was annealed by heating to 95°C for 5 min and then cooled on ice for an hour prior to use. The RNA was diluted in pH 7.4 fluorescence assay buffer (50 mM Tris-HCl, 50 mM KCl, 0.01% Trition-X). The G5-PEG was dissolved in the assay buffer and serially diluted to obtain aliquots of concentrations from 2 nM to 2000 nM. 100 nM TAR was incubated for 30 min in 1:1 volume with varying concentrations of the G5-PEG in a 384-well plate such that the final RNA concentration in each well was 50 nM and the N:P ratios varied from 0 to 28. Fluorescence intensities were measured in triplicates using an Omega star plate reader (BMG Labtech) with a 485 nm excitation and 520 nm detection. For the exchange assay, to selected N:P ratio sample wells, 0.3 μL of 500 μM untagged TAR was added and the resulting fluorescence intensity was measured in a similar fashion after 30 min incubation. The assay was also repeated for N:P points 1, 10, and 70 within 2 min of adding untagged TAR.

2.1.2 Results and Discussion

2.1.2.1 DLS Provides Evidence for a Major (~12-40 nm) and Minor (~140-200 nm) Polyplex Particles

We initially used DLS to characterize the size of TAR/G5-PEG polyplex particles formed at different N:P ratios. The hydrodynamic diameter obtained using cumulants based intensity mean (Z-average diameter),[39] which is the commonly used method to obtain particle size from light scattering data, yielded values of ~67-170 nm consistent with literature reported values for dendrimer based polyplex systems.[4,15,16,40] However, the polydispersity index (PDI), which reports on the homogeneity of the sample with respect to particle sizes was high (0.27-0.37) and peaks in the range of ~12-40 nm were also observed (S I). Since the Z-average diameter gives good description of size only for unimodal

distribution with narrow polydispersity (PDI < 0.1),[39] we also examined the intensity weighting by the number of particles (number average distribution) assuming that the conversion from intensity to number holds for our measurements (Figure 2.1 a). The number average analysis indicates that particles of ~12-34 nm size range are the major species in the population. The number average diameter increases from N:P of 0.25 to 1 and only slightly decreases at N:P of 5. Interestingly, such small polyplex sizes haven't been reported previously for similar polyplex systems using DLS. For example, DLS data previously reported for siRNA/G5-PEG polyplexes in tris-HCL buffer at N:P of 10 gave a diameter of ~100 nm based on Z-average analysis.[16] This could be due to different sample conditions or due to differences in size estimates obtained from Z-average versus number average analysis. Furthermore, it is known that larger particles scatter more light compared to smaller particles causing the average diameter obtained by DLS to be biased towards larger particles present in the solution.[39] Although DLS reported sizes are usually in the larger size range (> 50 nm), there have been reports of smaller sizes for unPEGylated PAMAM/ siRNA polyplexes using TEM and AFM (15-130 nm)[4] and nanoparticle tracking analysis (NTA) (10-80 nm).[41] Although the DLS experiments were carried out at room temperature compared to the NMR experiments at 37^{o}C (described below) which can affect the equilibrium populations, the sizes obtained by DLS are consistent with size estimates (~7.5-15 nm) from our NMR results.

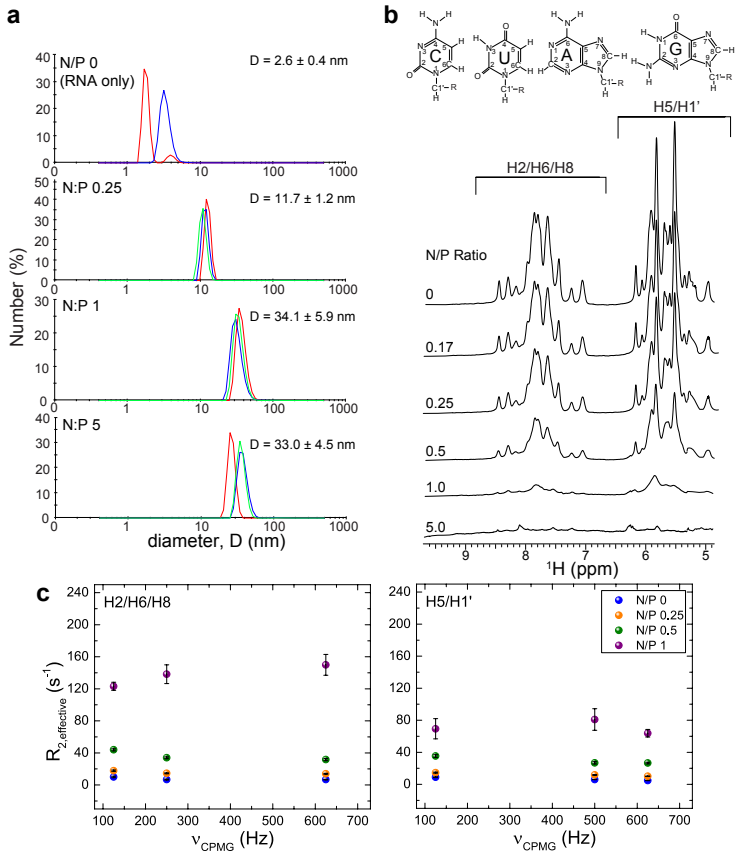

Figure 2.1 TAR exists in rapid exchange between free and polyplex-bound species. (a) DLS measurements of polyplex samples at N:P ratios 0 to 5 at NMR concentrations (200 μM TAR) showing presence of ~12-34 nm polyplexes. Data is presented as number average diameter. Overlay of three peaks in the same graph indicates triplicate measurements. Only two measurements were collected for N:P 0. The diameter of G5-PEG only was previously published to be 5.9 nm.[31] (b) Stacked overlay of ^{1}H NMR spectra (aromatic H2/H6/H8, sugar H1', and aromatic H5 region) of 200 μM TAR titrated to increasing N:P ratios with G5-PEG at 37°C in pH 7.4 NMR buffer (15mM sodium phosphate, 25mM NaCl, 0.01% EDTA) exchanged to 99.99% D_2O (c) $R_{2,effective}$ as a function of different CPMG fields in Hz for N:P ratios 0, 0.25, 0.5, and 1 measured independently for H2/H6/H8 and H5/H1' protons.

2.1.2.2 TAR Exists in Rapid Exchange (< ms) between Free and Polyplex-Bound Particles

1D ^{1}H NMR titrations of G5-PEG into a solution of unlabeled TAR showed gradual line broadening of TAR resonances without significant changes in the TAR chemical shifts (Figure 2.1 b). The line broadening indicates that TAR is interacting with G5-PEG but the lack of significant chemical shift

perturbations suggests that the interaction does not significantly affect the structural and dynamic properties of TAR. This is striking considering that TAR is a highly flexible molecule[24,42-44] and that chemical shift perturbations are observed when varying salt concentrations,[45] upon addition of DMSO,[46] and a wide variety of ligands that bind to TAR non-specifically.[22,47]

Analysis of the spectra did not reveal evidence for free RNA with sharp narrow lines, as would be expected if small and large species with similar chemical shifts exchange at slow timescales. The line broadening could arise due to microsecond-to-millisecond chemical exchange, which results in an exchange contribution (R_{ex}) to the observed effective "transverse" relaxation rate constant ($R_{2,effective} = R_2 + R_{ex}$, where R_2 is the intrinsic "transverse" relaxation rate constant). The exchange could represent transitions between free and bound RNA and/or changes in the RNA conformation in the bound state. Chemical exchange with a small particle can cause significant line broadening if there were significant differences in chemical shifts of free and bound state. For a low population of such a bound state, if the chemical shift difference is large enough, and on the slow to intermediate timescales, then the line broadening could be significant without inducing a change in the observed RNA chemical shift.

To assess R_{ex} contributions, we carried out ^{1}H Carr-Purcell-Meiboom-Gill (CPMG)[33,34] relaxation dispersion experiments (Figure 2.1 c) on polyplexes of unlabeled TAR and G5-PEG using an approach similar to that described previously for DNA.[15] In this experiment, $R_{2,effective}$ is measured during a relaxation period as a function of a time interval (τ_{cp}) between successive 180° refocusing pulses which serve to suppress the R_{ex} chemical exchange contribution. We relied on ^{1}H CPMG experiment rather than ^{13}C CPMG dispersion due to poor sensitivity in 2D ^{1}H-^{13}C HSQC spectra beyond N:P of 0.25. The regions of the ^{1}H NMR spectra representing H2/H6/H8 aromatic protons (6.6-9.0 ppm) and aromatic H5 and sugar H1' protons (5.1-6.3 ppm) were integrated separately and $R_{2,effective}$ values were obtained from monoexponential decay fits of the integrated area versus decay times (Appendix A, S II). $R_{2,effective}$ values were measured for various τ_{cp} delays and for N:P ratios of 0, 0.25, 0.5, and 1. We observed an increase in measured $R_{2,effective}$ with increasing N:P ratios even when using a short τ_{cp} delay of 0.8 ms to maximally suppress R_{ex} contributions. Increasing the N:P ratio from 0 to 1 resulted in an increase in

$R_{2,effective}$ from 6.7 ± 0.4 s^{-1} to 150 ± 13 s^{-1} for H2/H6/H8 and 4.7 ± 0.1 s^{-1} at N:P of 0 to 63.8 ± 4.7 s^{-1} at N:P of 1 for H5/H1'. These values are comparable to that reported previously published for DNA/G5-PEG where $R_{2,effective}$ also increased by ~20 fold from 8.1 ± 0.2 s^{-1} at N:P 0 to 135.6 ± 14.5 s^{-1} at N:P of 1 for H2/H6/H8 and 8.7 ± 0.4 s^{-1} at N:P 0 to 162.7 ± 13.5 s^{-1} at N:P 1.[33] The measured $R_{2,effective}$ values showed much smaller (< 10 Hz) variations when varying the τ_{cp} delay and carrying out the CPMG experiments at three field strengths (ν_{CPMG} = 625 Hz, 250 Hz, and 125 Hz) (Figure 2.1 c). These data indicate that the increase in line broadening and $R_{2,effective}$ is not principally due to an exchange contribution in the intermediate time scale but rather due to rapid exchange of the RNA with large polyplex particles which results in an increase in the intrinsic R_2 as reported previously for DNA polyplexes.[15] Indeed, the $R_{2,effective}$ values increase as the amount of dendrimer increases suggesting rapid exchange with polyplex particles growing in size (at least up to the N:P ratios probed by the experiment). This is consistent with DLS data that also showed an increase in the number average size from N:P of 0.25 to 1. We were, however, unable to measure $R_{2,effective}$ for N:P of 5 due to severe line broadening.

To estimate the $R_{2,effective}$ values for the polyplex-bound form, the $R_{2,effective}$ values measured at the highest CPMG field strength for different N:P ratios were globally fit to (2.6),[15]

$$R_{2,effective} = p_{free}R_{2,free} + p_{bound}R_{2,polyplex} \quad \textbf{(2.6)}$$

where, p_{bound} describes the fraction of RNA bound in the small-sized polyplexes in fast exchange with free RNA, and $p_{free} + p_{bound} = 1$. $R_{2,free}$ and $R_{2,polyplex}$ are the $R_{2,effective}$ rates for free RNA and RNA bound to small-sized polyplexes respectively. The large ~140-200 nm particles observed by DLS are likely in slow exchange which do not contribute to the observed $R_{2,effective}$ values. This equation expresses $R_{2,effective}$ as a population weighted average for free and polyplex-bound species assuming a two-state binding equilibrium for a fast exchange scenario where the chemical exchange rate constant ($k_{ex} = k_1 + k_{-1}$, where k_1 and k_{-1} are forward and backward rates respectively) is much larger than $2\pi \times \Delta\omega$ (where $\Delta\omega = \omega_{polyplex} - \omega_{free}$ is the chemical shift difference between free and bound species). The fits were obtained using random initial values of each parameter using the constraints $0 \leq p_{free} \leq 1$; $0 \leq R_{2,polyplex} \leq$

500. The $R_{2,polyplex}$ values (Table 3) obtained from the two-state fit are similar to those reported previously for DNA.[15]

Table 3 Exchange parameters obtained from global fitting of relaxation data using eq. 1 (see main text) for H2/H6/H8 (6.6-9.0 ppm) and H5/H1' (5.1-6.3 ppm). $p_{free} = 1 - p_{bound}$ where p_{bound} is the fraction of RNA bound in the small-sized polyplexes in fast exchange with free RNA.

N:P	p_{free}	$R_{2,polyplex}$ (s^{-1}) (H2/H6/H8)	$R_{2,polyplex}$ (s^{-1}) (H5/H1')
0	1		
0.25	0.97 ± 0.02	311 ± 111	236 ± 84
0.50	0.89 ± 0.06		
1.0	0.64 ± 0.21		

Based on the estimated value of $R_{2,polyplex}$, we can estimate the rate of exchange (k_{ex}) to be greater than $R_{2,polyplex} - R_{2,free}$ ~304 s^{-1} for H2/H6/H8 and ~231 s^{-1} for H5/H1'. The largest $\Delta\omega$ observed in the proton dimension observed in 2D ^{1}H-^{13}C HSQC spectra described below was ~0.08 ppm (~300 rad s^{-1} at 600 MHz spectrometer field). Therefore, for all chemical shift differences smaller than this the k_{ex} will be greater placing the system in fast exchange.

We employed the fitted $R_{2,polyplex}$ values to calculate approximate hydrodynamic diameter for the polyplex particles. Under the assumptions of isotropic tumbling with internal motions being much smaller than overall tumbling, and that dipole-dipole coupling dominates the "transverse" relaxation rate, the overall rotational correlation times obtained (see materials and method) were estimated to be ~36-240 ns. Assuming spherical shape, this corresponds to hydrodynamic diameter in the range 7.5-14 nm consistent with previously reported values for DNA polyplexes.[15] Using the population of free and bound at N:P of 0.25 from the two state fit of ^{1}H relaxation data shown in Table 3, ^{13}C $R_{2,polyplex}$ values were also calculated using residue specific ^{13}C relaxation data as a cross-validation (see experimental section). Despite a number of approximations employed, these values are close to number average size of the polyplexes (~12-40 nm) as measured by DLS.

It should be noted that in addition to line broadening, we observe a significant reduction in the integrated area of the ^{1}H NMR resonances with increasing N:P ratios. Even though this decrease in intensity could result due to relaxation during the experiment itself, we cannot rule out some degree of exchange with much larger particles such as the ~140-200 nm particles observed by DLS that are not directly observable by NMR.[48] A similar decrease in resonance signals was reported in the previous study[15] with 20-bp DNA duplex which was attributed to the small polyplexes in equilibrium with larger NMR 'invisible' particles.

2.1.2.3 Insights into RNA-Dendrimer Interactions from 2D NMR Chemical Shift Mapping Experiment

Previous studies relied primarily on ^{1}H NMR experiments to examine the impact of dendrimer binding on DNA structure.[15] These experiments did not allow for characterization of any structural and dynamic perturbations with site-specific resolution. Here, we used uniformly ^{13}C/^{15}N labeled TAR and 2D ^{1}H-^{13}C HSQC experiments to analyze TAR G5-PEG interactions and the effects on TAR structure and dynamics with site-specific resolution. The ability to measure ^{13}C and ^{15}N chemical shifts provides additional probes of structure and dynamics. Prior studies have shown that the TAR 2D ^{1}H-^{13}C HSQC spectra are very sensitive to changes in physicochemical conditions, including salt,[45] pH,[49] and presence of a wide range of added ligands.[46,47,50] This chemical shift sensitivity is a result of TAR's high degree of conformational flexibility and high susceptibility to structural and dynamic perturbations due to environmental cues. Remarkably, despite high susceptibility to chemical shift perturbations, we observed little change in the 2D ^{1}H-^{13}C HSQC spectra of TAR following the addition of dendrimer resulting in N:P ratio up to a value of 1. The only significant perturbations observed were for the flexible bulge residues U23 and C24, and the flexible apical loop residue A35 (Figure 2.2). These perturbations including other small chemical shift changes in both ^{1}H and ^{13}C dimensions are similar to those observed for TAR conformational changes induced by positively charged ions such as Na^{+} and Mg^{2+}.[45] At physiological pH, the terminal $–CH_2CH_2NH_2$ dendrimer surface is protonated yielding $–CH_2CH_2NH^{3+}$ end groups (up to ~101 per dendrimer molecule). These charged end groups of the dendrimer could be interacting with TAR in a manner similar to positively charged metal ions. In

addition to ^{1}H and ^{13}C chemical shifts, ^{15}N chemical shifts could also be used to obtain site-specific effects of dendrimer interaction, in particular on the base pairs. Such studies are intended to be carried out in future.

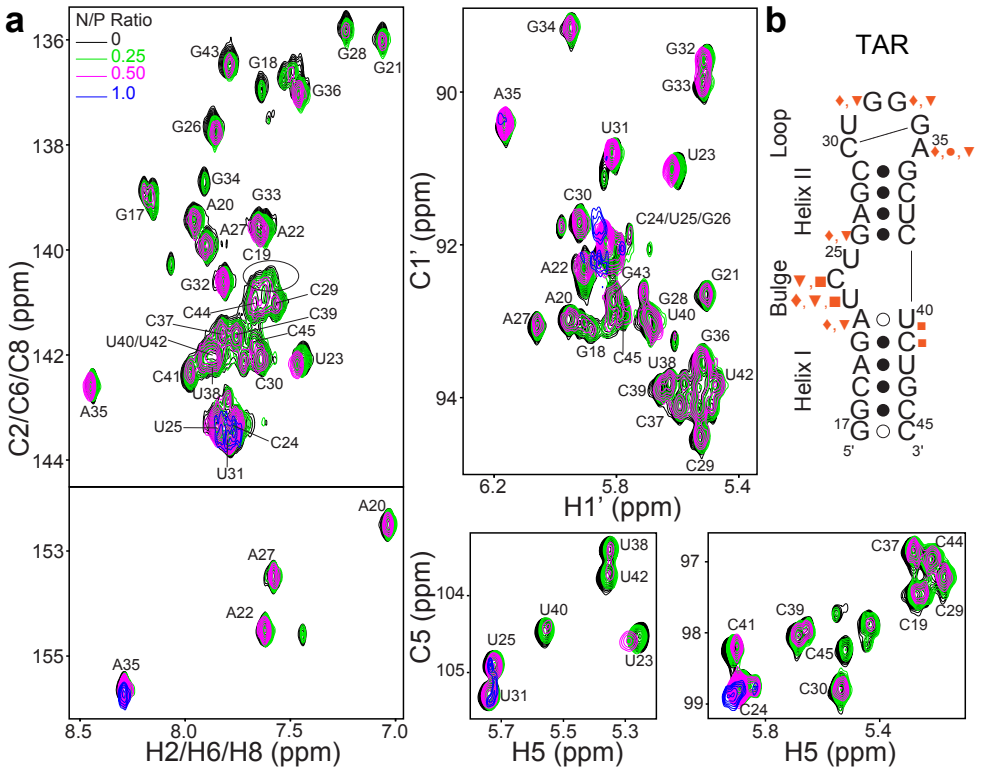

Figure 2.2 Effect of dendrimer interaction on RNA structure. (a) Overlay of 2D ^{13}C-^{1}H HSQC spectra of uniformly $^{13}C/^{15}N$ labeled 200 µM TAR titrated to increasing N:P ratios with G5-PEG at 37°C showing cross peaks for H2-C2/H6-C6/H8-C8, H1'-C1', and H5/C5 correlations. Spectra for N:P of 0.17 has been omitted for clarity (b) Secondary structure of TAR. Residues that show chemical shift perturbations are indicated by orange diamond, circle, triangle, and square symbols representing H8-C8, H2-C2, H1'-C1', and H5-C5 perturbations respectively. Larger symbol denotes greater magnitude of chemical shift perturbation.

2.1.2.4 Characterizing how Dendrimer Interactions affect RNA Dynamics

To more fully characterize the impact of dendrimer binding on the TAR dynamics we measured ^{13}C "longitudinal" relaxation rate (R_1) and "transverse" relaxation rates (R_2) values on the aromatic

(C2/C6/C8) and sugar (C1') carbons. The measured ^{13}C R_2/R_1 values for TAR in absence of dendrimer and at N:P ratio of 0.25 is shown in Figure 2.3 a. The R_2/R_1 ratio is widely used to estimate the overall correlation times as the ratio can be approximated to be independent of rapid internal motions.[36] The R_2/R_1 ratio is propotional to the overall correlation times which can be used to describe the relative flexibility of residues. The values obtained for free TAR are in agreement with previously published data.[23,24] In the presence of dendrimer, nearly all TAR residues show an increase in R_2/R_1, consistent with a slow-down in overall tumbling due to formation of small sized polyplex particles as indicated by ^{1}H NMR relaxation and DLS data. Although the overall tumbling of the RNA is slowed down, the bulge residues: U23, C24, U25 and the apical loop residues: U31, G32, G33, A35 retain lower R_2/R_1 values indicating that the RNA retains internal flexibility when bound to the small sized polyplexes. The correlation plot (Figure 2.3 b) of R_2/R_1 values at N:P of 0 vs N:P of 0.25 shows good aggrement indicating that the dynamic properties of TAR are not significantly affected upon interacting with dendrimers at this N:P ratio. The outlier points correspond to the terminal residue (C45) or near terminal residue (G18), which could be the most affected due to dendrimer interaction. Overall these results further support that despite interactions with the dendrimer that slow down overall tumbling, at this N:P ratio the RNA largely retains key elements of flexibility observed in the free state, including high flexibility at the bulge and apical loop.

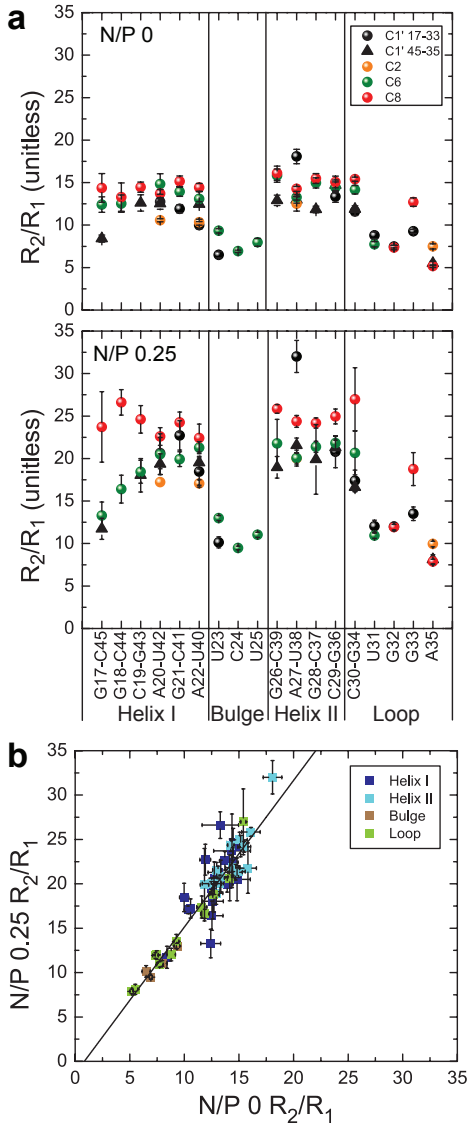

Figure 2.3 Examining impact of dendrimer interaction on TAR dynamics by ^{13}C spin relaxation (a) Ratio of ^{13}C "transverse" relaxation (R_2) to "longitudinal" relaxation (R_1) values (R_2/R_1) measured on TAR at N:P 0 and 0.25 plotted as a function of the nucleotide residue (as base-paired in the helices or unpaired in the bulge and apical loop). Values for different nuclei are denoted using different symbols and colors (b) Correlation of measured R_2/R_1 values at N:P 0 and 0.25.

To cross validate ^{1}H NMR relaxation based overall tumbling time/ hydrodynamic diameter, we employed eq. 1 to obtain ^{13}C $R_{2,polyplex}$ using p_{free} and p_{bound} values obtained from ^{1}H relaxation experiment for N:P of 0.25 (Table 3) and ^{13}C R_2 values. The ^{13}C $R_{2,polyplex}$ ranged from 460-840 s^{-1} for the

helical, non-terminal residues, and 140-670 s^{-1} for terminal, loop, and bulge residues for C2/C6/C8. For C1' carbons, the $R_{2,polyplex}$ values ranged from 380-680 s^{-1} for helical, non-terminal residues, and 180-450 s^{-1} for terminal, bulge, and loop residues. Overall tumbling times obtained using these ^{13}C $R_{2,polyplex}$ values (see experimental section) ranged bewteen ~80-280 ns. Assuming spherical shape and using Stokes-Einstein's relation[15] the diameter obtained was in the range ~10-15 nm. These values are close to the range obtained from ^{1}H relaxation (~7.5-14 nm).

2.1.2.5 Effect on Dendrimer Structure upon Polyplex Formation

MD simulations have shown that the flexibility of PAMAM dendrimers play a crucial role in the binding interactions with nucleic acids.[12] However, few atomic level experiments[13,15] have been used to provide insights into how the dendrimer structure is affected upon polyplex formation.[13,15] To this end, we performed 1D ^{1}H NMR titrations of 5 μM G5-PEG with increasing TAR concentrations (0-67 μM) resulting in decreasing N:P ratios from ∞ to 0.25 (Figure 2.4). These titrations were focused on the resonances belonging to G5-PEG. We observe no significant chemical shift perturbations on the proton signals (*a, b, c, d, e, f*) from the PAMAM framework[15] of G5-PEG or the PEG proton signals (*i, j, k*),[15,51] suggesting that the interaction with RNA doesn't significantly alter the polymer structure and dynamic flexibility. Although we do not observe large changes in chemical shift, the proton signals from the PAMAM framework broaden with decreasing N:P ratios. The proton signal *d*, assignable to the methylene group alpha to the tertiary amine of the PAMAM framework shows an unusual behaviour in which it initially broadens nearly out of detection as the N:P decreases, and then reappears as a broad signal at N:P < 2. This could reflect structural reorganization in the polyplex around this N:P ratio, which is also suggested by our fluorescence experiments described below. The overall broadening of the proton signals from the PAMAM framework is consistent with a dynamic equilibrium between free RNA and polyplex-bound RNA as observed from the RNA perspective. Pavan *et al.* also observed such broadening of PAMAM peaks of unPEGylated G5 PAMAM dendrimer upon complexation with siRNA at low N:P ratios.[13] By way of contrast, the PEG proton signals in our titration spectra remain sharp with integrated area and chemical shifts remaining essentially constant. This behavior is consistent with the

PEG arms of the dendrimer remaining highly flexible in the polyplex. Absence of broadening of the PEG proton peaks also suggests that broadening of both the PAMAM and RNA peaks is due to polyplex formation and broadening associated with slower tumbling of the larger particles and not due to overall viscosity changes.

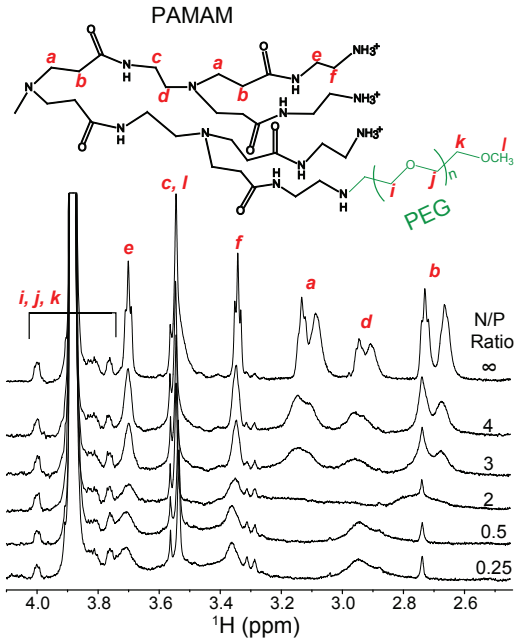

Figure 2.4 Effect of RNA interaction on the dendrimer. ^{1}H NMR spectra of 5 μM G5-PEG titrated with increasing concentrations of TAR to decreasing N:P ratios with assignments of ^{1}H NMR peaks of G5-PEG mapped onto its chemical structure shown above the NMR spectra. Peak assignments are based on previously published studies.[12,31] Peaks representing PAMAM framework of G5-PEG are broadened while PEG peaks remain sharp suggesting that the RNA is binding to the PAMAM part while the PEG arms remain flexible.

2.1.2.6 Competitive Exchange of Polyplex-Bound RNA Measured using Fluorescence

The NMR experiments indicate that the free RNA and DNA[15] exists in rapid exchange with polyplex-bound forms at N:P ≤ 1. Such a dynamic exchange behavior may help explain the mechanism by which polyplexes play a dual role of both protecting the nucleic acids from nuclease degradation as well as allowing for oligonucleotide release from the polyplexes that make it into the cells. A dynamic equilibrium between free and bound RNA does suggest that the time spent by the RNA in the free state

can allow for interaction with nucleases in the cell depending on the off-rate of the polyplex equilibrium and on-rate of nuclease binding equilibrium. However, a fast exchange would allow for the RNA to spend less time as 'free' and 'attackable' by nucleases. While we have not specifically tested nuclease activity in this work, reports in literature have suggested that association with polyplexes slows down but does not completely prevent degradation by nucleases in a N:P ratio dependent manner.[52,53] However, the NMR experiment is unable to probe what happens beyond N:P > 1 due to severe line broadening of the measured signals. To determine if RNA is still exchangeable at higher N:P ratios, we designed a fluorescence-based competition experiment (Figure 2.5). In the experiment, TAR containing a fluorescein tag on the 3' end (TAR-FL) was mixed with increasing concentrations of G5-PEG to obtain N:P ratios ranging from 0 to 28. The fluorescence intensity was measured at a wavelength of 520 nm for each of the N:P points. We observe that the fluorescence intensity of TAR-FL decreases as the concentration of G5-PEG increases up to N:P ratio of 2, after which the intensity recovers to about 55% of initial fluorescence, and finally levels off at higher N:P ratios. A possible explanation for the initial decrease in TAR-FL fluorescence is that due to polyplex formation, RNA molecules come in close proximity leading to dye-dye quenching.

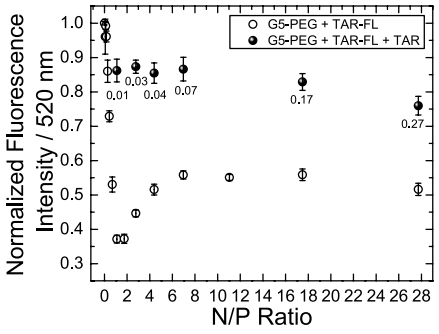

Figure 2.5 Fluorescence quenching based competitive displacement assay demonstrating release of fluorescein tagged TAR from polyplexes with G5-PEG. Open circles indicate fluorescence of polyplex mixture at different charge ratios before adding untagged TAR. Filled circles indicate fluorescence of the polyplex mixtures after adding untagged 0.3 µL of 500 µM TAR with numbers below the filled circles indicating resulting N:P ratios. The total concentration of tagged TAR in all N:P ratios was 50 nM. Buffer condition used is 50mM Tris-HCl, 50mM KCl, 0.01% Trition-X, pH 7.4.

An interesting feature of the fluorescence intensity binding curve is that the fluorescence recovers partially beyond ~N:P 2. Van Rompaey *et al.*[54] and Zheng *et al.*[55] have previously used similar fluorescence quenching assays to assess binding of other types of polycationic polymers with oligonucleotides. Zheng *et al.*[55] also observed similar recovery in an assay with Tye563-labeled siRNA and hyperbranched PEI, which they attributed to molecular reorganization of the polyplexes. Interestingly in our case, beyond N:P ratio 2 we also observe in our ^{1}H NMR titration spectra recovery of the resonance assigned to methylene group alpha to the tertiary amine of the PAMAM framework. This observation is consistent with molecular reorganization leading to conformational changes close to this region in the PAMAM framework. Increased electrostatic repulsion as more cationic polymer is added may causes an average increase in dye-dye distance. Increase in the volume of polyplex around these N:P points also may be a plausible explanation for partial reversal of fluorescence quenching. Beyond N:P of 6 the fluorescence intensity is constant. This is suggestive of no further changes in the structural organization of the polyplex particle. These results are consistent with the DLS results in which the number average size increases up to N:P 1 and remains more or less constant at N:P of 5.

Next we used this assay to test whether the RNA bound at N:P ratios greater than 1:1 remains exchangeable. Our prediction was if the RNA is exchangeable, it would be possible to rapidly recover the fluorescence intensity observed at low N:P ratios by simple addition of untagged TAR. Excess of untagged TAR was added to the preformed polyplex mixture at each N:P ratio described above and the resulting fluorescence intensity was measured. In all cases, addition of excess untagged TAR resulted in recovery of TAR-FL fluorescence intensity within < 30 min. For selected N:P ratios (1, 10, and 70) the fluorescence intensity was re-measured within 2 min of adding untagged TAR (Appendix A, S I). The fluorescence intensity was also recovered in this case. Adding excess RNA introduces competition of binding; however, this condition also provides a model for the competition with other biomolecules when polyplex is introduced to cell culture or an organism. These data indicate that at N:P ratios > 1:1, which are not probed by NMR, the polyplex RNA remains exchangeable and that this process is rapid on the fluorescence experiment time scale (< 2 min).

2.1.2.7 *Comparison with Prior DNA Study*

Overall, the exchange behaviour observed for polyplexes of TAR/G5-PEG is similar to that observed previously for 20-bp DNA/G5-PEG polyplexes,[15] i.e. the exchange is rapid on the NMR timescale. Similar $R_{2,polyplex}$ values were obtained in both studies indicating presence of similar sized particles (~8-15 nm). However, we did observe differences in the ^{1}H NMR spectra. In studies of DNA, the nucleic acid resonances broaden with increasing N:P ratio and are nearly undetectable at N:P ratio of 1. However, they reappear at N:P ratio of 5 either due to release of the DNA or increased local dynamics at the pico-nanosecond timescale. However, for the RNA polyplexes, peaks did not reappear beyond N:P of 1. Although it is difficult to hypothesize the origin of differences between RNA and DNA at these N:P ratios, there are some literature evidences suggesting local structural differences may exist between RNA and DNA polyplexes. For example, as the closest comparison, CD spectra of polyplexes of PEGylated PAMAM G4 and a double stranded RNA showed little changes at N:P of 5 and above whereas polyplexes with a 20-nucleotide antisense DNA showed significant spectral changes at same N:P ratios, suggesting conformational changes in the antisense DNA.[6]

As for the DLS measurements on the DNA polyplexes, a bimodal distribution was observed only for N:P ratio of 0.25 based on intensity where the second peak was observed ~8-20 nm. A unimodal distribution was observed for higher N:P ratios with the intensity average diameter ~60 nm. For the RNA, particles in the size range ~12-40 nm were observed for all N:P charge ratios in addition to ~140-200 nm particles. In addition, number average analysis indicated the smaller size particles represented the majority population. Overall, both studies suggest the presence of small sized polyplexes as well as the larger particles in the more commonly reported size range in exchange with free RNA.

2.1.2.8 *Proposed Model of Exchange in the Polyplex System of RNA and Dendrimer*

Combining results from NMR, DLS, and fluorescence experiments, we can propose a model for dynamic exchange illustrated in Scheme 2-I. The scheme shows smaller polyplexes in rapid exchange with free RNA as indicated by NMR line broadening without chemical shift perturbations. We hypothesize that this intrinsic rapid exchange in the polyplex could provide a mechanism for RNA

release and protection from nuclease degradation. It is also conceivable that these dynamics affect interaction with other biomolecules in the cell such as plasma membrane components, and intracellular RNA, lipids, and proteins. For example, our recent study has shown that in polyplex treated cells the induced plasma membrane current is the same value as obtained for POCP-treated cell alone and persists even after the cells were allowed to recover by rapidly exchanging with POCP-free ECS solution. These data indicate that the POCPs are released into the cell plasma membrane and remain intercalated in the form of a stabilized pore or carpet structure.[56] The size range for these smaller polyplexes were comparable between our NMR (~7.5-15 nm) and DLS (~12-40 nm) diameter measurements. Polyplex particles in this size range have been hypothesized to be the active form for effective gene delivery.[57-59] The lower size limit for first pass elimination by kidneys has been estimated to be 10 nm diameter based on sieving coefficients simulated for proteins, Ficoll, and Dextran particles using pore theory of glomerular permselectivity.[60] The upper size limit for particles to successfully reach target locations has been suggested[57] to be ~70 nm diameter based on a study[61] which showed that gylcolipid/liposome particles > 70 nm diameters were not recognized by the asialogycoprotein receptor on hepatocytes. The NMR data suggests that in the small sized polyplex particle, the RNA maintains its structural and dynamic properties without any differences localized in the flexible bulge residues and are consistent with effects observed with divalent cations.[45] This is consistent with previous circular dichroism (CD) spectroscopy studies on RNA polyplexes with PEGylated G4 PAMAM[6] and a variety of unPEGylated dendrimers[7] where the overall CD spectral pattern of polyplexes remained similar to that of A-form RNA, minimally indicating that the RNA remains in its A-form helical secondary structure. Similar results were also inferred for transfer RNA (t-RNA) polyplexes from both CD spectroscopy and infrared (IR) spectroscopy.[8] In addition, we also have evidence for presence of larger polyplex particles in the size range ~140-200 nm as measured by DLS. It is possible that these larger particles are in exchange with either free RNA or the smaller polyplex particles, as suggested by the decrease in integrated area of NMR resonances. We note that our data is consistent with the number of particles in the ~12-40 nm size range being dominant but a greater volume of material being present in the large ~140-200 nm particles. This

leads us to put forward a picture of the polyplex system as an 'ion-cloud' like environment where the RNA and dendrimer molecules are held together by transient non-specific interactions preserving the RNA local structure and dynamics and are in dynamic exchange between free and bound forms.

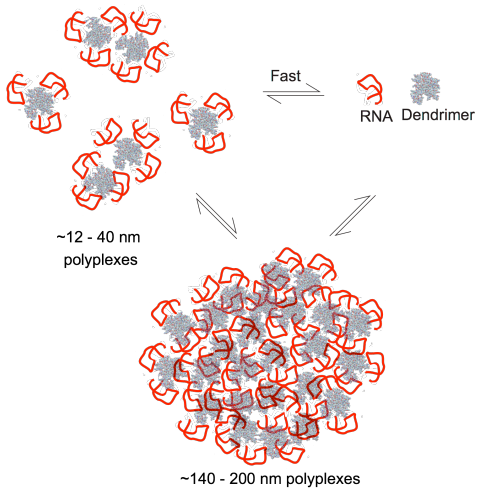

Scheme 2-I Proposed exchange model between polyplex bound forms and free RNA. As suggested by DLS, the ~12-40 nm particles represent the majority of polyplex population.

2.2 Role of Polymer Structure and Oligonucleotide Structure on Compexation and Intramolecular Exchange of Polyplexes

While intraction between nucleic acids and POCPs are largely viewed as non-specific electrostatic interactions, owing to the involvement of large number of charges, there are several instances in literature (discussed in 0) suggesting that the structural details of the POCP as well as the nucleic acids play a role in determining the overall interactions in these complex systems. Here we test three common nucleic acid delivery polymers of the roughly similar average molecular weights (25 kDa) and having amines as the protonable groups with respect to their ability to complex and exchange HIV-1 TAR using fluorescence based competition assay described in section 2.1.1.12. Using fluorophore tag on G5-PAMAM we show that the degree of complexation as monitored by amount of fluorescence quenched, depends on whether the oligonucleotides favor unstructured or hairpin structures irrespective of their

molecular weights. It was also shown that when competed with untagged G5-PAMAM, bound G5-PAMAM were able to be exchanged in solution.

2.2.1 Dependence of Degree of Complexation and Release of Bound Oligo on POCP Structure

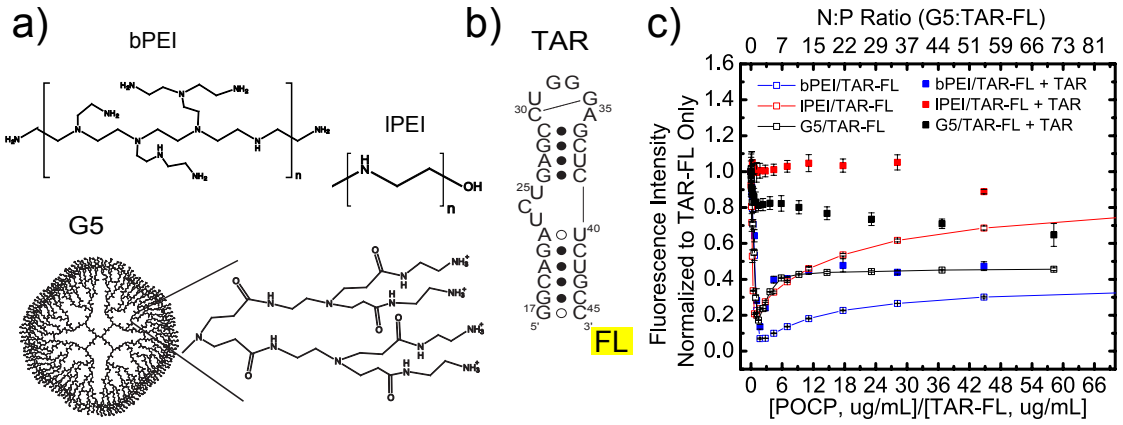

Figure 2.6 Binding and exchange of TAR-FL in different polyplexes as monitored by quenching of TAR-FL fluorescence. (a) Chemical structure of different POCPs tested. (b) Open circles with lines represent TAR-FL fluorescence intensity upon binding with the POCPs at different concentration ratios (N:P ratios is provided for G5). Filled dots represent fluorescence intensity after exchange with excess untagged TAR.

Figure 2.6 a shows the different POCPs tested in this study. All three POCPs are known to form polyplexes with nucleic acids, with the interactions largely mediated by the protonable amine groups. The two forms of PEI are chemically very similar with every third atom being protonable (monomer unit -CH_2-CH_2-NH-). However, they differ significantly in the arrangement of protonable sites along the main chain. The hyperbranched architecture of bPEI results in primary, secondary, and tertiary amines in an estimated ratio 1:2:1. lPEI only has secondary amines except at the chain end which is terminated by primary amine. The repeating unit of PAMAM has amide as well as amine functional groups. The branching in PAMAM also results in primary, secondary, and tertiary amines, however the dendritic architecture results in unique polymer properties. Figure 2.6 b shows the secondary structure of the nucleic acid used in this study with fluorophore tag at the 3' end. It is observed, as seen in Figure 2.6 c

that the total amount of TAR complexed as measured by total amount of fluorescence quenched, which we will define as the degree of complexation, is significantly different for the three tested POCPs. At the concentration ratio where maximum amount of quenching is observed for all POCPs, the order of the amount of quenching is bPEI > lPEI ~ G5. Although the exact effect of protonation in PEIs have been difficult to understand, additionally complicated by the molecular weight inhomogeinity, the stronger affinity of bPEI compared to lPEI may be attributed to differences in protonation behavior between the two types of PEI. The primary amines have the highest pKa followed by secondary and tertiary amines. Therefore for a given mass of PEI at physiological pH, bPEI is expected to be protonated to a greater extent compared to lPEI, which only has secondary amines. However, this may nontrivial owing to the effect on protonation of a amine by its surrounded by its already protonated neighboring amines. For e.g. Theoretical analysis and simulations have shown that under physiological pH, the protonated sites in lPEI alternate with un-protonated sites along the chain.[62] In bPEI, there is an additional energetic penalty to protonate amines due electrostatic effects from the easily protonable neighboring primary or secondary nitrogen atoms.[63] Secondly, the branched topology makes bPEI more rigid compared to lPEI.[64] Moreover, binding to nucleic acids can alter the protonation of the POCP, which can be structure dependent. Therefore, in addition to the overall charge in polymer structural features can play a role in determining how many oligonucleotides can bind to a single polymer molecule.

Beyond the maximum quenching ratio fluorescence is recovered for all three POCPs to some extent. This type of quenching profiles, i.e., initial quenching up to ~ N:P 1 and some degree of recovery of fluorescence has been attributed to the capability of polyplexes to undergo molecular reorganization leading to either increased separation of fluorophore molecules. This also coincides with the "charge inversion" behavior of polyplexes in presence of excess positive charges. Theories developed to explain "charge inversion" behavior of polyplexes predict that when there are excess positively charged polymers present, preformed charge neutral polyplexes can accommodate the excess charges resulting in an overall positive charge on the polyplex. This kind of accommodation can result in redistribution of the nucleic acid molecules in the polyplexes. Interestingly, while the fluorescence quenching profiles of

lPEI and bPEI (ignoring the absolute fluorescence values) are similar, the profile is significantly different for G5 suggesting some differences in molecular reorganization of the polyplexes. However, the exact nature of these differences cannot be accessed simply from fluorescence quenching. Upon adding untagged TAR to the preformed polyplex solutions, fluorescence is recovered for POCPs. However, the total amount of fluorescence recovered after the competition is different for different POCP which follows the order lPEI> G5 > bPEI. This suggests that the exchange of bound RNA is most favored for lPEI while for bPEI the RNA is more tightly bound.

2.2.2 Dependence of Degree of Complexation of Bound Oligo and Release of Bound POCP on Oligo Secondary Structure.

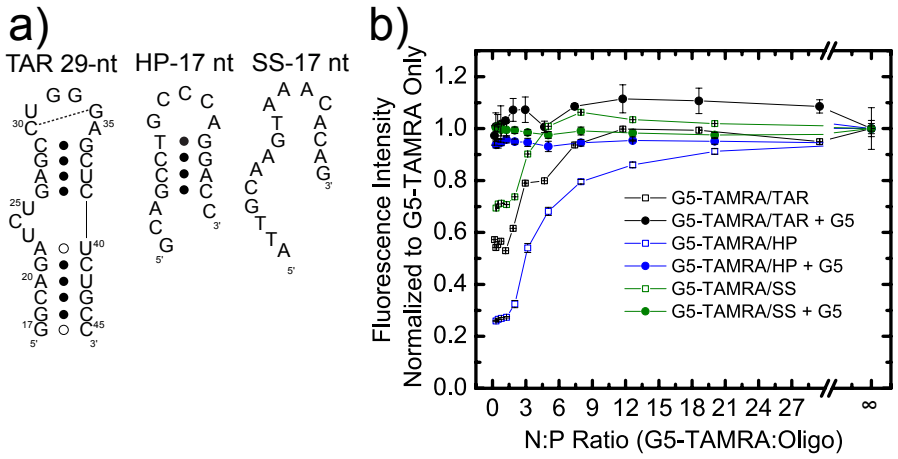

Figure 2.7 Binding and exchange of G5-TAMRA in different polyplexes as monitored by quenching of G5-TAMRA fluorescence. (a) **Chemical structure of different oligonucleotides tested.** (b) **Open circles represent TAMRA fluorescence intensity upon binding with the olignucleotides different N:P atios. Filled dots represent fluorescence intensity after exchange with excess untagged G5.**

Secondly, we tested the effect of oligo structure on the degree of complexation with G5 and exchange of G5. Figure 2.7 a shows the different oligonucleotides used in this study. The first is the 29-nt RNA used in our previous experiment, while the latter two (HP and SS) are of equal nucleotide length and hence comparable masses. However, due to their sequence context, the is HP is predicted to thermodynamically favor hairpin structures whereas the free energy of hairpin formation is very high for

SS. Sequences for these constructs were obtained from studies by Sundaram *et al.* [65] where they showed, using single stranded oligo binding dye, that the amount of uncomplexed oligo was greater for single stranded oligo/polylysine (PLL) complexes compared to hairpin/pLL polyplexes. Figure 2.7 b shows quenching of fluorescence of TAMRA conjugated to G5 (G5-TAMRA) upon polyplex formation with the three oligos as a function of N:P ratio. In this assay, a constant amount of G5-TAMRA was mixed with varying amounts of oligo. As the N:P decreases (equivalently as the oligo concentration increases), the TAMRA fluorescence quenches and reaches a saturation around N:P 1. A significant difference in the amount of fluorescence quenching for the different oligonucleotides is observed even when normalized for the N:P ratios. It is worth mentioning that unlike in the assay where the POCP is varied where the estimation of N:P ratio and hence the charge balance is prone to errors due to large molecular weight inhomogeneity, in this assay the N:P ratios can closely represent the charge ratio as both the G5 molecular weight and oligo molecular weights are more precise. Consistent with the studies by Sundaram *et al.*, we observed that the HP oligo quenched G5-TAMRA fluorescence the most and the SS oligo quenched the least suggesting hairpin structure complex with POCPs to a greater extent compared to unstructured oligos. This may be explained by higher charge density of double helical regions compared to single stranded regions. However, the flexibility of the unstructured regions may also play a role as the higher molecular weight RNA which has twice the number of helices compared to the HP, but has a very flexible junction showed lower degree of complexation compared with HP but higher compared to SS. When excess of untagged dendrimer was added to the preformed polyplexes, fluorescence was recovered for polyplexes of all oligonucleotides used. This indicates that the bound dendrimer can be exchanged into the solution. However, the amount of complexed G5 exchanged does not appear to be dependent on the oligonucleotide structure.

2.3 Conclusions

Using a combination of experimental approaches we describe a coherent picture for the structure and dynamics of soluble nanoscopic complexes of a small RNA with polycationic dendrimer. DLS and NMR experiments support the view that the RNA-dendrimer polyplexes form two distinct populations

with sizes of ~12-40 nm and ~140-200 nm. The smaller polyplexes are expected to be the more functional form as this size range falls within the proposed size limits for delivery vehicles. While the RNA rapidly exchanges between free and bound forms, we find no significant effect on the secondary structure and fast local dynamics of the RNA upon polyplex formation. However, both polymer and nucleic acid structure affects the composition of the the polyplexes and the intermolecular exchange as indicated by fluorescence experiments. The intermolecular exchange dynamics is crucial for biological function, as the nucleic acid cargo needs to be both protected and released. The prospect of having functionally active RNA/DNA bound to a dendrimer delivery vehicle is extremely promising for future design. Lastly, we hypothesize that the small, active population of polyplexes are in free exchange with the larger aggregates observed in DLS. By considering all of these data, we propose a picture of how polyplexes may exist in solution that includes rapidly exchanging RNA/DNA molecules on smaller RNA-dendrimer polyplexes, as well as on the larger polyplexes aggregating and exchanging. The data presented here should prove useful for future engineering of polyplexes for the purpose of therapeutic nucleic acid delivery.

2.4 References

1. Aliabadi, H. M.; Landry, B.; Sun, C.; Tang, T.; Uludag, H. Supramolecular Assemblies in Functional siRNA Delivery: Where Do We Stand? *Biomaterials* 2012, *33*, 2546-2569.
2. Ainalem, M. L.; Nylander, T. DNA Condensation Using Cationic Dendrimers-Morphology and Supramolecular Structure of Formed Aggregates. *Soft Matter* 2011, *7*, 4577-4594.
3. Wan, L.; Manickam, D. S.; Oupicky, D.; Mao, G. DNA Release Dynamics from Reducible Polyplexes by Atomic Force Microscopy. *Langmuir* 2008, *24*, 12474-12482.
4. Perez, A. P.; Romero, E. L.; Morilla, M. J. Ethylendiamine Core PAMAM Dendrimers/siRNA Complexes as in Vitro Silencing Agents. *Inter. J. of Pharm.* 2009, *380*, 189-200.
5. Prevette, L. E.; Kodger, T. E.; Reineke, T. M.; Lynch, M. L. Deciphering the Role of Hydrogen Bonding in Enhancing pDNA-Polycation Interactions. *Langmuir* 2007, *23*, 9773-9784.
6. Reyes-Reveles, J.; Sedaghat-Herati, R.; Gilley, D. R.; Schaeffer, A. M.; Ghosh, K. C.; Greene, T. D.; Gann, H. E.; Dowler, W. A.; Kramer, S.; Dean, J. M.; Delong, R. K. mPEG-PAMAM-G4 Nucleic Acid Nanocomplexes: Enhanced Stability, RNase Protection, and Activity of Splice Switching Oligomer and Poly I:C RNA. *Biomacromolecules* 2013, *14*, 4108-4115.
7. Ionov, M.; Lazniewska, J.; Dzmitruk, V.; Halets, I.; Loznikova, S.; Novopashina, D.; Apartsin, E.; Krasheninina, O.; Venyaminova, A.; Milowska, K.; Nowacka, O.; Gomez-Ramirez, R.; de la

Mata, F. J.; Majoral, J. P.; Shcharbin, D.; Bryszewska, M. Anticancer siRNA Cocktails as a Novel Tool to Treat Cancer Cells. Part (a). Mechanisms of Interaction. *Inter. J. of Pharm.* 2015, *485*, 261-269.

8. Froehlich, E.; Mandeville, J. S.; Kreplak, L.; Tajmir-Riahi, H. A. Aggregation and Particle Formation of tRNA by Dendrimers. *Biomacromolecules* 2011, *12*, 2780-2787.
9. Su, C. J.; Chen, H. L.; Wei, M. C.; Peng, S. F.; Sung, H. W.; Ivanov, V. A. Columnar Mesophases of the Complexes of DNA with Low-Generation Poly(amidoamine) Dendrimers. *Biomacromolecules* 2009, *10*, 773-783.
10. Jensen, L. B.; Mortensen, K.; Pavan, G. M.; Kasimova, M. R.; Jensen, D. K.; Gadzhyeva, V.; Nielsen, H. M.; Foged, C. Molecular Characterization of the Interaction between siRNA and PAMAM G7 Dendrimers by SAXS, ITC, and Molecular Dynamics Simulations. *Biomacromolecules* 2010, *11*, 3571-3577.
11. Mills, M.; Orr, B.; Holl, M. M. B.; Andricioaei, I. Microscopic Basis for the Mesoscopic Extensibility of Dendrimer-Compacted DNA. *Biophys. J.* 2010, *98*, 834-842.
12. Pavan, G. M.; Albertazzi, L.; Danani, A. Ability to Adapt: Different Generations of PAMAM Dendrimers Show Different Behaviors in Binding siRNA. *J. Phys. Chem. B* 2010, *114*, 2667-2675.
13. Pavan, G. M.; Posocco, P.; Tagliabue, A.; Maly, M.; Malek, A.; Danani, A.; Ragg, E.; Catapano, C. V.; Pricl, S. PAMAM Dendrimers for siRNA Delivery: Computational and Experimental Insights. *Chem. Euro. J.* 2010, *16*, 7781-7795.
14. Mills, M.; Orr, B. G.; Holl, M. M. B.; Andricioaei, I. Attractive Hydration Forces in DNA-Dendrimer Interactions on the Nanometer Scale. *J. Phys. Chem. B* 2013, *117*, 973-981.
15. Prevette, L. E.; Nikolova, E. N.; Al-Hashimi, H. M.; Holl, M. M. B. Intrinsic Dynamics of DNA-Polymer Complexes: A Mechanism for DNA Release. *Mol. Pharm.* 2012, *9*, 2743-2749.
16. Tang, Y.; Li, Y.-B.; Wang, B.; Lin, R.-Y.; van Dongen, M.; Zurcher, D. M.; Gu, X.-Y.; Holl, M. M. B.; Liu, G.; Qi, R. Efficient in Vitro siRNA Delivery and Intramuscular Gene Silencing Using PEG-Modified PAMAM Dendrimers. *Mol. Pharm.* 2012, *9*, 1812-1821.
17. Rinnenthal, J.; Buck, J.; Ferner, J.; Wacker, A.; Furtig, B.; Schwalbe, H. Mapping the Landscape of RNA Dynamics with NMR Spectroscopy. *Acc. of Chem. Res.* 2011, *44*, 1292-1301.
18. Mustoe, A. M.; Brooks, C. L.; Al-Hashimi, H. M. Hierarchy of RNA Functional Dynamics. *Annu. Rev. Biochem.* 2014, *83*, 441-466.
19. Puglisi, J. D.; Tan, R.; Calnan, B. J.; Frankel, A. D.; Williamson, J. R. Conformation of the TAR RNA-Arginine Complex by NMR Spectroscopy. *Science* 1992, *257*, 76-80.
20. Zhao, H.; Li, J. R.; Xi, F.; Jiang, L. Polyamidoamine Dendrimers Inhibit Binding of Tat Peptide to TAR RNA. *FEBS Lett.* 2004, *563*, 241-245.
21. Wang, W.; Guo, Z. P.; Chen, Y.; Liu, T.; Jiang, L. Influence of Generation 2-5 of PAMAM Dendrimer on the Inhibition of Tat Peptide/TAR RNA Binding in HIV-1 Transcription. *Chem. Biol. & Drug Des.* 2006, *68*, 314-318.
22. Zhang, Q.; Sun, X.; Watt, E. D.; Al-Hashimi, H. M. Resolving the Motional Modes That Code for RNA Adaptation. *Science* 2006, *311*, 653-656.

23. Hansen, A. L.; Al-Hashimi, H. M. Dynamics of Large Elongated RNA by NMR Carbon Relaxation. *J. Am. Chem. Soc.* 2007, *129*, 16072-16082.
24. Dethoff, E. A.; Hansen, A. L.; Musselman, C.; Watt, E. D.; Andricioaei, I.; Al-Hashimi, H. M. Characterizing Complex Dynamics in the Transactivation Response Element Apical Loop and Motional Correlations with the Bulge by NMR, Molecular Dynamics, and Mutagenesis. *Biophys. J.* 2008, *95*, 3906-3915.
25. Lee, J.; Dethoff, E. A.; Al-Hashimi, H. M. Invisible RNA State Dynamically Couples Distant Motifs. *Proc. Natl. Acad. Sci. USA* 2014, *111*, 9485-9490.
26. Meltzer, A. D.; Tirrell, D. A.; Jones, A. A.; Inglefield, P. T.; Hedstrand, D. M.; Tomalia, D. A. Chain Dynamics in Poly(amidoamine) Dendrimers - a Study of ^{13}C NMR Relaxation Parameters. *Macromolecules* 1992, *25*, 4541-4548.
27. Meltzer, A. D.; Tirrell, D. A.; Jones, A. A.; Inglefield, P. T. Chain Dynamics in Poly(amidoamine) Dendrimers - a Study of ^{2}H NMR Relaxation Parameters. *Macromolecules* 1992, *25*, 4549-4552.
28. Hu, J.; Fang, M.; Cheng, Y.; Zhang, J.; Wu, Q.; Xu, T. Host-Guest Chemistry of Dendrimer-Drug Complexes. 4. An in-Depth Look into the Binding/Encapsulation of Guanosine Monophosphate by Dendrimers. *J. Phys. Chem. B* 2010, *114*, 7148-7157.
29. Mullen, D. G.; Fang, M.; Desai, A.; Baker, J. R.; Orr, B. G.; Banaszak Holl, M. M. A Quantitative Assessment of Nanoparticle-Ligand Distributions: Implications for Targeted Drug and Imaging Delivery in Dendrimer Conjugates. *ACS Nano* 2010, *4*, 657-670.
30. Mullen, D. G.; Desai, A.; van Dongen, M. A.; Barash, M.; Baker, J. R., Jr.; Holl, M. M. B. Best Practices for Purification and Characterization of PAMAM Dendrimer. *Macromolecules* 2012, *45*, 5316-5320.
31. van Dongen, M. A.; Desai, A.; Orr, B. G.; Baker, J. R.; Holl, M. M. B. Quantitative Analysis of Generation and Branch Defects in G5 Poly(Amidoamine) Dendrimer. *Polymer* 2013, *54*, 4126-4133.
32. Delaglio, F.; Grzesiek, S.; Vuister, G. W.; Zhu, G.; Pfeifer, J.; Bax, A. NMRPipe - a Multidimensional Spectral Processing System Based on UNIX Pipes. *J. Biomol. NMR* 1995, *6*, 277-293.
33. Carr, H. Y.; Purcell, E. M. Effects of Diffusion on Free Precession in Nuclear Magnetic Resonance Experiments. *Phys. Rev.* 1954, *94*, 630-638.
34. Meiboom, S.; Gill, D. Modified Spin-Echo Method for Measuring Nuclear Relaxation Times. *Rev. Sci. Instrum.* 1958, *29*, 688-691.
35. Jarymowycz, V. A.; Stone, M. J. Fast Time Scale Dynamics of Protein Backbones: NMR Relaxation Methods, Applications, and Functional Consequences. *Chem. Rev.* 2006, *106*, 1624-1671.
36. Boisbouvier, J.; Wu, Z.; Ono, A.; Kainosho, M.; Bax, A. Rotational Diffusion Tensor of Nucleic Acids from ^{13}C NMR Relaxation. *J. Biomol. NMR* 2003, *27*, 133-142.

37. Aboul-ela, F.; Karn, J.; Varani, G. The Structure of the Human Immunodeficiency Virus Type-1 TAR RNA Reveals Principles of RNA Recognition by Tat Protein. *J. Mol. Biol.* 1995, *253*, 313-332.
38. Hansen, A. L.; Al-Hashimi, H. M. Insight into the CSA Tensors of Nucleobase Carbons in RNA Polynucleotides from Solution Measurements of Residual CSA: Towards New Long-Range Orientational Constraints. *J. Magn. Reson.* 2006, *179*, 299-307.
39. Hassan, P. A.; Rana, S.; Verma, G. Making Sense of Brownian Motion: Colloid Characterization by Dynamic Light Scattering. *Langmuir* 2015, *31*, 3-12.
40. Liu, X.; Liu, C.; Laurini, E.; Posocco, P.; Pricl, S.; Qu, F.; Rocchi, P.; Peng, L. Efficient Delivery of Sticky siRNA and Potent Gene Silencing in a Prostate Cancer Model Using a Generation 5 Triethanolamine-Core PAMAM Dendrimer. *Mol. Pharm.* 2012, *9*, 470-481.
41. Jensen, L. B.; Pavan, G. M.; Kasimova, M. R.; Rutherford, S.; Danani, A.; Nielsen, H. M.; Foged, C. Elucidating the Molecular Mechanism of PAMAM-siRNA Dendriplex Self-Assembly: Effect of Dendrimer Charge Density. *Int. J. Pharm.* 2011, *416*, 410-418.
42. Al-Hashimi, H. M.; Pitt, S. W.; Majumdar, A.; Xu, W.; Patel, D. J. Mg^{2+}-Induced Variations in the Conformation and Dynamics of HIV-1 TAR RNA Probed Using NMR Residual Dipolar Couplings. *J. Mol. Biol.* 2003, *329*, 867-873.
43. Zhang, Q.; Throolin, R.; Pitt, S. W.; Serganov, A.; Al-Hashimi, H. M. Probing Motions between Equivalent RNA Domains Using Magnetic Field Induced Residual Dipolar Couplings: Accounting for Correlations between Motions and Alignment. *J. Am. Chem. Soc.* 2003, *125*, 10530-10531.
44. Musselman, C.; Al-Hashimi, H. M.; Andricioaei, I. Ired Analysis of TAR RNA Reveals Motional Coupling, Long-Range Correlations, and a Dynamical Hinge. *Biophys. J.* 2007, *93*, 411-422.
45. Casiano-Negroni, A.; Sun, X. Y.; Al-Hashimi, H. M. Probing Na^{+}-Induced Changes in the HIV-1 TAR Conformational Dynamics Using NMR Residual Dipolar Couplings: New Insights into the Role of Counterions and Electrostatic Interactions in Adaptive Recognition. *Biochemistry* 2007, *46*, 6525-6535.
46. Lee, J.; Vogt, C. E.; McBrairty, M.; Al-Hashimi, H. M. Influence of Dimethylsulfoxide on RNA Structure and Ligand Binding. *Anal. Chem.* 2013, *85*, 9692-9698.
47. Stelzer, A. C.; Frank, A. T.; Kratz, J. D.; Swanson, M. D.; Gonzalez-Hernandez, M. J.; Lee, J.; Andricioaei, I.; Markovitz, D. M.; Al-Hashimi, H. M. Discovery of Selective Bioactive Small Molecules by Targeting an RNA Dynamic Ensemble. *Nat. Chem. Biol.* 2011, *7*, 553-559.
48. Callaghan, P. T. Principles of Nuclear Magnetic Resonance Spectroscopy. *Clarendon Press* 1991, *Oxford*.
49. Dethoff, E. A.; Petzold, K.; Chugh, J.; Casiano-Negroni, A.; Al-Hashimi, H. M. Visualizing Transient Low-Populated Structures of RNA. *Nature* 2012, *491*, 724-728.
50. Stelzer, A. C.; Kratz, J. D.; Zhang, Q.; Al-Hashimi, H. M. RNA Dynamics by Design: Biasing Ensembles Towards the Ligand-Bound State. *Angew. Chem. Int. Edit.* 2010, *49*, 5731-5733.

51. Kim, Y.; Klutz, A. M.; Jacobson, K. A. Systematic Investigation of Polyamidoamine Dendrimers Surface-Modified with Poly(Ethyleneglycol) for Drug Delivery Applications: Synthesis, Characterization, and Evaluation of Cytotoxicity. *Bioconjug. Chem.* 2008, *19*, 1660-1672.
52. Bielinska, A. U.; Kukowska-Latallo, J. F.; Baker, J. R., Jr. The Interaction of Plasmid DNA with Polyamidoamine Dendrimers: Mechanism of Complex Formation and Analysis of Alterations Induced in Nuclease Sensitivity and Transcriptional Activity of the Complexed DNA. *Biochim. Biophys. Acta.* 1997, *1353*, 180-190.
53. Ainalem, M. L.; Bartles, A.; Muck, J.; Dias, R. S.; Carnerup, A. M.; Zink, D.; Nylander, T. DNA Compaction Induced by a Cationic Polymer or Surfactant Impact Gene Expression and DNA Degradation. *PLOS One* 2014, *9*, e92692.
54. Van Rompaey, E.; Chen, Y.; Muller, J. D.; Gratton, E.; Van Craenenbroeck, E.; Engelborghs, Y.; De Smedt, S.; Demeester, J. Fluorescence Fluctuation Analysis for the Study of Interactions between Oligonucleotides and Polycationic Polymers. *Biol. Chem.* 2001, *382*, 379-386.
55. Zheng, M.; Pavan, G. M.; Neeb, M.; Schaper, A. K.; Danani, A.; Klebe, G.; Merkel, O. M.; Kissel, T. Targeting the Blind Spot of Polycationic Nanocarrier-Based siRNA Delivery. *ACS Nano* 2012, *6*, 9447-9454.
56. Vaidyanathan, S.; Anderson, K. B.; Merzel, R. L.; Jacobovitz, B.; Kaushik, M. P.; Kelly, C. N.; van Dongen, M. A.; Dougherty, C. A.; Orr, B. G.; Banaszak Holl, M. M. Quantitative Measurement of Cationic Polymer Vector and Polymer-pDNA Polyplex Intercalation into the Cell Plasma Membrane. *ACS Nano* 2015, *9*, 6097-6109.
57. Bartlett, D. W.; Davis, M. E. Physicochemical and Biological Characterization of Targeted, Nucleic Acid-Containing Nanoparticles. *Bioconj. Chem.* 2007, *18*, 456-468.
58. Meyer, M.; Philipp, A.; Oskuee, R.; Schmidt, C.; Wagner, E. Breathing Life into Polycations: Functionalization with pH-Responsive Endosomolytic Peptides and Poly(ethyleneglycol) Enables siRNA Delivery. *J. Am. Chem. Soc.* 2008, *130*, 3272-3275.
59. Ulasov, A. V.; Khramtsov, Y. V.; Trusov, G. A.; Rosenkranz, A. A.; Sverdlov, E. D.; Sobolev, A. S. Properties of PEI-Based Polyplex Nanoparticles That Correlate with Their Transfection Efficacy. *Mol. Ther.* 2011, *19*, 103-112.
60. Venturoli, D.; Rippe, B. Ficoll and Dextran Vs. Globular Proteins as Probes for Testing Glomerular Permselectivity: Effects of Molecular Size, Shape, Charge, and Deformability. *Am. J. Physiol-Renal* 2005, *288*, F605-F613.
61. Rensen, P. C. N.; Sliedregt, L. A. J. M.; Ferns, A.; Kieviet, E.; van Rossenberg, S. M. W.; van Leeuwen, S. H.; van Berkel, T. J. C.; Biessen, E. A. L. Determination of the Upper Size Limit for Uptake and Processing of Ligands by the Asialoglycoprotein Receptor on Hepatocytes in Vitro and in Vivo. *J. Biol. Chem.* 2001, *276*, 37577-37584.
62. Ziebarth, J. D.; Wang, Y. M. Understanding the Protonation Behavior of Linear Polyethylenimine in Solutions through Monte Carlo Simulations. *Biomacromolecules* 2010, *11*, 29-38.

63. Borkovec, M.; Koper, G. J. M. Proton Binding Characteristics of Branched Polyelectrolytes. *Macromolecules* 1997, *30*, 2151-2158.
64. Sun, C. B.; Tang, T.; Uludag, H. Molecular Dynamics Simulations for Complexation of DNA with 2 kDa PEI Reveal Profound Effect of PEI Architecture on Complexation. *J. Phys. Chem. B* 2012, *116*, 2405-2413.
65. Sundaram, S.; Viriyapthakorn, S.; Roth, C. M. Oligonucleotide Structure Influences the Interactions between Cationic Polymers and Oligonucleotides. *Biomacromolecules* 2005, *6*, 2961-2968.

CHAPTER 3 LOCAL MICROENVIRONMENTS IN POLYPLEXES

The work presented in section 3.2 of this chapter has been submitted for review in the following paper:

Shakya, A.; Al-Hashimi, H. M.; Holl, M. M. B. "Three Microenvironments Detected in Fluxional Gene Delivery Polyplexes", under review.

3.1 Local/Interfacial Solvent Structure and Ionic Composition of upon Interaction of Charged Polymers

When two charged surfaces interact large perturbations on the local solvent and ion environment is expected.[1,2] Interactions close to charged surfaces have been difficult to understand despite being a subject of immense theoretical and experimental research. As has been discussed in 0, polyplexes present themselves as complex hierarchical assembly of charged surfaces. One of the interesting properties that arises due the stoichiometric charge excess when polyplexes are prepared in excess of either the POCP or nucleic acid charges, is the so called phenomenon of "charge inversion".[3] From ion correlation theories[4,5] it follows that under these conditions favorable accommodation of excess of the like charge on to a polymer surface occurs resulting into an overall charge. Therefore, in a hierarchically assembled polyplex multiple distinct local environments can be expected, for e.g. regions on the polymer surface that is completely neutralized by the oppositely charge polyion and regions where charges are not compensated by the oppositely charged polyion resulting in differences in the distribution of counterion density and identity (positive vs. negative counterions).[6,7] Such differences can result into regions with local environment very different from bulk. Furthermore it is well known that the water structure close to surfaces is significantly different from bulk, although the precise nature is not clearly understood.[8] Since both PCOPs and nucleic acids present different hydrophobic/hydrophilic surfaces, polyplex can have complex ordering of water molecules.[9] Such local/interfacial properties become important,

especially for reactions that pH dependent reactions such as enzyme catalysis.[10] However, these properties are difficult to measure using bulk measurements. Using small molecule probes that can detect local changes is a useful approach. Fluorescein is one such molecule that shows a variety of prototropic and solvatochromic response.

3.1.1 Solvatochroism

A basic tenant of optical excitation is the molecule undergoes a significant change to the molecules dipole moment. Often, the ground and electronically excited states both have a dipole moment, though, during excitation and relaxation, the dipole moment undergoes a significant change. In a bath of polar solvent molecules, organization of solvent molecules around a chromophore can stabilize the inherent dipole moments of the chromophore in the ground and excited states. In this case, the solvent molecules must reorganize following excitation, as the sudden change in the chromophores dipole moment drives solvent reorganization around the new dipole moment (Figure 3.1).

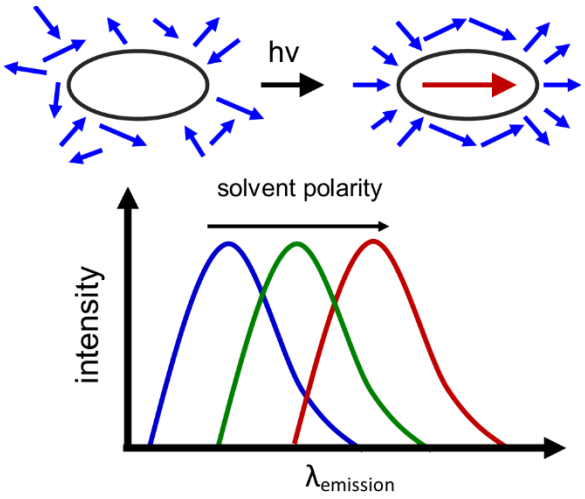

Figure 3.1 Solvatochromism. In a polar solvent, the solvent dipole moments can align to stabilize the excited state dipole of a fluorescent molecule. This solvent organization stabilizes the excited state, and a resulting red-shift can be measured in the fluorescence emission wavelength. This predictable phenomenon can be used to measure solvent polarities, and can also be used to characterize complex solvent environments.

The stabilization of the ground and excited states of a chromophore by a polar solvent affects the energy levels probed by absorption and fluorescence. For instance, the stabilization of the electronic excited state relative to the ground state lowers the energy gap, and thus fluorescence emission red shift when the chromophore is in a polar solvent. The tuning of the emission wavelength can be calibrated and used as an analytical method for determining a solvents polarity. In the case of complex environments, such as systems with nanoscale heterogeneity, solvatochroism can be used to characterize complex solvent environments, heterogeneous compositions and preferential solvation.

3.1.2 Fluorescein Protrotopism

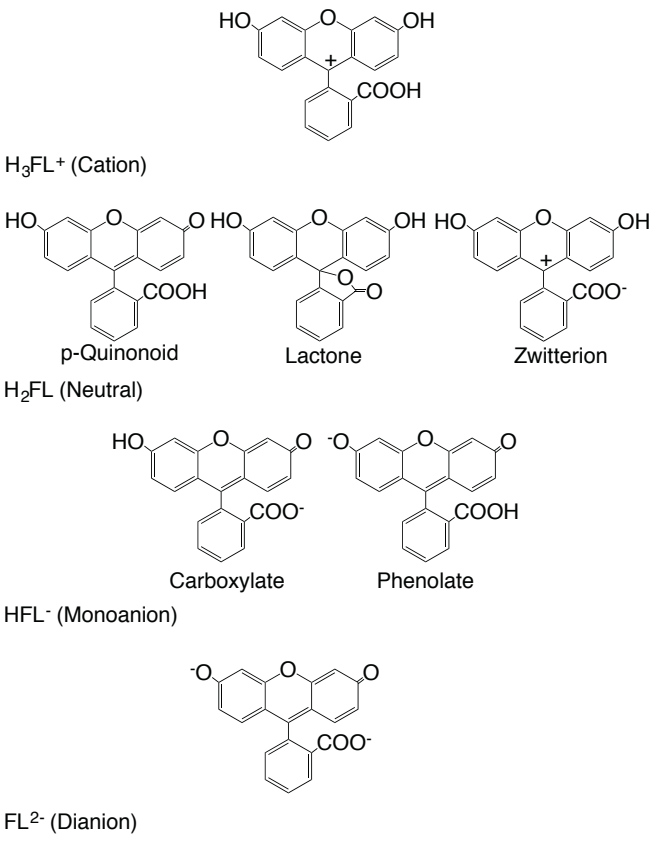

Figure 3.2 Protrotopism of fluorescein

Owing to is high molar absorptivity, quantum yield, and photostability fluorescein is one of the most commonly used dyes. It exhibits a rich prototropic and solvatochromic behavior making it very useful to

study a variety of environments around a molecule. Depending on the pH, fluorescein can exist as dianionic, anionic, neutral, and zwitterionic forms, which have unique spectral signatures. The different prototropic forms of fluorescein are shown in Figure 3.2. Although a range of different pKa values for the protolytic equilibria between the different forms have been reported, the approximate values are illustrated in Scheme 3-I.[11,12]

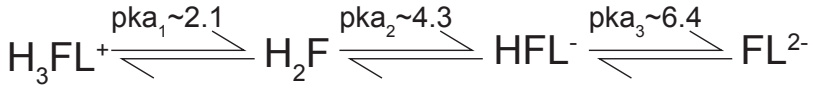

Scheme 3-I Prototropic equilibria of fluorescein.

3.2 Local Microenvironments in Polyplexes

Polycationic polymers (POCP) have long been studied for applications in nucleic acid-based therapy due to their ability to compact genetic material and transport it within the cell.[13-16] They form nanoparticulate complexes (polyplexes) with nucleic acids by simple mixing in aqueous solutions. Several polyelectrolyte complex models[3,17-23] have explained effective attraction (as close as a few angstroms) of the highly negatively charged phosphate backbone of nucleic acids in the presence of polycations, which constitute the basis for understanding polyplex formation. The emerging picture of the polyplex structure in solution is a hierarchical assembly where several nucleic acid molecules bind to a polymer (or vice versa depending on relative sizes) and several loaded polymers ("primary" complexes) aggregate to form nanoparticulate clusters.[24-28]

Studies also suggest the presence of vacant spaces within the clusters[26,29,30] that could be a source of local water and ionic microenvironments that differ from that of the bulk solution. The functional importance of local water and ionic environment at charged interfaces has been highlighted in studies of activity of enzymes assembled on charged surfaces.[1,10,31] At POCP concentrations greater than that required for the most effective charge neutralization (typically around the protonable POCP nitrogen to nucleic acid phosphate formulation ratio (N:P) of 1:1), so called "charge inversion" is predicted to occur. Favorable non-stoichiometric accommodation of excess POCP molecules via local effects on the surface

potential of already neutralized surfaces confers an effective positive charge to the polyplex.[4,5,32] Due to the effective positive surface charge, an electrostatic double layer and a counterion gradient that decreases with increasing distance from the surface (1-100 nm)[33] is expected to be present. By virtue of this electrostatic double layer and counterion gradients or hydrophilic pockets within the assembly, polyplexes can have local water and ions whose physical and chemical properties are dramatically different from that of bulk solution. In particular, interactions between charged surfaces result in uneven distribution of ions near the interface. This can result in local pH values to be different from bulk pH of the solution, which can have functional implications.[1,33] For example, enhanced activity of catalytic peptides assembled on gold nanoparticles coated with charged monolayers is attributed to an increase in interfacial local pH compared to bulk solution.[1,34] As for polyplexes, it is conceivable that local water and ionic properties are important not only for properties like polyplex mobility often linked with the electrostatic double layer charge, but also for functional intracellular events like cargo and target nucleic acid hybridization and nuclease activity owing to their sensitivity to local pH, ionic strength, and solvent structure.

This study leverages the rich prototropisim[11,12,35,36] and sensitivity to solvatochromic effects[37,38] of fluorescein to detect multiple microenvironments present in polyplex nanoparticles with local site specificity. In particular, fluorescein is a very sensitive reporter of hydronium ion concentrations making it ideal for probing microenvironments with different pH.[39-41] A variety of fluorophores, including fluorescein, have been previously employed to assess nucleic acid-POCP binding employing quenching of fluorophore fluorescence upon interaction with POCP.[25,42-44] However, in addition to quenching, information on solvent structure and composition that fluorophore spectral properties can provide has not been tapped to study the local environment of polyplex nanoparticles. The data obtained herein employing fluorescein (FL) covalently tagged to the 3' end of a 29-nt RNA (Trans Activator Response Element, TAR-FL) indicate that the RNA in polyplexes exists in at least three different microenvironments: a) RNA in association with the polyplex that experience local pH changes; possibly on the electrostatic double layer ("Stern layer" or "diffuse layer" that is dependent on POCP to RNA N:P

ratio) b) RNA that experience relatively acidic local pH that remains constant in polyplexes formed after a charge neutral N:P ratio c) RNA that are packed close enough to mediate fluorophore/fluorophore quenching. The magnitude of these changes observed as a function of POCP to nucleic acid N:P ratio depends upon the exact type of polymer employed.

3.3 Experimental

1.1.1 Materials

Sodium chloride (NaCl), 0.1 N hydrochloric acid (HCl), tris (hydroxymethyl)-aminomethane and Triton-X were purchased from Sigma, St. Louis, MO. G5 PAMAM dendrimer was purchased from Dendritech Inc. (Midland, MI) and dialysed before use. bPEI was obtained from Sigma Aldrich Corporation with Mw of ~25,000. lPEI was obtained from Polysciences, Inc., with Mw ~25,000. HPLC purified TAR tagged with fluorescein at the 3' end was purchased from Dharmacon (Lafayette, CO).

3.3.1 Fluorescence Spectroscopy

All oligos were annealed by heating to 95^{o}C for 5 min and then cooled on ice for an hour prior to use. The oligos were diluted in pH 7.54 fluorescence assay buffer (50 mM Tris-HCl, 50 mM KCl, 0.01% Trition-X). Polymers were dissolved in the assay buffer and serially diluted to obtain aliquots of concentration from 2 nM to 2000 nM. 100 nM oligo was incubated for 30 min in 1:1 volume with varying concentrations of the dendrimer in a 384 well plate such that the final oligo concentration in each well was 50 nM and varying concentration ratios. Fluorescence emission at wavelengths 500 – 600 nm with stepwidth of 1 nm using 472 nm excitation wavelength and 16 nm bandwidth of excitation. Measurements were done in triplicates using a CLARIOStar Omega plate reader (BMG Labtech) at room temperature.

3.3.2 Bulk pH Measurements

Polyplex solutions were prepared in the same buffer conditions and concentrations as prepared for fluorescence experiments, but in higher volumes in order to facilitate pH measurement using a pH

probe. The probe was dipped into the polyplex solution and allowed to equilibrate until the pH reading was stable. Both calibration and measurements were performed at room temperature.

3.4 Results and Discussion

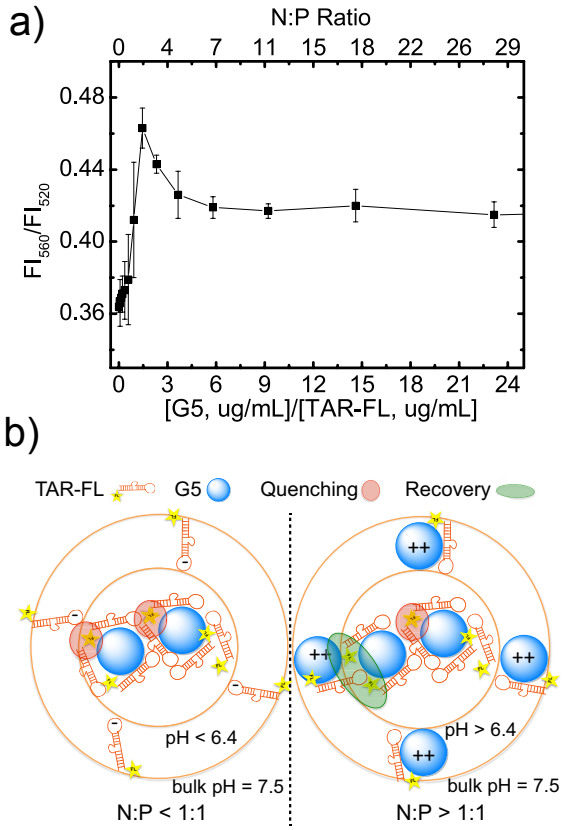

Figure 3.3 Effect of G5 PAMAM polyplex formation on the fluorescence emission spectrum of FL conjugated to the 3' end of TAR. (a) Ratio of fluorescence intensity at 560 nm (FI_{560}, fluorescein monoanion emission maximum) versus 520 nm (FI_{520}, fluorescein dianion emission maximum) plotted as a function of N:P. Corresponding concentration ratios are also denoted. b) A scheme illustrating the different microenvironments in the G5/TAR-FL polyplexes formed at N:P less and greater than 1:1.

The positive to negative charge balance, represented by N:P ratio, is one of the key formulation parameters known to affect the structure, size, colloidal stability, surface charge properties, and

fluorophore spectral properties of polyplex nanoparticles. For G5 PAMAM dendrimers, only the primary amine nitrogens are considered as they are the only ones predicted to be fully protonated at physiological pH.[45] Owing to very low pKa (~1.5) nucleic acid phosphates are always deprotonated at physiological pH. Figure 3.3 summarizes representative changes in the emission profile of TAR-FL upon polyplex formation with G5 at different N:P ratios. A key observation is that the monoanion (FL^-) fluorescence intensity relative to dianion (FL^{2-}) intensity, approximately captured by FI_{560}/FI_{520} ratio, increases as N:P increases up to 1.7 (assuming 108 primary amines per molecule of G5 and 29 phosphates per molecule of RNA). This indicates a ground state equilibrium shift towards the protonated form FL^-, reflecting an increase in hydronium ion concentration surrounding the fluorescein, given the pKa of FL^{2-} to FL^- conversion to be ~ 6.3.[38] It is important to note that no bulk pH change was observed as a function of N:P ratio as measured using pH electrodes (Appendix B, T I). Moreover, despite increasing dendrimer (a weak polybase) concentration, increased fluorophore protonation is observed (increase in FI_{560}/FI_{520}) up to N:P 1.7. This indicates, under the well-buffered solution condition, a local increase in hydronium ion concentration in the immediate environment of the fluorophore; and not bulk changes in the solution pH. It should also be noted that the emission spectrum of free fluorescein itself does not change at different POCP concentrations used in this study (Figure 3.4).

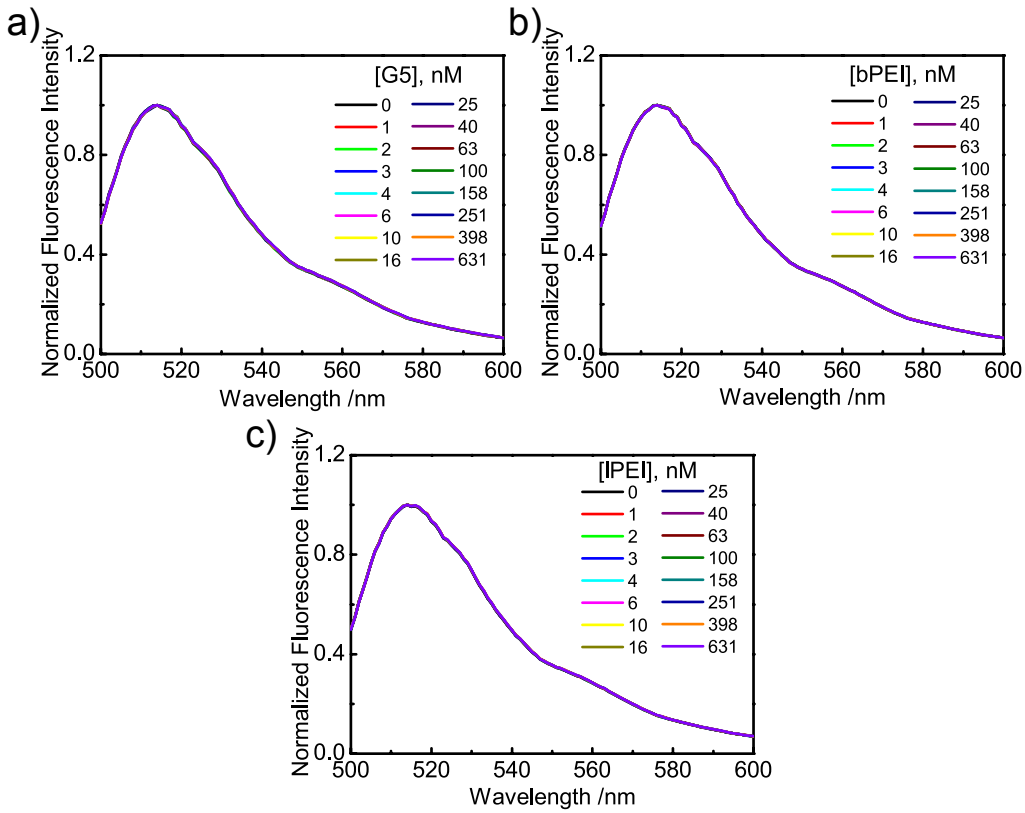

Figure 3.4 Effect of (a) G5, (b) bPEI, and (c) LPEI on free fluorescein spectrum. The concentration of fluorescein was 50 nM and the concentrations of POCP used were same as in presence of polyplex formation experiments. All the spectra at different POCP concentrations overlap with each other due to insignificant changes in the free fluorescein spectrum.

Beyond N:P 1.7, the amount of FL^- decreases and subsequently saturates at N:P 7. Such a dependence of FL protonation/deprotonation on POCP to RNA N:P ratio may be understood based on condensation/decondensation behavior of nucleic acid chains in the presence of polycations. It is well established for large DNA molecules that as the concentration of polycation is increased, the nucleic acid chains become increasingly condensed (compacted).[22,46] In the case of shorter nucleic acid chains aggregation becomes more dominant, although basic principles of polynucleotide chain attraction in the presence of polycations are expected to hold. MD simulations of small aggregates of short DNA chains in presence of polycations show that the DNA-DNA distance decreases as the positive to negative charge ratio is increased.[47] The ratio that allows for the most condensed state of separate nucleic acid chains

(close to charge neutral ratios, i.e. N:P 1:1) could provide the most acidic microenvironment due to the acidic nucleic acid phosphate groups. Beyond this ratio, the nucleic acid chains are predicted to become "charge inverted" and can reenter the bulk solution phase from the condensed/aggregated phase or reorganize in order to minimize repulsive interactions.[22,46] This is consistent with an increase in local pH (equilibrium shift from FL^- to FL^{2-}) observed after N:P 1.7. However, the local pH appears to remain slightly more acidic compared to that experienced by free TAR-FL (N:P 0) suggesting that the RNA remains in interaction with other RNA molecules in the complex. This supports the notion of molecular rearrangement of "primary" complexes leading to more sparsely distributed RNA in the polyplex aggregate.[25]

The initial decrease in local pH surrounding the chromophore until charge neutral ratios are reached, followed by subsequent increase and saturation, is also reminiscent of the dependence of zeta potential on the charge ratios commonly reported in literature. Zeta potential measurement, which is based on mobility of colloidal/nanoparticles in an applied electric field, reports on the effective charge on the electrostatic double layer surrounding the particles. However, unlike hard nanoparticles, polyplex nanoparticles are soft and fluxional; and are expected to have a heterogenous interface and a non-ideal electrostatic double layer.[48] Nonetheless, zeta potential measurements are often used as a useful tool to qualitatively compare the effective charge on the double layer among particles formed at different N:P ratios.[49] The general trend observed is that zeta potential value decreases as the N:P ratio increases and reverses in sign beyond the charge neutral condition. Based on this model, it is likely that the observed pH changes reflected by FI_{560}/FI_{520} ratio are reporting on pH changes within the electrostatic double layer surrounding the polyplex nanoparticles.

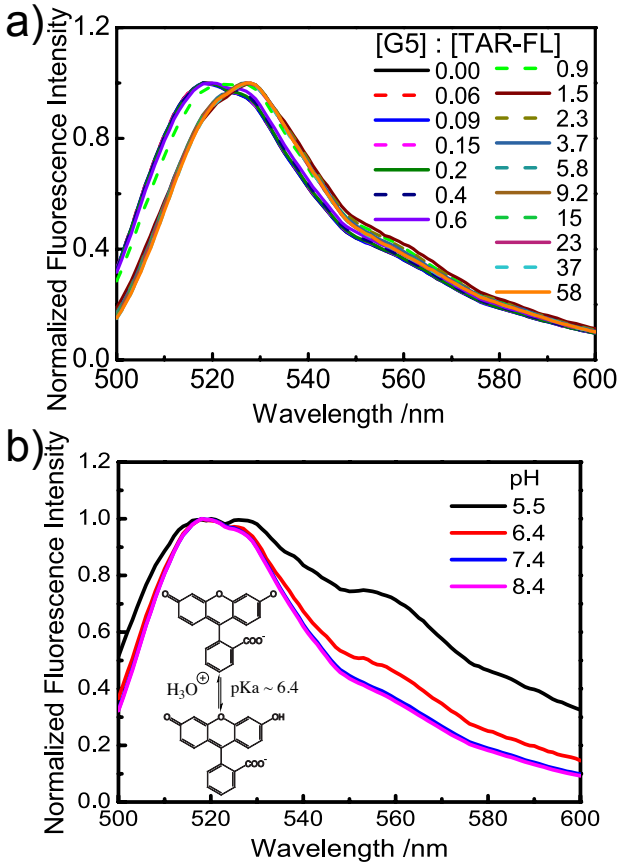

Figure 3.5 (a) Normalized steady state emission spectra (excitation wavelength, λ_{ex} = 472 nm) of TAR-FL at various G5:TAR-FL concentration(ug/mL) ratios. Solutions were buffered at a pH of 7.54 using tris-HCL. (b) Normalized emission spectra of TAR-FL at different buffer (tris-HCl) pH (λ_{ex} = 472 nm).

Secondly, a bathochromic shift of up to ~6 nm is observed for the FL^{2-} emission maximum ca. 520 nm (Figure 3.5 a). Bathochromic spectral shifts of FL^{2-} are observed when solvent polarity increases and/or the FL^{2-} experiences a change in hydrogen bonding status molecules in its ground state.[38] The observed red shift in emission from the dianionic chromophore suggests either electrostatic interaction of FL^{2-} with the POCP charged amines, which is consistent with an increased extent of terminal amine protonation, and/or lowered hydrogen bonding interactions with water molecules due to competition with RNA phosphates as local water molecules are expected to deplete or change their ordering upon POCP/nucleic acid interaction.[9] Another feature of the emission spectra that indicates local pH changes is a less prominent shoulder peak ca. 526 nm. As seen in emission spectra of TAR-FL at different buffer

pH (Figure 3.5 b), the relative intensity of this peak also increases as the pH is lowered. This intensity of this low pH fluorescent species increases up to the same N:P ratio at which maximum FL^- emission observed. However, unlike the FL^- emission at 560 nm, it does not decrease on further increasing the N:P ratio. This suggests the presence of a separate relatively acidic polyplex microenvironment that remains unperturbed as the POCP is increased beyond the charge balance condition. Although precise structural descriptions of the polyplex assembly cannot be made solely based on these fluorescence data, the concept of vacant spaces[26,29,30] in these soft nanoparticles is consistent with an internal solvent microenviroment that is relatively acidic compared to the electrostatic double layer on the surface of the polyplex as the latter will have a higher probability of interacting with the excess free POCP in the solution.

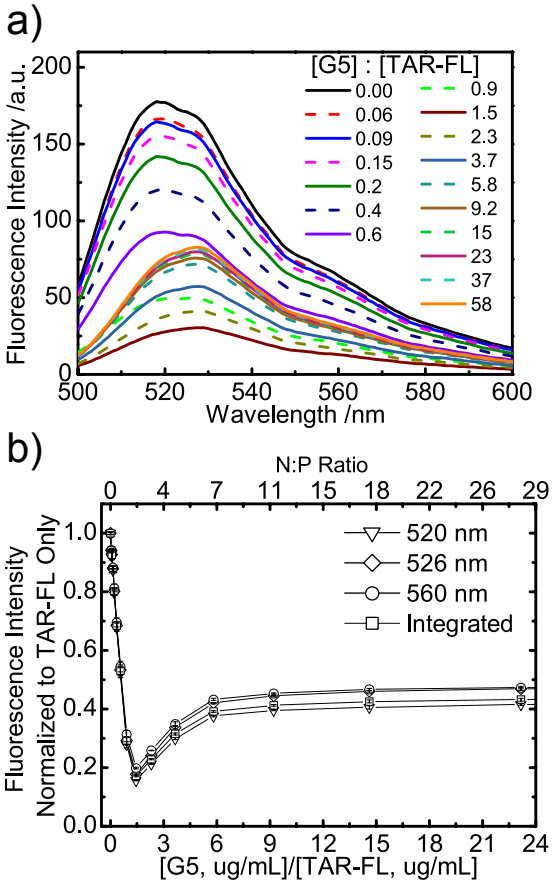

Figure 3.6 Quenching of FL fluorescence at different G5 to TAR-FL N:P (ug/mL) ratios a) Raw emission spectra (λ_{ex} = 472 nm). b) Comparison of fluorescence intensities at wavelengths 520, 526,

560 nm with the total intensity integrated over 500-600 nm. Fluorescence intensities are normalized to TAR-FL only sample. Error bars represent standard deviation from triplicate measurements.

The near charge neutral ratio N:P 1.7, is also the ratio where maximum fluorescence quenching occurs (Figure 3.6 a). Such quenching is generally attributed to increased proximity between fluorophores molecules upon complex formation.[25,44] The degree of quenching at this ratio is essentially same regardless of the wavelength of detection and is the same as when the entire spectrum is integrated (Figure 3.6 b) indicating that quenching is a general effect, regardless of the relative concentration of fluorescing species present. Partial recovery of fluorescence is observed beyond the near charge neutral ratio. This dependence of quenching on the N:P ratio has been observed for assays involving other covalently attached dye molecules as well. The partial recovery supports the model that beyond the critical N:P ratio polyplex nanoparticles undergo molecular reorganization of the assembled "primary" complexes in the polyplexes, that allows for increased dye-dye distance[25,28] possibly due to the favorable accommodation of excess POCP as predicted by ion-ion correlation based "charge inversion" effects.

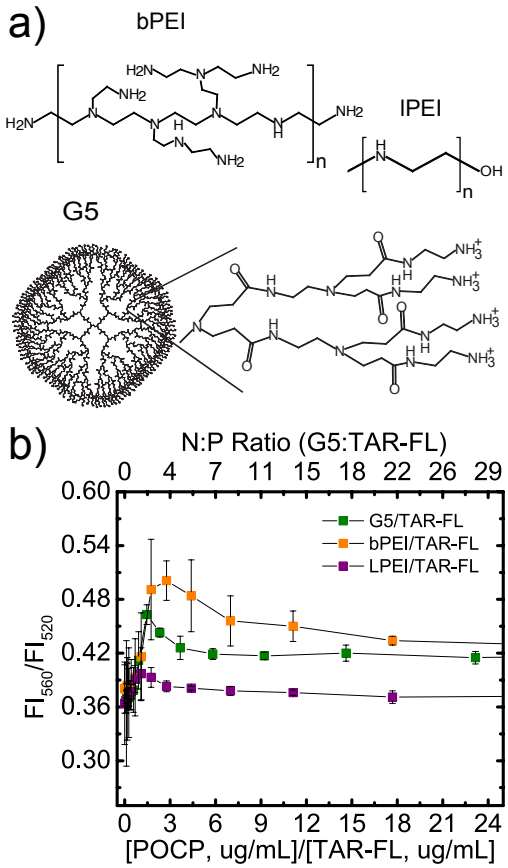

Figure 3.7 Effect of POCP type on FL emission upon polyplex formation. a) Chemical structures of G5, bPEI and lPEI b) Comparison of FI_{560} /FI_{520} ratio, reflecting on relative F^-/F^{2-} concentrations for polyplexes of TAR-FL with different POCPs. The N:P ratio is provided for G5.

Two other commonly studied POCPs, ~25 kDa lPEI and bPEI were also tested, the polyplexes of which differ substantially in their functional efficiency. Figure 3.7 shows that the magnitude of changes observed in the fluorescence spectrum of TAR-FL at different POCP concentrations is largely dependent on the type of POCP. Bathochromic shifts follow the trend G5(6 nm) > bPEI (4 nm) > lPEI (3 nm) (Figure 3.5 a, Figure 3.8). The magnitude of bathochromic shift observed when a fluorescently labeled molecule is in a binding interaction has been attributed to the increased strength of interaction of the fluorophore in the bound state compared to its hydrogen bonding interaction with the solvent.[38] Increased ordering of solvent molecules around fluorophore molecules can also induce red shifts.[50] The increased bathochromic shift observed for G5 and bPEI compared to lPEI suggests their branched

architecture may allow for more stable aggregation of the RNA into the polyplex nanoparticles; and/or increased ordering of solvent molecules leading to reduced hydrogen bonding interactions between the fluorophore and the solvent. This is consistent with MD studies that suggest greater affinity of higher generation dendrimers with nucleic acids compared with the more flexible lower generation dendrimers[51] and more stable aggregation of bPEI polyplexes compared to lPEI polyplexes.[52] On the other hand, the FI_{560}/FI_{520} ratio is highest for bPEI polyplexes suggesting the most acidic local pHs are seen for bPEI polyplexes followed by G5 polyplexes and lPEI polyplexes (Figure 3.7 b). The same trend follows for total amount of fluorescence quenching observed (Figure 2.6) consistent with a greater degree of complexation (more RNA bound per polyplex) for bPEI followed by G5 and lPEI. Comparing the two forms of PEI, chemically they are very similar with every third atom being protonable (monomer unit $-CH_2-CH_2-NH-$). However, they differ significantly in the arrangement of protonated sites along the main chain. The hyperbranched architecture of bPEI results in primary, secondary, and tertiary amines in an estimated ratio 1:2:1. lPEI only has secondary amines except at the chain end which is terminated by primary amine. Under physiological pH and salt, the protonated sites in lPEI alternate with un-protonated sites along the chain.[53] In bPEI, there is an additional energetic penalty to protonate the already acidic tertiary amines due to electrostatic effects from three easily protonable neighboring primary or secondary nitrogen atoms.[54] Secondly, the branched topology makes bPEI more rigid compared to lPEI.[52] Differences in the arrangement of protonated sites along with differences in chain flexibility has been attributed to different modes of binding with nucleic acid molecules[52] which may subsequently lead to differences in the hierarchical assembly and hence the observed differences on the fluorophore spectrum.

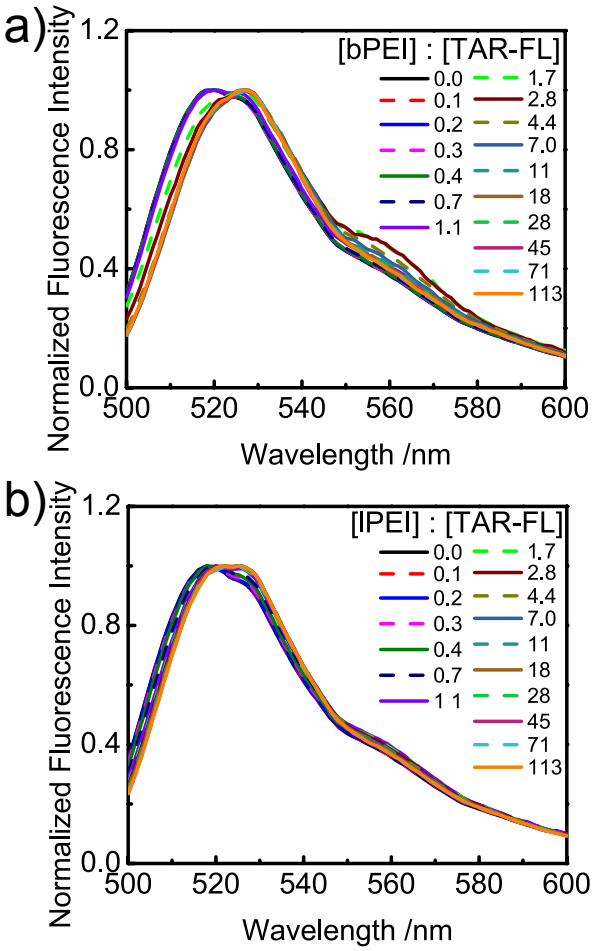

Figure 3.8 Normalized emission spectra (λ_{ex} = 472 nm) of a) bPEI/TAR-FL polyplexes at different bPEI to TAR-FL concentration (ug/mL) ratios b) lPEI/TAR-FL polyplexes at different lPEI to TAR-FL concentration (ug/mL) ratios.

3.5 Conclusion

From these observations, the following descriptions of the polyplex microenvironment can be assessed: a) RNA in association with the polyplex experiences an N:P dependent local pH change, possibly at the electrostatic double layer) b) RNA experiences relatively acidic local pH that remains constant in polyplexes formed with N:P 1:1 c) closely packed RNA experiences fluorophore/fluorophore quenching. The N:P ratio giving maximal bathochromic shift and maximal quenching slightly differs for the various POCPs. This may reflect the different levels of charge on the POCPs due to differences in the degree of protonation of amine groups. This could lead to different stoichiometry of the polyplex

resulting in a different degree of interaction of the fluorophore with the polyplex environment. The local microenvironment of polyplex may be important for the practical use of polyplexes. It is expected to change to a much lesser extent compared to bulk solution upon exposure of the polyplex particles to cellular conditions. The surface or the vicinity of the nanoparticles would provide an ideal milieu for hybridization of the cargo with target nucleic acids, as nucleic acids not in association with the polyplex are prone to nuclease degradation.[55,56] Additionally, the different microenvironments may represent the functional hierarchy of polyplex bound oligonucleotides. For example, RNA in the more acidic microenvironment (possibly internal RNA) compared to the RNA that are close to the electrostatic double-layer would be less prone to pH dependent nuclease attack as nuclease activity is reduced at low pH. Also in general, lower pH is more favorable for base pairing interactions. Assessment of such microenvironments of the polyplex and the dependence on polymer choice can help identify POCPs that can provide most favorable microenvironments for optimal function.

3.6 References

1. Hartvig, R. A.; van de Weert, M.; Ostergaard, J.; Jorgensen, L.; Jensen, H. Protein Adsorption at Charged Surfaces: The Role of Electrostatic Interactions and Interfacial Charge Regulation. *Langmuir* 2011, *27*, 2634-2643.
2. Biesheuvel, P. M.; van der Veen, M.; Norde, W. A Modified Poisson-Boltzmann Model Including Charge Regulation for the Adsorption of Ionizable Polyelectrolytes to Charged Interfaces, Applied to Lysozyme Adsorption on Silica. *J. Phys. Chem. B* 2005, *109*, 4172-4180.
3. Grosberg, A. Y.; Nguyen, T. T.; Shklovskii, B. I. Colloquium: The Physics of Charge Inversion in Chemical and Biological Systems. *Rev. Mod. Phys.* 2002, *74*, 329-345.
4. Shklovskii, B. I. Screening of a Macroion by Multivalent Ions: Correlation-Induced Inversion of Charge. *Phys. Rev. E.* 1999, *60*, 5802-5811.
5. Nguyen, T. T.; Shklovskii, B. I. Model of Inversion of DNA Charge by a Positive Polymer: Fractionalization of the Polymer Charge. *Phys. Rev. Lett.* 2002, *89*.
6. Antila, H. S.; Harkonen, M.; Sammalkorpi, M. Chemistry Specificity of DNA-Polycation Complex Salt Response: A Simulation Study of DNA, Polylysine and Polyethyleneimine. *Phys. Chem. Chem. Phys.* 2015, *17*, 5279-5289.
7. Ziebarth, J.; Wang, Y. Molecular Dynamics Simulations of DNA-Polycation Complex Formation. *Biophys. J.* 2009, *97*, 1971-1983.
8. Chandler, D. Interfaces and the Driving Force of Hydrophobic Assembly. *Nature* 2005, *437*, 640-647.

9. Mills, M.; Orr, B. G.; Holl, M. M. B.; Andricioaei, I. Attractive Hydration Forces in DNA-Dendrimer Interactions on the Nanometer Scale. *J. Phys. Chem. B* 2013, *117*, 973-981.
10. Talbert, J. N.; Goddard, J. M. Enzymes on Material Surfaces. *Colloids Surf. B Biointerfaces* 2012, *93*, 8-19.
11. Klonis, N.; Sawyer, W. H. Spectral Properties of the Prototropic Forms of Fluorescein in Aqueous Solution. *J. Fluoresc.* 1996, *6*, 147-157.
12. Sjoback, R.; Nygren, J.; Kubista, M. Absorption and Fluorescence Properties of Fluorescein. *Spectrochim. Acta A* 1995, *51*, L7-L21.
13. Lachelt, U.; Wagner, E. Nucleic Acid Therapeutics Using Polyplexes: A Journey of 50 Years (and Beyond). *Chem. Rev.* 2015, *115*, 11043-11078.
14. Scomparin, A.; Polyak, D.; Krivitsky, A.; Satchi-Fainaro, R. Achieving Successful Delivery of Oligonucleotides-from Physico-Chemical Characterization to in Vivo Evaluation. *Biotechnol. Adv.* 2015, *33*, 1294-1309.
15. Prabhu, R. H.; Patravale, V. B.; Joshi, M. D. Polymeric Nanoparticles for Targeted Treatment in Oncology: Current Insights. *Int. J. Nanomedicine* 2015, *10*, 1001-1018.
16. Germershaus, O.; Nultsch, K. Localized, Non-Viral Delivery of Nucleic Acids: Opportunities, Challenges and Current Strategies. *Asian. J. Pharm. Sci.* 2015, *10*, 159-175.
17. Manning, G. S. The Molecular Theory of Polyelectrolyte Solutions with Applications to the Electrostatic Properties of Polynucleotides. *Q. Rev. Biophys.* 1978, *11*, 179-246.
18. Guldbrand, L.; Jonsson, B.; Wennerstrom, H.; Linse, P. Electrical Double-Layer Forces - a Monte-Carlo Study. *J. Chem. Phys.* 1984, *80*, 2221-2228.
19. Kornyshev, A. A.; Leikin, S. Electrostatic Zipper Motif for DNA Aggregation. *Phys. Rev. Lett.* 1999, *82*, 4138-4141.
20. Khan, M. O.; Jonsson, B. Electrostatic Correlations Fold DNA. *Biopolymers* 1999, *49*, 121-125.
21. Kornyshev, A. A.; Lee, D. J.; Leikin, S.; Wynveen, A. Structure and Interactions of Biological Helices. *Rev. Mod. Phys.* 2007, *79*, 943-996.
22. Teif, V. B.; Bohinc, K. Condensed DNA: Condensing the Concepts. *Prog. Biophys. Mol. Bio.* 2011, *105*, 208-222.
23. Ran, S. Y.; Jia, J. L. A Multi-Field Approach to DNA Condensation. *Chinese. Phys. B.* 2015, *24*, 128702.
24. Jensen, L. B.; Pavan, G. M.; Kasimova, M. R.; Rutherford, S.; Danani, A.; Nielsen, H. M.; Foged, C. Elucidating the Molecular Mechanism of PAMAM-siRNA Dendriplex Self-Assembly: Effect of Dendrimer Charge Density. *Int. J. Pharm.* 2011, *416*, 410-418.
25. Zheng, M.; Pavan, G. M.; Neeb, M.; Schaper, A. K.; Danani, A.; Klebe, G.; Merkel, O. M.; Kissel, T. Targeting the Blind Spot of Polycationic Nanocarrier-Based siRNA Delivery. *ACS Nano* 2012, *6*, 9447-9454.
26. Perevyazko, I. Y.; Bauer, M.; Pavlov, G. M.; Hoeppener, S.; Schubert, S.; Fischer, D.; Schubert, U. S. Polyelectrolyte Complexes of DNA and Linear PEI: Formation, Composition and Properties. *Langmuir* 2012, *28*, 16167-16176.

27. Pavan, G. M. Modeling the Interaction between Dendrimers and Nucleic Acids: A Molecular Perspective through Hierarchical Scales. *Chemmedchem* 2014, *9*, 2623-2631.
28. Shakya, A.; Dougherty, C. A.; Xue, Y.; Al-Hashimi, H. M.; Holl, M. M. B. Rapid Exchange between Free and Bound States in RNA-Dendrimer Polyplexes: Implications on the Mechanism of Delivery and Release. *Biomacromolecules* 2016, *17*, 154-164.
29. Clamme, J. P.; Azoulay, J.; Mely, Y. Monitoring of the Formation and Dissociation of Polyethylenimine/DNA Complexes by Two Photon Fluorescence Correlation Spectroscopy. *Biophys. J.* 2003, *84*, 1960-1968.
30. Hou, S.; Ziebacz, N.; Wieczorek, S. A.; Kalwarczyk, E.; Sashuk, V.; Kalwarczyk, T.; Kaminski, T. S.; Holyst, R. Formation and Structure of PEI/DNA Complexes: Quantitative Analysis. *Soft Matter* 2011, *7*, 6967-6972.
31. Johnson, B. J.; Algar, W. R.; Malanoski, A. P.; Ancona, M. G.; Medintz, I. L. Understanding Enzymatic Acceleration at Nanoparticle Interfaces: Approaches and Challenges. *Nano Today* 2014, *9*, 102-131.
32. Perel, V. I.; Shklovskii, B. I. Screening of a Macroion by Multivalent Ions: A New Boundary Condition for the Poisson-Boltzmann Equation and Charge Inversion. *Physica A* 1999, *274*, 446-453.
33. Trefalt, G.; Behrens, S. H.; Borkovec, M. Charge Regulation in the Electrical Double Layer: Ion Adsorption and Surface Interactions. *Langmuir* 2016, *32*, 380-400.
34. Zaramella, D.; Scrimin, P.; Prins, L. J. Self-Assembly of a Catalytic Multivalent Peptide-Nanoparticle Complex. *J. Am. Chem. Soc.* 2012, *134*, 8396-8399.
35. Martin, M. M.; Lindqvist, L. pH-Dependence of Fluorescein Fluorescence. *J. Lumin.* 1975, *10*, 381-390.
36. Batistela, V. R.; Cedran, J. D.; de Oliveira, H. P. M.; Scarminio, I. S.; Ueno, L. T.; Machado, A. E. H.; Hioka, N. Protolytic Fluorescein Species Evaluated Using Chemometry and Dft Studies. *Dyes Pigments* 2010, *86*, 15-24.
37. Ali, M.; Dutta, P.; Pandey, S. Effect of Ionic Liquid on Prototropic and Solvatochromic Behavior of Fluorescein. *J. Phys. Chem. B* 2010, *114*, 15042-15051.
38. Klonis, N.; Clayton, A. H.; Voss, E. W., Jr.; Sawyer, W. H. Spectral Properties of Fluorescein in Solvent-Water Mixtures: Applications as a Probe of Hydrogen Bonding Environments in Biological Systems. *Photochem. Photobiol.* 1998, *67*, 500-510.
39. Mordon, S.; Devoisselle, J. M.; Maunoury, V. In Vivo pH Measurement and Imaging of Tumor Tissue Using a pH-Sensitive Fluorescent Probe (5,6-Carboxyfluorescein): Instrumental and Experimental Studies. *Photochem. Photobiol.* 1994, *60*, 274-279.
40. Khodorov, B.; Valkina, O.; Turovetsky, V. Mechanisms of Stimulus-Evoked Intracellular Acidification in Frog Nerve Fibres. *FEBS Lett.* 1994, *341*, 125-127.
41. Han, J.; Burgess, K. Fluorescent Indicators for Intracellular pH. *Chem. Rev.* 2010, *110*, 2709-2728.

42. Trubetskoy, V. S.; Slattum, P. M.; Hagstrom, J. E.; Wolff, J. A.; Budker, V. G. Quantitative Assessment of DNA Condensation. *Anal. Biochem.* 1999, *267*, 309-313.
43. Van Rompaey, E.; Chen, Y.; Muller, J. D.; Gratton, E.; Van Craenenbroeck, E.; Engelborghs, Y.; De Smedt, S.; Demeester, J. Fluorescence Fluctuation Analysis for the Study of Interactions between Oligonucleotides and Polycationic Polymers. *Biol. Chem.* 2001, *382*, 379-386.
44. Trubetskoy, V. S.; Hagstrom, J. E.; Budker, V. G. Self-Quenched Covalent Fluorescent Dye-Nucleic Acid Conjugates as Polymeric Substrates for Enzymatic Nuclease Assays. *Anal. Biochem.* 2002, *300*, 22-26.
45. Cakara, D.; Kleimann, J.; Borkovec, M. Microscopic Protonation Equilibria of Poly(Amidoamine) Dendrimers from Macroscopic Titrations. *Macromolecules* 2003, *36*, 4201-4207.
46. Lando, D. Y.; Teif, V. B. Modeling of DNA Condensation and Decondensation Caused by Ligand Binding. *J. Biomol. Struct. Dyn.* 2002, *20*, 215-222.
47. Bagai, S.; Sun, C. B.; Tang, T. Potential of Mean Force of Polyethylenimine-Mediated DNA Attraction. *J. Phys. Chem. B* 2013, *117*, 49-56.
48. Delgado, A. V.; Gonzalez-Caballero, E.; Hunter, R. J.; Koopal, L. K.; Lyklema, J. Measurement and Interpretation of Electrokinetic Phenomena - (IUPAC Technical Report). *Pure Appl. Chem.* 2005, *77*, 1753-1805.
49. Shcharbin, D.; Pedziwiatr, E.; Bryszewska, M. How to Study Dendriplexes I: Characterization. *J. Control. Release* 2009, *135*, 186-197.
50. Lakowicz, J. R. 3rd ed.; Springer: New York, 2006; p xxvi, 954 p.
51. Pavan, G. M.; Mintzer, M. A.; Simanek, E. E.; Merkel, O. M.; Kissel, T.; Danani, A. Computational Insights into the Interactions between DNA and siRNA with "Rigid" and "Flexible" Triazine Dendrimers. *Biomacromolecules* 2010, *11*, 721-730.
52. Sun, C. B.; Tang, T.; Uludag, H. Molecular Dynamics Simulations for Complexation of DNA with 2 kDa PEI Reveal Profound Effect of PEI Architecture on Complexation. *J. Phys. Chem. B* 2012, *116*, 2405-2413.
53. Ziebarth, J. D.; Wang, Y. M. Understanding the Protonation Behavior of Linear Polyethylenimine in Solutions through Monte Carlo Simulations. *Biomacromolecules* 2010, *11*, 29-38.
54. Borkovec, M.; Koper, G. J. M. Proton Binding Characteristics of Branched Polyelectrolytes. *Macromolecules* 1997, *30*, 2151-2158.
55. Bielinska, A. U.; Kukowska-Latallo, J. F.; Baker, J. R., Jr. The Interaction of Plasmid DNA with Polyamidoamine Dendrimers: Mechanism of Complex Formation and Analysis of Alterations Induced in Nuclease Sensitivity and Transcriptional Activity of the Complexed DNA. *Biochim. Biophys. Acta.* 1997, *1353*, 180-190.
56. Ainalem, M. L.; Bartles, A.; Muck, J.; Dias, R. S.; Carnerup, A. M.; Zink, D.; Nylander, T. DNA Compaction Induced by a Cationic Polymer or Surfactant Impact Gene Expression and DNA Degradation. *PLOS One* 2014, *9*, e92692.

CHAPTER 4 NUCLEIC ACID CATALYSIS IN PRESENCE OF POLYCATIONIC POLYMERS

4.1 Introduction

4.1.1 Catalytic Nucleic Acids

The discovery that RNA could catalyze reactions independent of proteins[1,2] formed the basis of the 'RNA World' hypothesis. According to this hypothesis, existing life evolved from organisms whose machinery was dependent solely on RNA molecules capable of both genetic coding and catalysis.[3] All catalytic RNA molecules (ribozymes) identified so far have been assigned to 11 distinct classes.[4] Some of the naturally occurring catalytic RNA molecules have well known cellular roles such as protein synthesis (RNA subunit in the ribosome),[5] splicing (group I and II introns),[6,7] and tRNA processing (RNaseP that occurs as a RNA-protein complex).[2] The roles of few ribozymes in gene regulation have also been identified.[8-11] However, biological functions of several other ribozymes, especially those identified as small self-cleaving motifs (nucleolytic ribozymes) that occur in diverse bacterial and eukaryotic species and genetic contexts,[4,12-14] are yet to be recognized and clarified. While the naturally occurring ribozymes identified so far all catalyze phosphoryl transfer reactions (except ribosomal RNA that catalyzes amino acyl transfer), ribozymes capable of catalyzing chemically different reactions have also been created using *in vitro* selection methods. Examples include RNA that can catalyze Diels-Alder reaction,[15] Michael addition,[16] and aldol condensation.[17,18]

The discovery of ribozymes has also fuelled much research interest towards understanding RNA structure-function relationship as these catalytic molecules fold into intricate 3D structures in order to achieve the perfect geometry needed to catalyze the specific reactions.[19-21] Due to their ability to catalyze sequence-specific cleavage, ribozymes have been also explored as nucleic acid based therapeutics.[22] In addition, based on the knowledge of catalytic RNA, different catalytic DNA (deoxyribozymes) has also been designed for several applications even though the latter are not known to exist naturally.[23-25]

The phosphoryl transfer reaction catalyzed by nucleolytic ribozymes is a S_N2 trans esterification reaction in which the O2' of a ribose attacks the adjacent 3' phosphate yielding cleaved sequences containing a 2', 3'–cyclic phosphate and 5'-OH (Scheme 4-I).[26] These ribozymes also catalyze the reverse reaction (ligation). Even though these ribozymes catalyze the same basic reaction and appear to have similar geometry at the catalytic site, the reaction is highly sequence specific and the ribozymes belonging to different classes adopt different global architectures in order to orient the catalytic sites.[19,26,27] The reaction mechanism of nucleolytic enzymes fall into the general theme of acid base catalysis with the nucleobases acting as general acid or base and except in few cases, Mg^{2+} is thought to only play a structural role.[26] Another interesting feature of ribozymes and complex RNA structures in general, is that the pKa of the nucleobases in the active sites are often significantly shifted from values in free or unstructured forms. This has been explained based on differences in the local electrostatic environment arising due to the relative positioning of negatively charged phosphate groups.[26,28,29] How these RNA achieve such shifted pKa values is a matter of significant interest because protonated/deprotonated states of nucleobases are implicated to act as general acid/base in catalysis of nucleolytic ribozymes. [26,27]

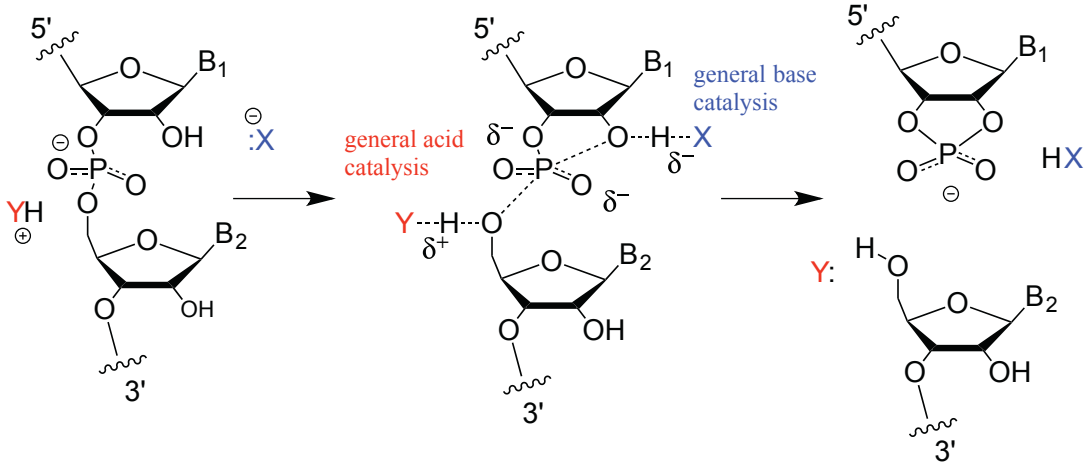

Scheme 4-I Trans esterification reaction catalyzed by nucleolytic ribozymes.

4.1.2 Effect of Charged Polyelectrolytes on Catalysis

Driven by several biotechnological and biomedical applications, there has been significant interest in assembly of protein enzymes on bulk interfaces, hard and soft nanoparticles, or lipid vesicles.[30] The nature of the interacting surface (hydrophobicity/hydrophillicity, surface charge density, covalent modifications e.t.c) can significantly influence protein folding and catalytic activity.[31] Protein enzymes interacting with charged surfaces (or polyelectrolyte coated surfaces) can show enhancement or reduction/inhibition of catalytic activity depending on whether the surface is positively or negatively charged and the overall charge on the protein.[32-34 35] In addition, there are increasing number of reports showing that nanosized charged surfaces accelerate enzymatic activity as opposed to bulk interfaces.[36] However, similar studies for nucleic acid enzymes are rare, primarily because their chemical repertoire of nucleic acid enzymes is not as diverse as that of protein enzymes. Nonetheless, they are capable of catalyzing important classes of chemical reactions described in section 4.1.1 that can go beyond therapeutic application of nucleolytic cleavage, for example in chemical sensing and nanobiotechnological applications.[37]

As has been observed for protein enzymes [30] effects on the global fold of nucleic acid enzymes can be expected upon interaction with polyelectrolyte surfaces. As discussed in the section 1.2 of Chapter 1, since nucleic acids are polyelectrolytes themselves, there is a complex interplay of nucleic acid structure and its counterion environment, which can be modulated by binding to oppositely charged polyelectrolytes in ways not yet completely understood. Additionally the local solvent environment, pH, pKa at charged interfaces are known to be significantly different from bulk (Chapter 3).[30] This can have a direct impact on the catalytic activity of nucleic acid enzymes as they depend strongly on the microenvironment of their catalytic sites. Another important aspect is polyelectrolyte exchange; in particular for polycationic polymers (POPC) mediated delivery of ribozymes or deoxyribozymes for therapeutic application because both protection and release of bound nucleic acid is necessary for effective function.[38-41]

Recently, enhanced catalytic activity of a 10-23 deoxyribozyme in presence of cationic comb type copolymer was reported by Gao *et al.* under substrate excess conditions.[42] On the other hand, in an earlier study by Wu *et al.*[43] reduced product yields of a Candida ribozyme in presence of triethanolamine core dendrimers in a generation dependent manner was reported. Although the mechanisms behind these different observations remain to be understood, this suggests that both polycation structure and the catalytic nucleic acid structure are intricately related in defining the functional role of polyplex systems. Here, we set out to explore how the interaction with POCP influences the structure and activity of a ribozyme (env22 twister) belonging to the twister class, a recently discovered class of nucelolytic ribozymes that are relatively small in size and seem to follow general acid/base catalysis by nucleobases.[14] We chose this ribozyme, as its 3D structure has been determined via X-ray crystallography [44] clearly showing long-range tertiary contacts important for catalysis. Knowledge of these tertiary contacts helps us to predict, using TOPRNA simulations, mutations distant from active sites that can play a role in catalysis The secondary and tertiary structure of env22 twister (twister, in short) used in this study is shown in Figure 4.1. We also tested how small structural mutations in one of the helices of the ribozyme, predicted by TOPRNA simulations to affect the tertiary contacts in the ribozyme, can affect the catalytic activity upon polyplex formation.

We find that the interaction with the POCP does not disrupt preformed tertiary contacts of the twister ribozyme as judged based on NMR studies and that the ribozyme is able to fold and thus function in presence of POCP. Consistent with Gao *et al.*'s results under multiple turnover conditions,[42] we also observed significantly enhanced rate and product yield with wild type twister in presence of POCP. However, this trend was not maintained for catalytically active twister mutants that topologically disfavor the native tertiary structure, even when the mutations were small and distant from the active site. The observed (apparent) rates and yields in presence of POCP were significantly different for the different mutants, with enhanced rates observed only for those mutants that were less or as active compared to the wild type in absence of POCP. In addition, different yields were observed for different POCP type. For the POCPs the yields correlated with the ability of the POCP to exchange as well as the

acidity of the local microenvironment. This strongly highlights the role of structural details of polyplex components, intermolecular exchange, as well as local solvent microenvironment in modulating ribozyme catalysis. Additionally, from a practical application point of view, ability of twister ribozymes to function, and in some instances be catalytically enhanced, also demonstrates that two POCPs used in this study, PAMAM dendrimers and lPEI, can be used for delivery of twister ribozymes for therapeutic applications.

4.1.3 Twister Ribozyme Structure

The twister ribozyme motif has been identified in bacteria and several eukaryotic species as relatively short sequences occurring in genetic contexts very similar to that of hammerhead ribozymes.[14] They were found to have high catalytic rates,[14] comparable to the fastest cleaving hammerhead ribozymes[45] and ~100-500 fold faster than other self-cleaving ribozymes of comparable sizes.[46,47] However, the mechanism of catalysis of this class of ribozyme is still under investigation.[48,49] The twister construct employed in this study is a bimolecular construct of env22 twister[44] comprising a 19-nt substrate strand (S) and a 37-nt strand, which will be called the ribozyme strand (Rz) (Figure 4.1). The secondary structure of the bimolecular construct of twister employed in this study comprises; an apical loop, four helixes (P1, H1, H2, H3), a three-way junction connecting P1, H3, and H2, an internal loop joining H2 and H1 and containing the cleavage site (U5-A6). Biochemical studies have shown that the long-range base pairing interactions are essential for the catalytic activity of the twister. In the presence of Mg^{2+}, the ribozyme-substrate complex (RzS) folds into a catalytically active structure forming five long-range Watson-Crick and one non-canonical base pair, as depicted in the crystal structure (Figure 4.1 b).[44]

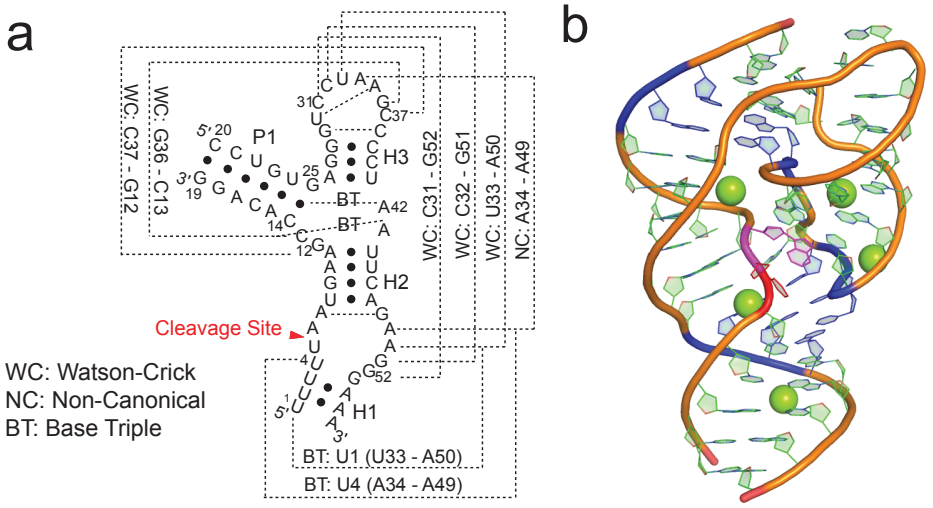

Figure 4.1 Structure of env22 twister (a) Secondary structure of env22 twister RzS complex with dotted lines showing tertiary contacts observed in crystal structure (b) Crystal structure (PDB 4OIJ) of env22 twister with base pairs in tertiary contacts shown in blue. The UA cleavage site is colored red and pink. Green balls represent Mg^{2+} ions

4.2 The Tertiary Structre of Wild Type Twister is not Disrupted upon POCP Interaction at Low N:P

It has generally been implied from studies based on CD spectroscopy and IR that the secondary structure of nucleic acids in polyplexes is not significantly altered.[50-53] However, atomic-resolution studies providing information on the local structure of nucleic acids in polyplex form is scarce in the literature.[54-58] Our recent atomic-resolution study based on NMR showed that while the highly stable structure of A-form helices are not significantly perturbed, the flexible regions such as the single stranded loop and bulge regions are amenable to changes in the local chemical environment upon POCP interaction.[57]

Much less is known about how POCP interactions might influence RNA tertiary structure and catalytically important bound metals. Such larger RNA molecules rely on the collective interactions of the highly dynamic loop and bulge regions to form long-range base pairs, stabilized by metal cations, to form precise 3D structures capable of catalysis. To test whether interaction with a polycationic polymer alters the critical base pairing interactions involved in the tertiary contacts of twister, imino proton spectra of a two piece twister construct (pre-folded in presence of Mg^{2+}) was collected upon titration

with G5 PAMAM with ~10% of the primary amines conjugated to 5 kDa poly(ethyleneglycol) (G5-PEG). PEGylation of the POCP has been previously shown to reduce aggregation and subsequent precipitation frequently observed at the high concentrations necessary for NMR measurements.[57,58] The substrate strand was synthesized with deoxy sugar at the U5 residue in order to prevent cleavage activity during NMR experiments.[44]

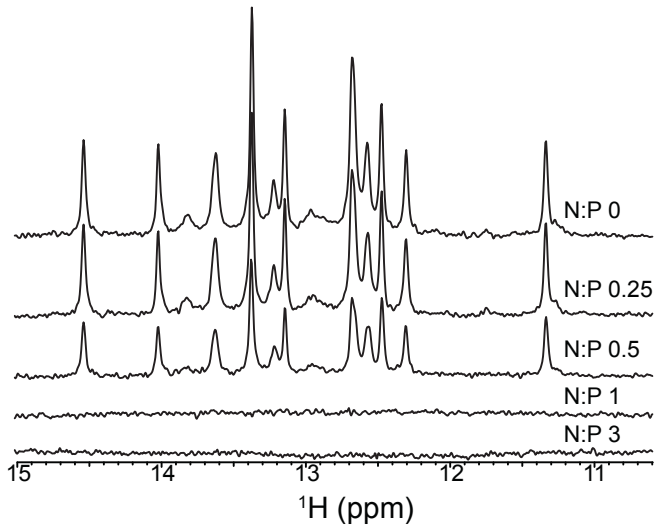

Figure 4.2 Effect of G5-PEG on the tertiary base pairs of twister. Proton NMR spectrum of twister in presence of Mg^{2+} upon titration of G5-PEG under to increasing N:P. The spectra as collected at 25°C on an 800 MHz Varian instrument. Buffer used was 10 mM sodium phosphate, pH 6.4, 0.01mM EDTA.

The imino proton region (chemical shift range ~10-15 ppm) of 1D NMR spectrum was collected to obtain evidence for base pair formation. Each peak in this region represents a base pair arising due to hydrogen bonding of the imino protons of Guanine and Uracil bases. Upon annealing of the substrate strand with the ribozyme strand, additional imino peaks are observed indicating hybridization between the two strands and secondary structure formation. After adding Mg^{2+} several new imino proton peaks appear which indicates formation of long-range tertiary base pairs in addition to secondary structure base pairs shown in Figure 4.2. These imino proton signals of the RzS pre-folded in presence of Mg^{2+} decreases in intensity upon adding increasing amounts of G5-PEG to increasing N:P indicating polyplex

formation. However, no significant chemical shift perturbation was observed indicating that all base pairs of the observed free RzS at N:P <1 remain intact, i.e both secondary and tertiary structure of twister is not affected. The disappearance of resonances indicates formation of large polyplex particles in which the RNA structure could potentially be altered, especially if the exchange between free and bound states was slow on the NMR timescale. While this suggests that the free RNA observed at N:P < 1 can still be catalytically active, the effects on twister catalysis cannot be predicted at N:P > 1 as all the imino signals were broadened out of detection.

4.3 Twister is Catalytically Active upon Formation of Polyplex Nanoparticles

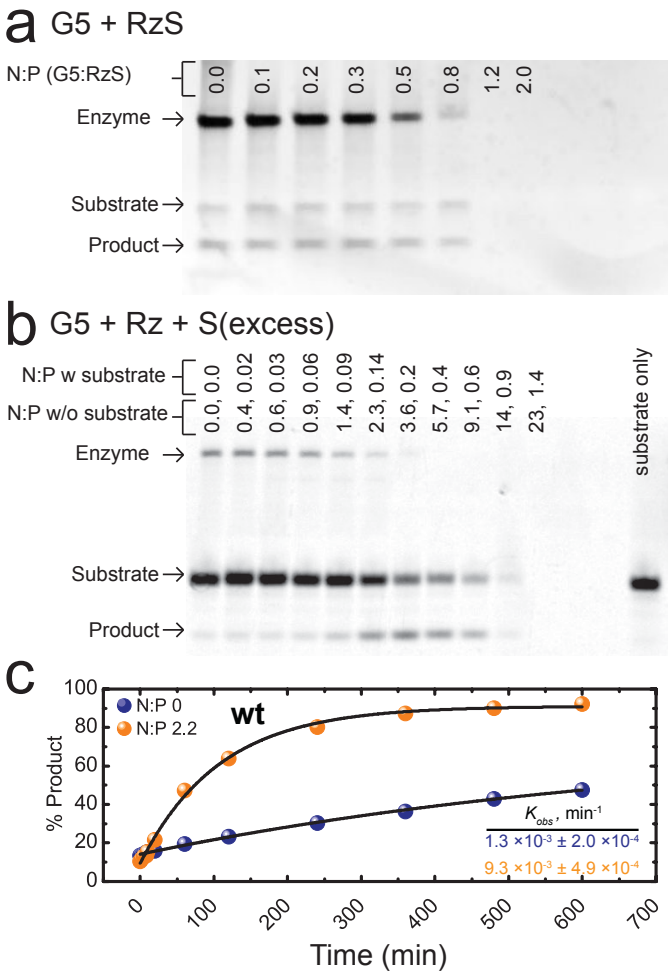

Figure 4.3 Twister activity in presence of polyplexes with G5 (a) Denaturing PAGE analysis of activity when polyplex is prepared with preannealed RzS at different N:P. The reaction (at 25°C) was stopped 5 min after addition of Mg^{2+} (final concentration of 10mM). The expected 5-nt product is not observable as it doesn't stain well with nucleic acid binding dyes owing to the small size (b) Denaturing PAGE analysis of activity when preformed polyplexes of G5 and Rz at different N:P are treated with excess substrate in presence of Mg^{2+} (final concentration of 10mM). The reaction was stopped after 1hr of incubation at 37°C. N:P w/o substrate represents N:P ratio with respect to only the Rz strand. N:P w substrate represents N:P ratio taking into account the added excess substrate (c) Observed rate of product formation in absence (N:P 0) and in presence of polyplexes (N:P 2.2) under the reaction conditions used in (b), see Scheme 4-II. The reaction buffer for all experiments contained 30 mM HEPES, 100 mM KCl at pH 7.5.

As follows from NMR experiments, preformed 1:1 RzS complex was expected to be active upon interaction with G5 at low N:P. Indeed, we observe product formation in activity assays (Figure 4.3a). At higher N:P ratios, retardation of electrophoretic mobility of polyplex precludes analysis of product formation. The next set of conditions tested is illustrated in Scheme 4-II in which the Rz strand was first assembled in the polyplex with G5 at different N:P ratios and subsequently allowed to exchange and react with excess of substrate strand (30 fold). This design strategy was adopted envisioning delivery of Rz/POCP complex to target specific substrate RNA. As the overall concentration of S was in excess over the Rz used to form polyplex, this mimics a multiple turnover enzymatic reaction, given that the Rz bound to the POCP is exchanged and becomes available to react with the excess substrate. Figure 4.3 b shows the denaturing PAGE analysis of the cleavage reaction under these conditions. The 14-nt product is clearly observable up to N:P 14 with respect to Rz strand in the preformed polyplex (0.9 accounting for the added substrate to the Rz/G5 polyplex solution). Beyond this ratio, migration of all of the RNA content is retarded as expected in presence of excess POCP owing to the net positive charge. The observations illustrates two important points: even at N:P much higher than 1:1 with respect to Rz strand 1) the bound Rz strand is able to exchange with the added substrate 2) the RzS complex is able to

form and fold into catalytically active conformation in presence of G5. The more interesting observation, is that at N:P ratios > 1.4 with respect to Rz, the product yield is much higher than in absence of G5. The observed rates of product formation was ~an order of magnitude higher when G5 was present (Figure 4.3 c). Multiple thermodynamic and kinetic effects could result into such high activity of the twister as the process involves multiple steps; intermolecular exchange of bound RNA, stabilization of helices and tertiary structure formation, cleavage reaction, and product release. Moreover, increase in local pH (as discussed in Chapter 3) could also contribute to enhanced rates. Gao *et al.*[42] from the analysis of observed rates under single turnover conditions (when the total concentrations of substrate and enzyme was similar) vs multiple turnover (when the enzyme was in excess), concluded that the enhanced activity was due to the polymer promoting turnover and not the chemical cleavage step. Here our goal is not to deconvolute the effects on the kinetic steps, given the complexity of the system. Instead we focus on establishing whether such observations can be generalized for different POCPs, reinforcing the general view of non-specificity of polycation/polyanion interactions or knowing if subtle changes in structure of the constituents play a role.

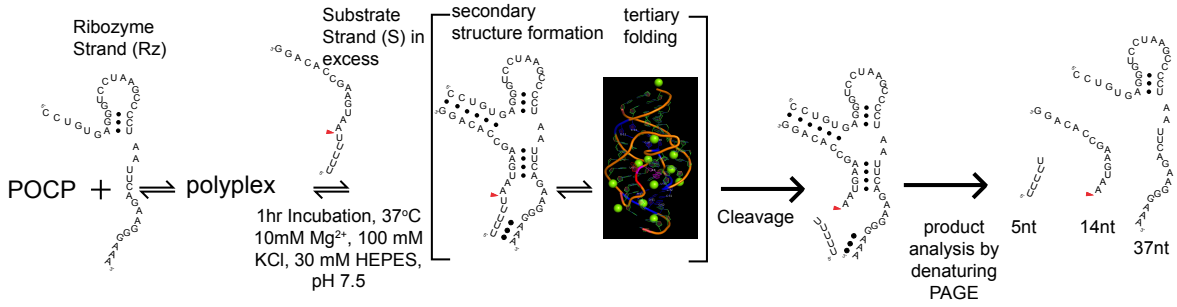

Scheme 4-II Experimental design of twister cleavage reaction under multiple turnover conditions in presence of POCP

4.4 POCPs that Favour Exchange of RNA Promote Activity

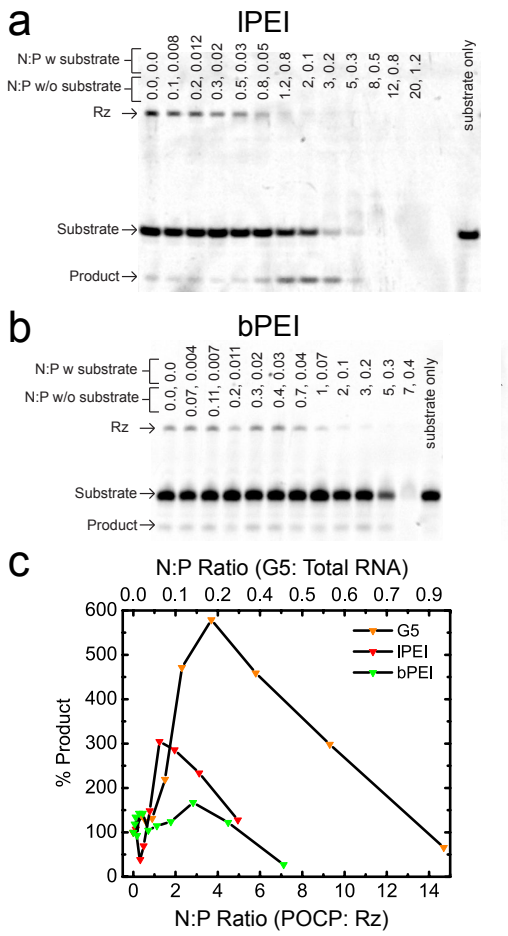

Figure 4.4 Comparison of twister activity in presence of different POCP under multiple turnover conditions. Denaturing PAGE analysis of cleavage reactions at different N:P ratios after 1 hr incubation at 37°C in presence of (a) lPEI (b) bPEI. (c) Quantitative comparison of amount of product formed in presence of G5, lPEI, and bPEI.

As discussed in Chapter 2 and from the review of polyelectrolyte complexes in general, intermolecular (interpolymer) exchange is an important property of polyplexes, which is highly dependent on the properties of the constituent polymers. We had previously observed based on fluorescence quenching assays that three POCPs (G5, bPEI, lPEI) with similar size (~25 kDa) were significantly different in their ability to exchange bound TAR RNA in solution at a given N:P. The amount of RNA exchanged (released) was significantly higher for lPEI compared to bPEI, which has chemically similar monomer units but differs in branching topology from lPEI. For G5 polyplexes, the

amount exchanged was intermediate therefore allowing us hypothesize that if RNA release was a limiting factor, the apparent product yield would be highest for lPEI as at any given time the concentration of Rz strand available for catalysis would be greatest for lPEI. Consistent with this hypothesis we observed that the product yield after 1hr incubation at 37°C, was the higher for lPEI, while bPEI did not show any yield enhancement at any N:P when the activity was tested using Scheme 4-II. However, the product yield was highest for G5 compared to lPEI and bPEI, suggesting that while polyplex exchange is important, chemical nature of the POCP itself may also contribute to the observed yields.

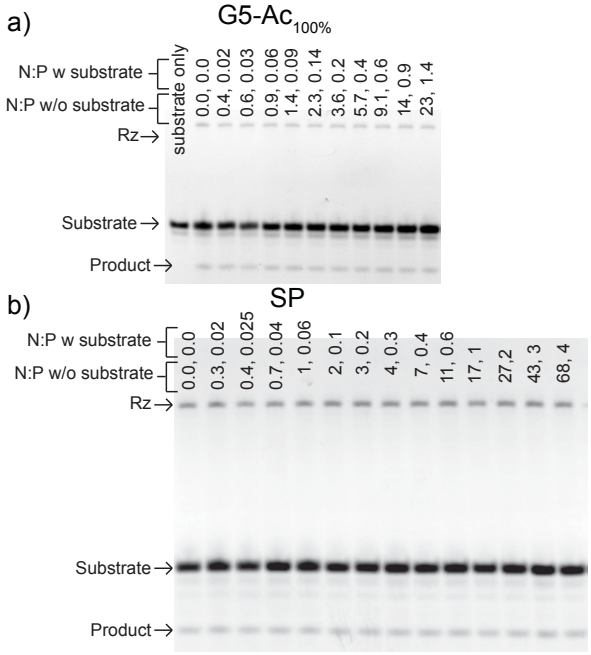

Figure 4.5 Effect of cation charge on twister activity. (a) In absence of cation charge. The primary amines on G5 were fully acetylated making the polymer unable to protonate at pH 7.5 (b) In presence of spermidine, which has two primary amines and one secondary amine capable of being protonated at physiological pH. The cleavage cleavage reaction was analyzed after 1hr incubation at 37°C under conditions mentioned above.

Additionally we observed no increased yield in presence of the small molecule cation spermidine (+3) or when there were no charges present in the polymer (fully acetylated G5). This indicates that the polyplex structure itself plays a key role, as it is well known that sufficient amount of cationic charge is

necessary in order to form such hierarchical complexes. We also provide evidence from DLS for one of the POCPs that nanoparticluate polyplexes are present under the reaction conditions. Interestingly, the average diameter (measured by DLS) remains more or less constant (~400 nm) when the substrate strand is added in excess to preformed polyplexes. However the PDI slightly increases (Figure 4.6). This indicates that the preformed polyplexes are not disintegrated into small particles. Instead the polyplexes could be either forming ternary complexes[59] having both Rz and S or rearrange to similar sized particles after the exchange of bound Rz with added S.

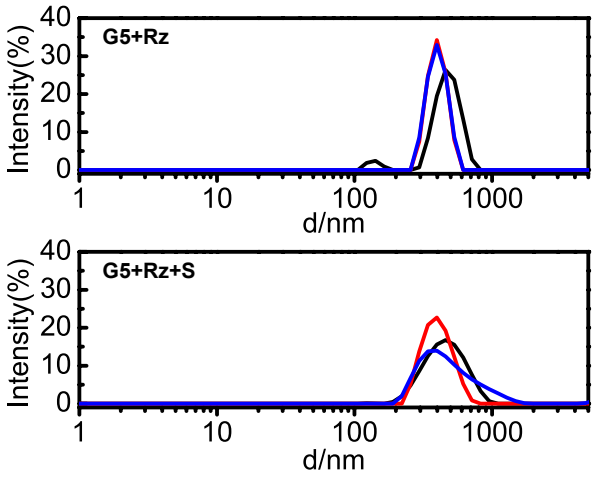

Figure 4.6 Average hydrodynamic diameter (*d*) of polyplexes measured by DLS (a) before (G5+Rz) and (b) after (G5+Rz+S) adding excess substrate at N:P 2.2. Triplicate measurements are reported.

4.5 Helix-3 (H3) Elongation Mutation and the Identity of Nucleotides at Three-way Junction Affects Observed Catalytic Rates and Yield in Presence of POCP

Next we examined whether POCP could rescue the activity of twister mutants that are topologically challenged to form the catalytic competent 3D structure. Using the coarse-grained simulation program TOPRNA (see techniques section of chapter 1), we explored mutations away from the active site that could topologically disfavor folding into the catalytically competent twister tertiary structures by disfavoring the positioning of residues involved in key tertiary interactions. These simulations indicate that the elongation of H3 would disrupt key tertiary contacts thereby potentially reducing overall product yield. We synthesized two-piece versions of these mutants in order to test how the observed

catalytic activity would be affected upon polyplex interaction. Activity assay was performed using the gel electrophoresis assay described earlier. Figure 4.7 shows the observed rates of product formation in presence and absence of G5 for the different mutants. In absence of POCP, interestingly, it was observed that except for +3 bp mutants, all mutants had higher or equal observed apparent rates and product yields compared to the wild type contrary to TOPRNA predictions. Nonetheless, the trend within the mutants themselves follows the prediction that the longer the H3, less active is the mutant owing to the thermodynamic destabilization of catalytically competent tertiary structure. Lower activity of wild type could be due to the less stable secondary structure (annealing) due to fewer base pairs. However, currently, our focus is not on the absolute reaction yield of the RNA mutants compared to the wild type. Instead we focus on the relative catalytic rate and yield of the mutants with and without POCP present.

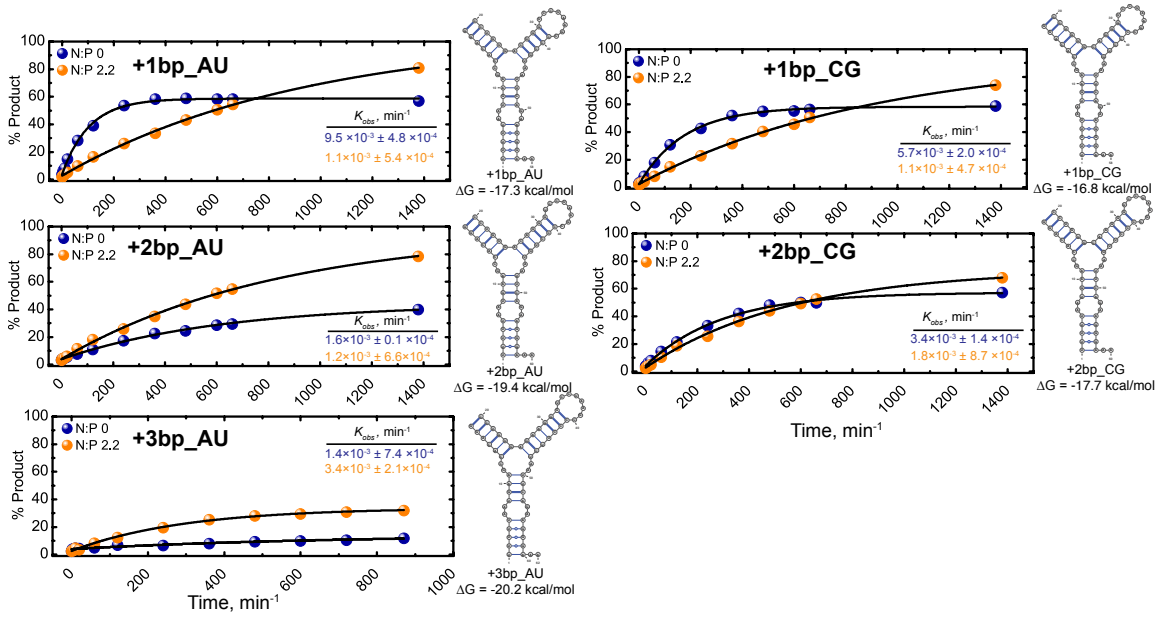

Figure 4.7 Observed rates of product formation of twister mutants elongated by 1-3 bp at helix 3 upon forming polyplexes with G5. H3 mutants with (a) AU (b) CG as the closing base pair at the three-way junction.

Even though polyplexes are generally viewed as non-specific electrostatic complexes we found that surprisingly subtle changes to the RNA sequence lead to drastically different responses of the catalysis to

the presence of polymer. In the case of the wild type RNA, we found that the reaction rate ***increased*** by an order of magnitude when POCP was added to the solution at an N:P of 2.2 (Figure 4.3). Surprisingly, this affect was not consistently observed in the cases of the mutants. Instead, elongation of H3 by a single-base pair (either AU or CG) lead to ***decrease*** of the apparent reaction rate by an order of magnitude for AU and five fold for CG compared to that in absence of POCP. Further elongation by 2 base pairs results in reaction rates that are nearly identical with and without the presence of polymer, and elongation by 3 base pairs recovers the trend observed in the wild type RNA.

The unexpected trend observed in Figure 4.7 adds to the evolving picture of polyplexes as complex structures that continually evade generalization. It is worth noting that the NMR data presented above is specific to low N:P. Direct observations of chemical shifts through NMR are not possible at the N:P ratios used in the catalysis experiments, however functional 3-dimensional folding and tertiary contacts must persist at these higher N:P as catalysis is still observed. While the NMR experiments suggest that the presence of polymers does not influence the structure and folding of the RNA, these results open the possibility that at higher concentrations the polymer can play an active role the RNA structure and catalysis. While the results are preliminary, the work suggests that a systematic engineering of dendrimers can strongly influence catalysis rates and yields, and that an appropriate approach to such engineering must take into account the mutual surface interactions between the RNA and polymer.

4.6 Conclusions

Based on results above following conclusions have been made 1) the long range tertiary contacts (base pairs) formed by twister in presence of Mg^{2+} are not disrupted due to interaction with the POCP at low N:P 2) Assembly of RNA chains into polyplex nanoparticles is essential for enhancement in activity 3) Only polyplexes that readily exchange bound RNA show significant enhancement of product formation 4) Small changes in the secondary structure of RNA can lead to drastic changes in observed rates and yields in presence of POCP. While, the effect of the POCP was predictable stemming from our results described in section 2.1.1.10 of Chapter 2, significant differences in observed rates and yields of the mutants in presence of the POCP were unexpected. This strongly highlights that polyplexes cannot

be simply viewed as non-specific assembly of positive and negative charges and that more advanced studies that elucidate the structure and dynamics of the interaction is necessary in order to develop these systems as successful delivery agents.

4.7 References

1. Kruger, K.; Grabowski, P. J.; Zaug, A. J.; Sands, J.; Gottschling, D. E.; Cech, T. R. Self-Splicing RNA: Autoexcision and Autocyclization of the Ribosomal RNA Intervening Sequence of Tetrahymena. *Cell* 1982, *31*, 147-157.
2. Guerrier-Takada, C.; Gardiner, K.; Marsh, T.; Pace, N.; Altman, S. The RNA Moiety of Ribonuclease P Is the Catalytic Subunit of the Enzyme. *Cell* 1983, *35*, 849-857.
3. Lilley, D. M.; Sutherland, J. The Chemical Origins of Life and Its Early Evolution: An Introduction. *Philos. Trans. R Soc. Lond. B Biol. Sci.* 2011, *366*, 2853-2856.
4. Weinberg, Z.; Kim, P. B.; Chen, T. H.; Li, S.; Harris, K. A.; Lunse, C. E.; Breaker, R. R. New Classes of Self-Cleaving Ribozymes Revealed by Comparative Genomics Analysis. *Nat. Chem. Biol.* 2015, *11*, 606-610.
5. Nissen, P.; Hansen, J.; Ban, N.; Moore, P. B.; Steitz, T. A. The Structural Basis of Ribosome Activity in Peptide Bond Synthesis. *Science* 2000, *289*, 920-930.
6. Cech, T. R. Self-Splicing of Group I Introns. *Annu. Rev. Biochem.* 1990, *59*, 543-568.
7. Michel, F.; Ferat, J. L. Structure and Activities of Group Ii Introns. *Annu. Rev. Biochem.* 1995, *64*, 435-461.
8. Teixeira, A.; Tahiri-Alaoui, A.; West, S.; Thomas, B.; Ramadass, A.; Martianov, I.; Dye, M.; James, W.; Proudfoot, N. J.; Akoulitchev, A. Autocatalytic RNA Cleavage in the Human Beta-Globin Pre-mRNA Promotes Transcription Termination. *Nature* 2004, *432*, 526-530.
9. Winkler, W. C.; Nahvi, A.; Roth, A.; Collins, J. A.; Breaker, R. R. Control of Gene Expression by a Natural Metabolite-Responsive Ribozyme. *Nature* 2004, *428*, 281-286.
10. Salehi-Ashtiani, K.; Luptak, A.; Litovchick, A.; Szostak, J. W. A Genomewide Search for Ribozymes Reveals an HDV-Like Sequence in the Human Cpeb3 Gene. *Science* 2006, *313*, 1788-1792.
11. Martick, M.; Horan, L. H.; Noller, H. F.; Scott, W. G. A Discontinuous Hammerhead Ribozyme Embedded in a Mammalian Messenger RNA. *Nature* 2008, *454*, 899-902.
12. Webb, C. H.; Luptak, A. HDV-Like Self-Cleaving Ribozymes. *RNA Biol.* 2011, *8*, 719-727.
13. Perreault, J.; Weinberg, Z.; Roth, A.; Popescu, O.; Chartrand, P.; Ferbeyre, G.; Breaker, R. R. Identification of Hammerhead Ribozymes in All Domains of Life Reveals Novel Structural Variations. *PLOS Comput. Biol.* 2011, *7*, e1002031.
14. Roth, A.; Weinberg, Z.; Chen, A. G.; Kim, P. B.; Ames, T. D.; Breaker, R. R. A Widespread Self-Cleaving Ribozyme Class Is Revealed by Bioinformatics. *Nat. Chem. Biol.* 2014, *10*, 56-60.
15. Seelig, B.; Jaschke, A. A Small Catalytic RNA Motif with Diels-Alderase Activity. *Chem. Biol.* 1999, *6*, 167-176.

16. Sengle, G.; Eisenfuhr, A.; Arora, P. S.; Nowick, J. S.; Famulok, M. Novel RNA Catalysts for the Michael Reaction. *Chem. Biol.* 2001, *8*, 459-473.
17. Oberhuber, M.; Joyce, G. F. A DNA-Templated Aldol Reaction as a Model for the Formation of Pentose Sugars in the RNA World. *Angew. Chem. Int. Ed. Engl.* 2005, *44*, 7580-7583.
18. Fusz, S.; Eisenfuhr, A.; Srivatsan, S. G.; Heckel, A.; Famulok, M. A Ribozyme for the Aldol Reaction. *Chem. Biol.* 2005, *12*, 941-950.
19. Lilley, D. M. Structure, Folding and Mechanisms of Ribozymes. *Curr. Opin. Struct. Biol.* 2005, *15*, 313-323.
20. Woodson, S. A. RNA Folding Retrospective: Lessons from Ribozymes Big and Small. *RNA* 2015, *21*, 502-503.
21. Strobel, E. J.; Watters, K. E.; Loughrey, D.; Lucks, J. B. RNA Systems Biology: Uniting Functional Discoveries and Structural Tools to Understand Global Roles of Rnas. *Curr. Opin. Biotechnol.* 2016, *39*, 182-191.
22. Mulhbacher, J.; St-Pierre, P.; Lafontaine, D. A. Therapeutic Applications of Ribozymes and Riboswitches. *Curr. Opin. Pharmacol.* 2010, *10*, 551-556.
23. Hollenstein, M. DNA Catalysis: The Chemical Repertoire of DNAzyme. *Molecules* 2015, *20*, 20777-20804.
24. Grimpe, B. Deoxyribozymes: New Therapeutics to Treat Central Nervous System Disorders. *Front. Mol. Neurosci.* 2011, *4*, 25.
25. Silverman, S. K. Pursuing DNA Catalysts for Protein Modification. *Acc. of Chem. Res.* 2015, *48*, 1369-1379.
26. Wilson, T. J.; Liu, Y. J.; Lilley, D. M. J. Ribozymes and the Mechanisms That Underlie RNA Catalysis. *Front. Chem. Sci. Eng.* 2016, *10*, 178-185.
27. Cochrane, J. C.; Strobel, S. A. Catalytic Strategies of Self-Cleaving Ribozymes. *Acc. Chem. Res.* 2008, *41*, 1027-1035.
28. Tang, C. L.; Alexov, E.; Pyle, A. M.; Honig, B. Calculation of Pkas in RNA: On the Structural Origins and Functional Roles of Protonated Nucleotides. *J. Mol. Biol.* 2007, *366*, 1475-1496.
29. Chin, K.; Sharp, K. A.; Honig, B.; Pyle, A. M. Calculating the Electrostatic Properties of RNA Provides New Insights into Molecular Interactions and Function. *Nat. Struct. Biol.* 1999, *6*, 1055-1061.
30. Talbert, J. N.; Goddard, J. M. Enzymes on Material Surfaces. *Colloids Surf. B Biointerfaces* 2012, *93*, 8-19.
31. Secundo, F. Conformational Changes of Enzymes Upon Immobilisation. *Chem. Soc. Rev.* 2013, *42*, 6250-6261.
32. You, C.-C.; Agasti, S. S.; De, M.; Knapp, M. J.; Rotello, V. M. Modulation of the Catalytic Behavior of α -Chymotrypsin at Monolayer-Protected Nanoparticle Surfaces. *J. Am. Chem. Soc.* 2006, *128*, 14612-14618.

33. Bhandari, S.; Gupta, V. K.; Singh, H. Enhanced Stabilization of Mungbean Thiol Protease Immobilized on Glutaraldehyde-Activated Chitosan Beads. *Biocatal. Biotransformation* 2009, *27*, 71-77.
34. Lopez-Gallego, F.; Betancor, L.; Hidalgo, A.; Dellamora-Ortiz, G.; Mateo, C.; Fernández-Lafuente, R.; Guisán, J. M. Stabilization of Different Alcohol Oxidases Via Immobilization and Post Immobilization Techniques. *Enzyme Microb. Technol.* 2007, *40*, 278-284.
35. Bahulekar, R.; Ayyangar, N. R.; Ponrathnam, S. Polyethyleneimine in Immobilization of Biocatalysts. *Enzyme Microb. Technol.* 1991, *13*, 858-868.
36. Johnson, B. J.; Algar, W. R.; Malanoski, A. P.; Ancona, M. G.; Medintz, I. L. Understanding Enzymatic Acceleration at Nanoparticle Interfaces: Approaches and Challenges. *Nano Today* 2014, *9*, 102-131.
37. Navani, N. K.; Li, Y. Nucleic Acid Aptamers and Enzymes as Sensors. *Curr. Opin. Chem. Biol.* 2006, *10*, 272-281.
38. Chen, H. H.; Ho, Y.-P.; Jiang, X.; Mao, H.-Q.; Wang, T.-H.; Leong, K. W. Quantitative Comparison of Intracellular Unpacking Kinetics of Polyplexes by a Model Constructed from Quantum Dot-Fret. *Mol. Ther.* 2008, *16*, 324-332.
39. Thibault, M.; Nimesh, S.; Lavertu, M.; Buschmann, M. D. Intracellular Trafficking and Decondensation Kinetics of Chitosan-pDNA Polyplexes. *Mol. Ther.* 2010, *18*, 1787-1795.
40. Schaffer, D. V.; Fidelman, N. A.; Dan, N.; Lauffenburger, D. A. Vector Unpacking as a Potential Barrier for Receptor-Mediated Polyplex Gene Delivery. *Biotechnol. Bioeng.* 2000, *67*, 598-606.
41. Gabrielson, N. P.; Pack, D. W. Acetylation of Polyethylenimine Enhances Gene Delivery Via Weakened Polymer/DNA Interactions. *Biomacromolecules* 2006, *7*, 2427-2435.
42. Gao, J.; Shimada, N.; Maruyama, A. Enhancement of Deoxyribozyme Activity by Cationic Copolymers. *Biomater. Sci.* 2015, *3*, 308-316.
43. Wu, J.; Zhou, J.; Qu, F.; Bao, P.; Zhang, Y.; Peng, L. Polycationic Dendrimers Interact with RNA Molecules: Polyamine Dendrimers Inhibit the Catalytic Activity of Candida Ribozymes. *Chem. Commun. (Camb)* 2005, 313-315.
44. Ren, A.; Kosutic, M.; Rajashankar, K. R.; Frener, M.; Santner, T.; Westhof, E.; Micura, R.; Patel, D. J. In-Line Alignment and Mg^{2+} Coordination at the Cleavage Site of the Env22 Twister Ribozyme. *Nat. Commun.* 2014, *5*, 5534.
45. Canny, M. D.; Jucker, F. M.; Kellogg, E.; Khvorova, A.; Jayasena, S. D.; Pardi, A. Fast Cleavage Kinetics of a Natural Hammerhead Ribozyme. *J. Am. Chem. Soc.* 2004, *126*, 10848-10849.
46. Emilsson, G. M.; Nakamura, S.; Roth, A.; Breaker, R. R. Ribozyme Speed Limits. *RNA* 2003, *9*, 907-918.
47. Breaker, R. R.; Emilsson, G. M.; Lazarev, D.; Nakamura, S.; Puskarz, I. J.; Roth, A.; Sudarsan, N. A Common Speed Limit for RNA-Cleaving Ribozymes and Deoxyribozymes. *RNA* 2003, *9*, 949-957.
48. Gaines, C. S.; York, D. M. Ribozyme Catalysis with a Twist: Active State of the Twister Ribozyme in Solution Predicted from Molecular Simulation. *J. Am. Chem. Soc.* 2016, *138*, 3058-3065.

49. Wilson, T. J.; Liu, Y.; Domnick, C.; Kath-Schorr, S.; Lilley, D. M. The Novel Chemical Mechanism of the Twister Ribozyme. *J. Am. Chem. Soc.* 2016, *138*, 6151-6162.
50. Braun, C. S.; Vetro, J. A.; Tomalia, D. A.; Koe, G. S.; Koe, J. G.; Middaugh, C. R. Structure/Function Relationships of Polyamidoamine/DNA Dendrimers as Gene Delivery Vehicles. *J. Pharm. Sci.* 2005, *94*, 423-436.
51. Froehlich, E.; Mandeville, J. S.; Kreplak, L.; Tajmir-Riahi, H. A. Aggregation and Particle Formation of tRNA by Dendrimers. *Biomacromolecules* 2011, *12*, 2780-2787.
52. Reyes-Reveles, J.; Sedaghat-Herati, R.; Gilley, D. R.; Schaeffer, A. M.; Ghosh, K. C.; Greene, T. D.; Gann, H. E.; Dowler, W. A.; Kramer, S.; Dean, J. M.; Delong, R. K. mPEG-PAMAM-G4 Nucleic Acid Nanocomplexes: Enhanced Stability, RNase Protection, and Activity of Splice Switching Oligomer and Poly I:C RNA. *Biomacromolecules* 2013, *14*, 4108-4115.
53. Dey, D.; Kumar, S.; Banerjee, R.; Maiti, S.; Dhara, D. Polyplex Formation between Pegylated Linear Cationic Block Copolymers and DNA: Equilibrium and Kinetic Studies. *J. Phys. Chem. B* 2014, *118*, 7012-7025.
54. Sato, Y.; Kim, W. J.; Choi, S. W.; Saito, M.; Kano, A.; Akaike, T.; Maruyama, A. Investigation of DNA Strand Exchange Mechanisms Mediated by Cationic Polymers. *Nucleic Acids Res. Suppl.* 2002, 59-60.
55. Sato, Y.; Kim, W. J.; Saito, M.; Kano, A.; Akaike, T.; Maruyama, A. Cationic Comb-Type Copolymers as an Artificial Nucleic Acid-Chaperone: Spectroscopic Analyses for DNA/Copolymer Interaction. *Nucleic Acids Res. Suppl.* 2003, 129-130.
56. Sato, Y.; Moriyama, R.; Choi, S. W.; Kano, A.; Maruyama, A. Spectroscopic Investigation of Cationic Comb-Type Copolymers/DNA Interaction: Interpolyelectrolyte Complex Enhancement Synchronized with DNA Hybridization. *Langmuir* 2007, *23*, 65-69.
57. Shakya, A.; Dougherty, C. A.; Xue, Y.; Al-Hashimi, H. M.; Holl, M. M. B. Rapid Exchange between Free and Bound States in RNA-Dendrimer Polyplexes: Implications on the Mechanism of Delivery and Release. *Biomacromolecules* 2016, *17*, 154-164.
58. Prevette, L. E.; Nikolova, E. N.; Al-Hashimi, H. M.; Holl, M. M. B. Intrinsic Dynamics of DNA-Polymer Complexes: A Mechanism for DNA Release. *Mol. Pharm.* 2012, *9*, 2743-2749.
59. Meneksedag-Erol, D.; Tang, T.; Uudag, H. Probing the Effect of Mirna on siRNA-PEI Polyplexes. *J. Phys. Chem. B* 2015, *119*, 5475-5486.

CHAPTER 5 NMR STUDIES OF SECONDARY STRUCTURE AND TERTIARY FOLDING OF TWISTER RIBOZYME

5.1 Introduction

Out of eleven naturally occurring classes of ribozymes identified to date, six (hammerhead, hairpin, hepatitis delta virus (HDV), Varkud Satellite (VS), glmS, twister) are self-cleaving (nucleolytic ribozymes).[1,2] Numerous sequences belonging to three classes (HDV, hammerhead, and twister) have been identified in diverse prokaryotic and eukaryotic genomes.[1,3-5] All nucleolytic ribozymes are known to catalyze the same chemical reaction (trans-esterification cleavage of the phosphodiester backbone) despite having different sequences, secondary structure and overall global (tertiary) fold.[2,6] The intricate teritary structures that these ribozymes need to adopt in order to catalyze seemingly simple reactions has generated a lot of interest in understanding the basis of RNA folding.[7,8]

The catalytic strategies employed by these ribozymes have been shown to conform to common theme of general acid-base catalysis utilizing nucleobases.[2,6] As depicted in their atomic resolution structures, a conserved guanine base is positioned close in space to the cleavage site in hammerhead,[9] hairpin,[10,11] glmS,[12,13] and twister[14-16] ribozymes that have been implicated to play the role of a general base although the precise mechanisms are not clear. For e.g. the N1 of guanine has a pKa of ~9.3,[17] therefore expected to be fully protonated at neutral pH and appearing unsuitable for nucleophillic attack of the 2'OH which has an even higher pKa ~13.[18] It has been proposed that guanines can adopt alternate transient tautomeric or ionized forms that can allow proton abstraction from 2'OH.[2,19] An alternative model is stabilization of the developing negative charge in the transition state by the guanines.[20,21] In HDV a hydrated metal ion has been suggested to act as a general base and a cytosine as a general acid.[22-24] In VS ribozymes, while the functional importance of guanines and adenines close to the cleavage site

have been realized, whether they act as acids or bases are not clear.[25,26] pH titration studies of site-specifically substituted nucleobases often demonstrate pKa values highly shifted[21,27] from their expected values in free or in unstructured forms, suggesting that the tertiary folds can stabilize electrostatically different local environment at the catalytic sites.[28] Therefore, atomic resolution techniques like NMR can significantly contribute to understand the site-specific environment[27,29] and dynamics at the active site such as formation of transient tautomeric and anionic bases[30] in order to understand the mechanisms of ribozyme catalysis.

Although recently discovered, there are already several published crystal structures[14-16] on different twister ribozyme sequences, which to some extent conform the initially predicted general secondary and important tertiary contacts in the twister class.[3] Biochemical studies[16,31] revealed an upper and a lower apparent pKa values which has been assigned to be due to the titrable groups of guanine and adenine bases respectively in close contact to the cleavage site. In a recently published computational study[32,33] it was observed that the N1 of the active site guanine and N3 of the active site adenine are positioned to act as a base and acid respectively. More interestingly it was observed that the pKa of N3 of adenine immediately 3' to the scissile phosphate was significantly shifted towards neutrality (by ~5 pKa units) thus providing additional support that nucleobases can have significantly shifted pKa values in complex electrostatic environments. The unexpected participation of N3 as opposed to the usual N1 of adenine was explained on the basis of its unique position of the adenine allowing the N6 to have multiple contacts with nearby phosphates.[6] An NMR study[27] on a mini variant of a different twister sequence also reported shifted pKa values of a ^{13}C2 labeled adenine in a similar position predicted to be involved as a general acid. The same study also revealed that in absence of N1 and N3 of the adenine, catalytic activity was absent indicating the critical role of N1 and N3 of adenine. While the active site guanine has been implicated as the general base, site-specific pKa values in twister ribozymes are not known. The guanine in the crystal structure is involved in a sheared GA basepair, which could potentially adopt transient taturomeric/anionic configuration in order to act as a general base, experimental evidence for which is still pending.

Another aspect that remains to be resolved is the role of Mg^{2+} (and other divalent metals) in catalysis of twister ribozymes. Except for HDV ribozymes, all nucleolytic ribozymes do not appear to involve Mg^{2+} in catalysis.[6] The role of Mg^{2+} is considered to be solely to stabilize the tertiary structure. Within the twister class, however, there is some disagreement on the role of Mg^{2+} ions among the different twister ribozymes studied. A major difference was observed between the crystal structures published by Ren *et al.*[14] (Env22 twister) and by Liu *et al.*[16] (O. Sativa twister). Only in the former, a co-ordination of Mg^{2+} ions to the non-bridging cleavable phosphate was observed that suggested a direct role of Mg^{2+} in the catalytic mechanism. Additional support for direct role of divalent metals in this twister sequence was also provided based on the activity employing phosphothioate modified substrates.[27]

Differences in the alignment of U-A cleavage site was also observed between the structures published in those two studies. While it is possible that difference in sequences can lead to such local differences, or that the crystal structures are simply capturing different structures of comparable energy in the dynamic ensemble, solution NMR studies could help resolve these discrepancies and provide further insights into the mechanism. However, the NMR spectra of ribozymes in general are difficult resolve due to not just the size being large (50 -150 nt) for a regular NMR sample, but also ribozymes sequences tend to have stretches of similar base pair repeats resulting into narrow dispersion of chemical shifts. Thus in absence of specific labeling schemes, obtaining full assignments of such RNA becomes difficult. Here, we initiate NMR studies of a two-piece env22 twister ribozyme (same sequence in the crystal structure published by Ren *et al.*[14]) and obtain insights into the structure and dynamics of this ribozyme under solution conditions.

5.2 Experimental

5.2.1 Solid Phase Synthesis, Deprotection, and Purification of Oligonucleotides and NMR Sample Preparation

The RNA strands were synthesized using solid phase synthesis using standard phosphoramide chemistry using 2' – TBDMS phosphoramidites. The synthesis was performed in a Mermade 6 synthesizer. Base deprotection was performed using the AMA (Ammonia/ Methylamine) reagent using

standard protocols. Deprotection of 2'- TBDMS protecting groups on the sugar was performed using standard protocols employing TEA-HF reagent. Purification was done using C_{18} cartridges purchased from Bioautomation Inc. followed by ethanol precipitation and buffer exchange. For NMR studies, the substrate strand was synthesized with a deoxy uridine at the cleavable uridine position in order to avoid cleavage during NMR studies.

Residue specific and atom specific labeling (^{13}C8/C6) of the enzyme strand was achieved using ^{13}C8/C6 labeled phosphoramides. Similar synthesis and purification protocols were followed as above.

The enzyme (Rz) strand and substrate (S) strands were annealed at high concentrations and presence of salt in order to promote hybridization.

5.2.2 NMR Experiments

1D Mg^{2+} titration experiments and ^{1}H-^{13}C HMQC (Heteronuclear Multiple Quantum Coherence) experiments using the SOFAST (band-Selective Optimized-Flip-Angle Short-Transient) pulse scheme[34,35] were carried out using a 600 mHz Bruker Spectrometer equipped with a cryoprobe. ^{1}H-^{15}N HMQC using the SOFAST pulse scheme and ^{1}H-^{1}H NOESY (Nuclear Overhauser Effect SpectroscopY) experiments were carried out in an 800 mHz Varian Spectrometer equipped with a cryoprobe. Use of the SOFAST pulse scheme enables fast acquisition of NMR which are useful for natural abundance samples which require long acquisition periods other wise to obtain sufficient signal to noise ratio. All NOESY spectra were collected using 150 ms mixing time. All experiments were carried out at 25^{o}C, unless mentioned otherwise. Two sets of buffer conditions were used in the experiments. For the NMR titration experiments to study the effect of Mg^{2+} on the folding of twister, the same buffer condition (30 mM HEPES, pH 7.5, 100 mM KCl) used for cleavage assays were used. However, for the assignment experiments a different buffer (10 mM phosphate buffer, 0.01 mM EDTA, pH 6.4) were used in order to improve the spectra quality.

5.3 Result and Discussion

5.3.1 Comparison of 1D Spectra of Unmodified and 2'-OH Modified Twister

Overlay of 1D ^{1}H spectra of deoxymodified and unmodified env22 twister in absence of Mg^{2+} is shown in Figure 5.1. The two spectra overlay very well suggesting the deoxy modifiation does not alter the hybridization (secondary structure formation) of the two strands, which was expected as it is only a small modification. However, the imino proton resonances were broadened indicating that in absence of Mg^{2+} the secondary structure may not be very stable and partial melting of base pairs allows for rapid exchange of the imino protons with water. In particular, the lower stem region comprising consecutive UA basepairs (U1A56 through U3A54) is expected to be less stable. This is supported by the recently published MD simulations on the same twiser sequence in which the stem was observed to be partially melted.[33]

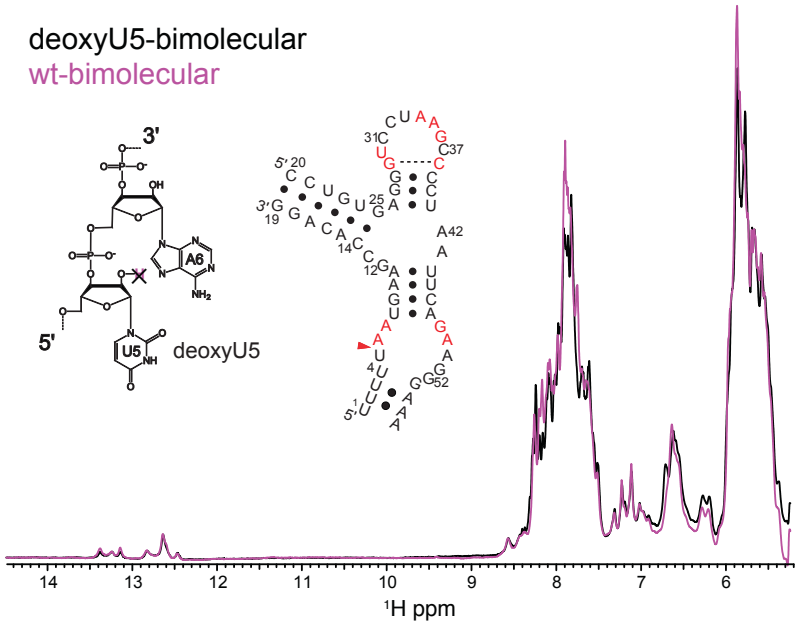

Figure 5.1 Comparison of 1D proton spectra of unmodified and 2'-OH twister bimolecular construct. Buffer conditions were 30mM HEPES at pH 7.5 and100 mM KCl. Spectra were collected at 25°C using excitation sculpting water suppression scheme in a 600 mHz Bruker Spectrometer.

5.3.2 Effect of Mg^{2+}

In presence of 20 mM Mg^{2+} however, many more resonances in the imino proton region emerge (Figure 5.2 a), which can arise both due stabilization of weak base pairs of the secondary structures or

new base pairs representing formation of long range tertiary contact. Mg^{2+} is known to have significant stabilization effects on nucleic acid structures compared to monovalent cations. Although the precise forces and mechanisms behind this significant stabilization are not yet understood fully, both non-specific electrostatic stabilization as well as specific interactions is widely discussed to play a role in stabilization. Control experiments titrating Mg^{2+} into substrate strand and the enzyme strand independently are shown in Figure 5.2 b and c. respectively. The substrate strand does not show any resonances in the imino region upon titrating with Mg^{2+}, suggesting that it does not undergo intra-strand base pairing or dimerization. The enzyme strand shows imino resonances in absence of Mg^{2+}, which is as expected because some intra strand base pairing is possible due to base complementary residues present further apart in sequence, also predicted by RNA folding algorithms. However, only minor perturbations of the imino proton chemical shifts are observed upon addition of Mg^{2+}. These control experiments thus exclude the possibility that the new imino chemical shifts observed upon titration of the annealed complex with Mg^{2+} are as a result of effect of Mg^{2+} on unannealed single strands. Rather, this more likely corresponds to Mg^{2+} induced folding of the ribozyme into a catalytically competent state.

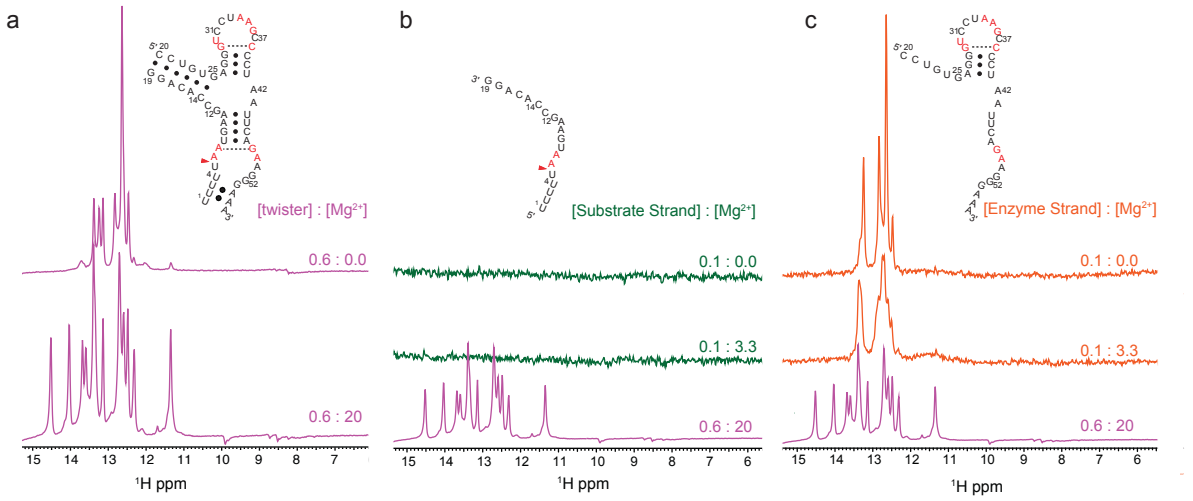

Figure 5.2 Effect of adding Mg^{2+} on the 1D imino proton spectra of twister bimolecular construct. a) Spectra of twister bimolecular construct before (top) and after (bottom) adding Mg^{2+} in the ratio [twister]:[Mg^{2+}] = [0.6 mM]:[20 mM]. b) Control experiment showing effect of Mg^{2+} on substrate

strand only. c) Control experiment showing effect of Mg^{2+} on enzyme strand only. The absolute concentration of RNA in the control experiments were 0.1 mM instead of 0.6 mM, however the relative concentration with respect of Mg^{2+} added was the same compared to the bimolecular construct. Buffer conditions were 30mM HEPES at pH 7.5 and100 mM KCl. Spectra were collected at 25°C using selective excitation of imino protons (SOFAST pulse scheme) using a 600 mHz Bruker Spectrometer

5.3.3 Comparison of C8/C6/C2 Chemical Shift Perturbations in Presence of Mg^{2+} with LARMORD Predictions of Chemical Shifts of the 3D Crystal Structure

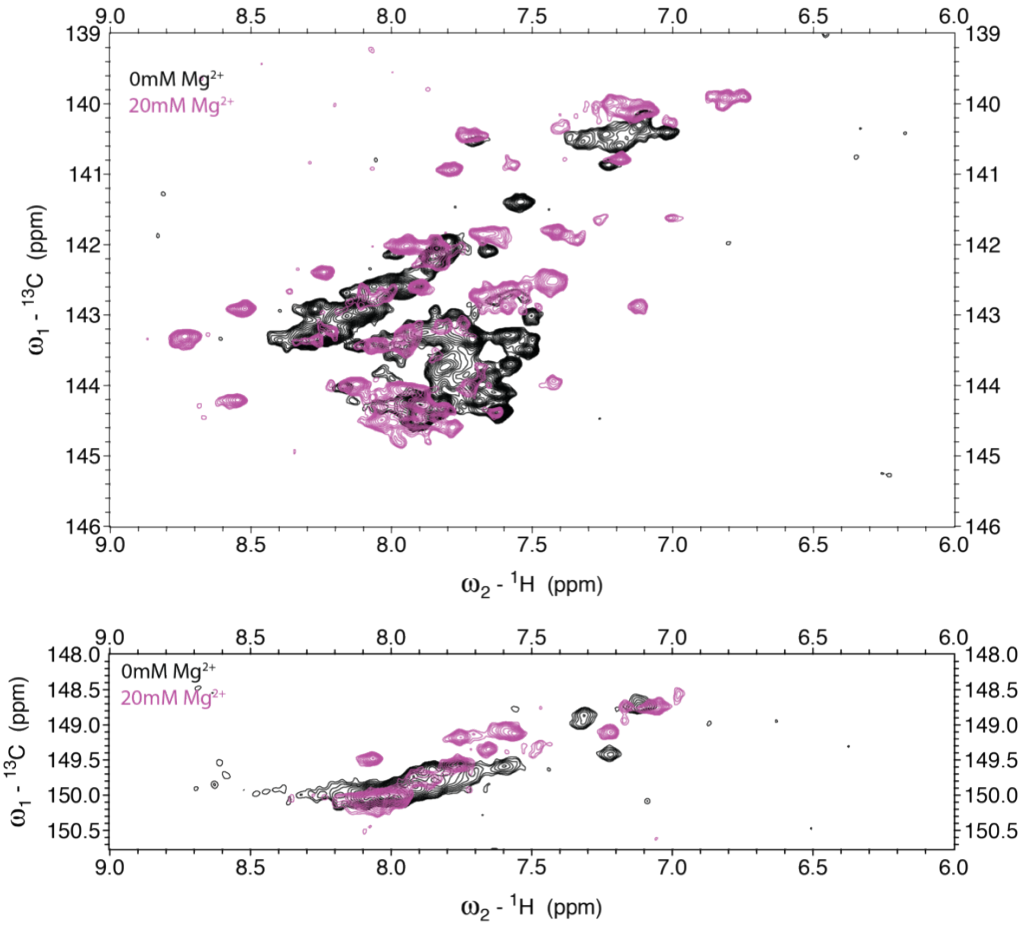

Figure 5.3 Effect of adding Mg^{2+} on the ^{1}H-^{13}C HMQC spectra of twister bimolecular construct. Top panel the H6/H8-C6/C8 correlations. Bottom panel show H2-C2 corrleations. [twister]:[Mg^{2+}] = [0.6 mM]:[20 mM]. Buffer conditions were 30mM HEPES at pH 7.5 and100 mM KCl. Spectra were

collected at 25°C using selective excitation of aromatic protons (SOFAST pulse scheme) using a 600 mHz Bruker Spectrometer

In absence of Mg^{2+}, the aromatic region of twister chemical shift shows severe overlap. However, in presence of Mg^{2+} the chemical shifts are fairly dispersed (Figure 5.3). This suggests that twister becomes more structured upon addition of Mg^{2+}. Tertiary structure formation often positions the nucleotide residues in unique conformations giving rise to more unique electronic environment around the nuclear spins of interest. In order to test, whether these chemical shift perturbations agree with those expected from the crystal structure, a chemical shift-predicting program $LARMOR^D$ (LARMOR frequency and Distance)[36] was employed. $LARMOR^D$ is an inter-atomic distance based chemical shift prediction software developed for predictions of the ^{13}C and non- exchangeable ^{1}H chemical shifts. Figure 5.4 shows the $LARMOR^D$ predicted aromatic ^{1}H-^{13}C correlation spectrum. The absolute chemical shifts appear to be systematically deviated compared to the experiments. However, qualitatively judging from the relative chemical shifts of different residues within the spectra, it can be suggested that the ^{1}H, ^{13}C chemical shifts observed in presence of Mg^{2+} represent a folded structure similar to that observed in the crystal structure. In particular, the residues A26, A34, A42, A43 appear to be consistent with prediction. The residues A26, A42, and A43 are a part of the three-way junction in which, as observed in the crystal structure, A42 and A43 form base triple with a Watson and Crick G-C base pairs. The A34 residue forms a non-canonical base pair with A49 as depicted in the crystal structure placing it in a unique electronic environment. These results suggest that in presence of Mg^{2+} the RNA adopts a conformation similar to that observed in the X-ray structure.[14]

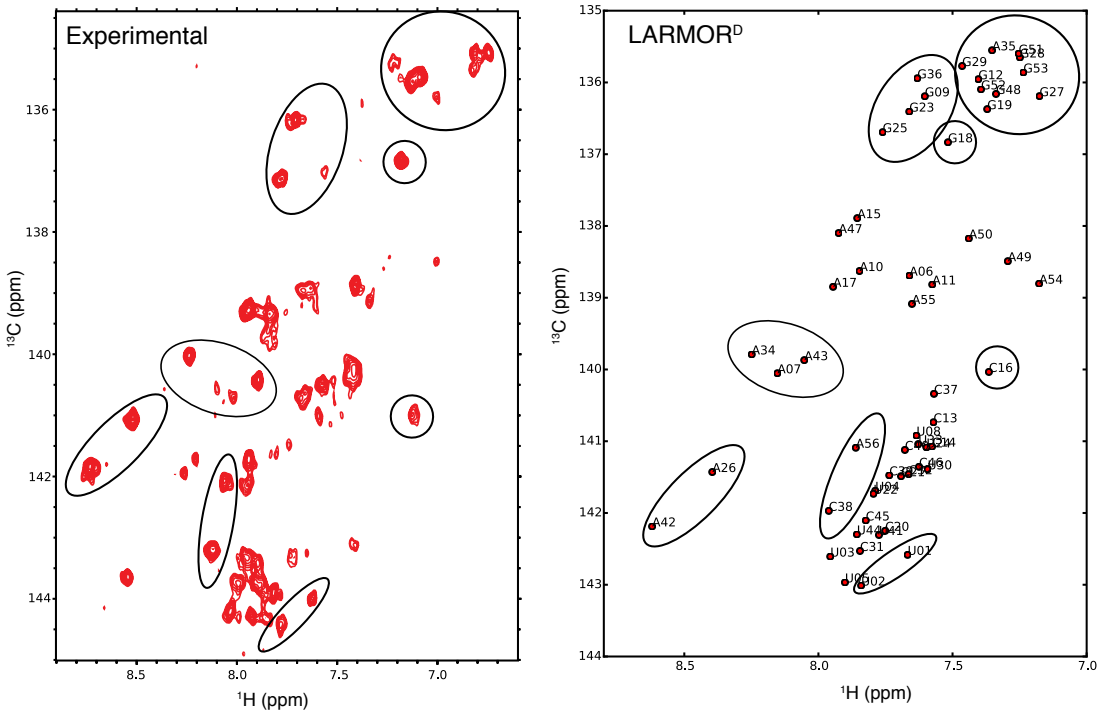

Figure 5.4 Comparison of experimental C6/C8-H6/H8 spectrum of twister in presence of Mg^{2+} with spectrum using LARMOR^D predicted chemical shifts.

5.3.4 Imino Proton Assignments

Since the buffer condition was changed to low salt phosphate buffer instead of HEPES buffer for imino proton assignments, in order to improve the quality of the spectra we first compared 1D spectra of samples in both buffers in presence of Mg^{2+} to see whether there was a significant effect on the secondary and tertiary base pairing. Shows that while some of the resonances shifted, as expected due to the differences in pH, overall the spectra were very similar. In addition some of the resonances in the canonical AU and GC resonances were stronger for samples prepared in the low salt low pH phosphate buffer.

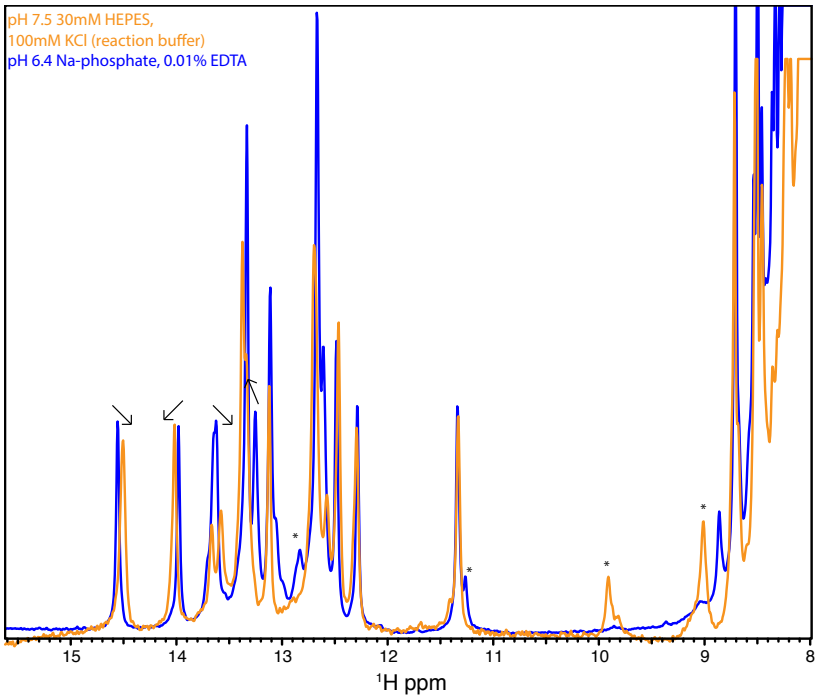

Figure 5.5 Comparison of imino proton spectra of twister in reaction buffer and in phosphate buffer in presence of Mg^{2+}

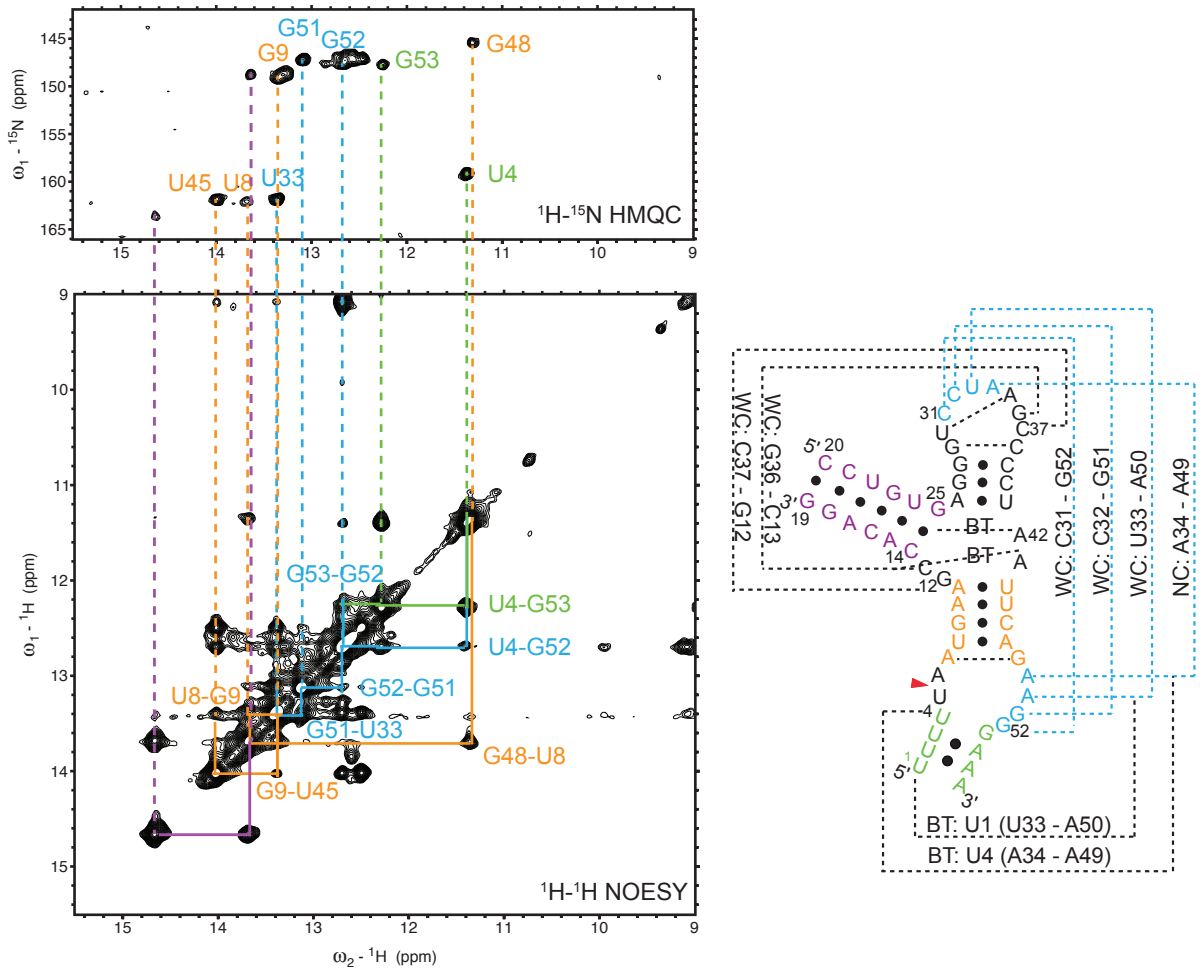

Figure 5.6 ^{1}H-^{1}H NOESY and ^{1}H-^{15}N HMQC spectra of bimolecular twister construct at natural abundance at 10°C. Tentative resonance assignment based on imino proton walk of helices formed after tertiary contact formation is provided with color codes mapped on to the twister secondary structure on the right.

Figure 5.6 shows the ^{1}H-^{1}H NOESY and ^{1}H-^{15}N HMQC spectra of twister ribozyme pre-folded in presence of Mg^{2+}. The NOESY spectra show several NOE cross peaks that can be sequentially walked suggesting formation of stacked helices which is expected when the RNA folds. However, the walks are non-degenerate, therefore unambiguous assignment of the imino-proton and imino-nitrogen resonances of the ^{1}H-^{15}N HMQC spectra were not possible using natural abundance samples. Nonetheless, a tentative assignment of resonances is given in Figure 5.6 based on the imino walk of helices formed after tertiary structure formation. Based on the sequential walks, formation of a tertiary

helix due to the long-range base pairing of residues A50 through G52 with U33 through C31 as depicted in crystal structure is evident. The formation of this tertiary contact has be shown to be important for catalysis from biochemical studies using substitution mutation of the residues in these locations such that they cannot undergo the long range base pairing.[3] The sequential walk was observed only in presence of Mg^{2+} which conforms the role of Mg^{2+} to stabilize the tertiary structure of twister. There is also evidence for a G48A7 sheared imino resonance as judged by the upfield shifted ^{1}H chemical shift. This GA mispair is of interest because the crystal structure evidences a conserved GA base pair close to the catalytic site that could potentially be involved in catalysis.

5.3.5 ^{13}C and ^{1}H Chemical Shifts of Residues Close to the Catalytic Sites

The conserved G48 residue is of special interest due to its suggested role as a general base in twister cleavage reaction. A high apparent pKa value of 9.5 observed in pH dependent biochemical studies by Liu *et al.*[16] on an environmental sequence of twister, which was attributed to a guanine in the same position. The high pKa value suggests that this guanine could potentially exist in an anionic form. pH dependence of NMR chemical shift can also be used to obtain pKa values of the specific residues. Samples with the G48 residue isotopically labeled only at the C8 carbon were successfully prepared using solid phase synthesis. The ^{13}C and ^{1}H chemical shifts of G48 with only the C8 carbon isotope labeled are shown in Figure 5.7. The chemical shifts also overlaid with that of a guanine base in the $^{13}C/^{15}N$ uniformly type-labeled sample thus with helping with the partial assignments of uniformly labeled samples. Similarly, samples with A49 residue isotopically labeled only at its C8 carbon were also prepared the spectrum of which are overlayed in Figure 5.7. The A49 is a conserved residue at the catalytic site, which forms a non-canonical base pair with a distant loop residue A34 in the crystal structure. Although the direct role of A49 in catalysis is not known, due to being adjacent to the proposed anionic G48, it could be an important probe of the structural dynamics at the catalytic site.

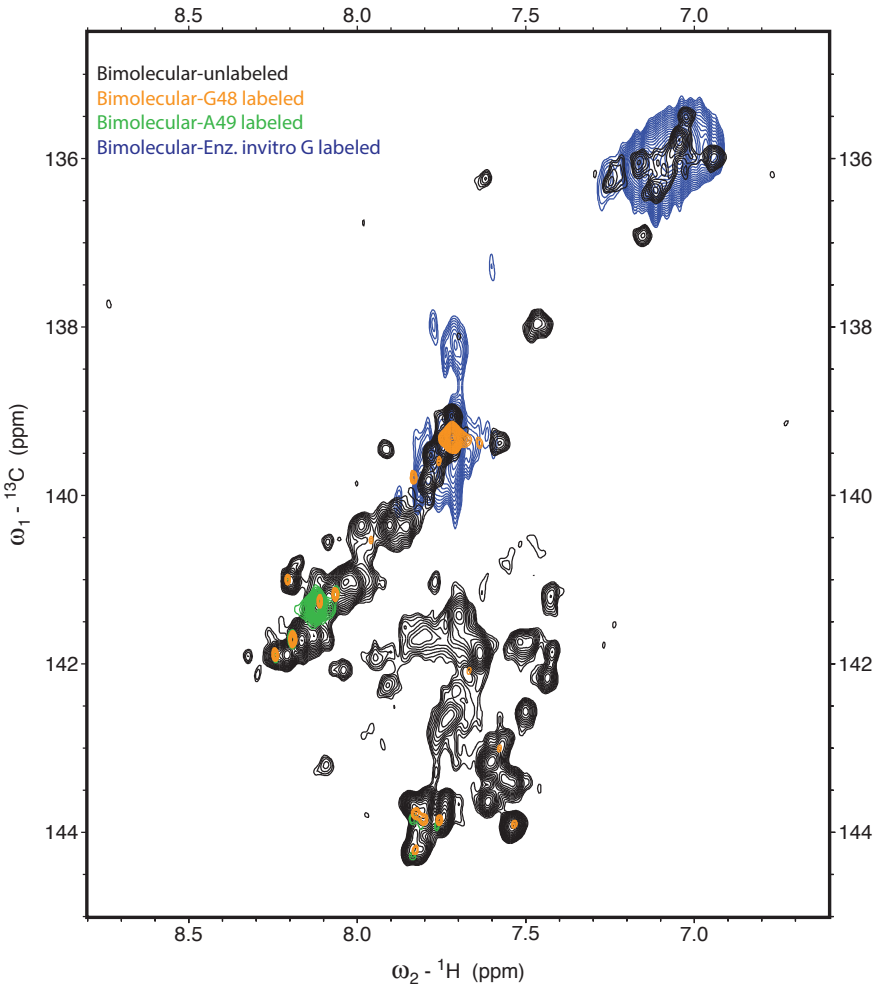

Figure 5.7 ^{1}H -^{13}C assignment of twister using isotope label at the C8 position of purine bases. All the spectra were collected on annealed bimolecular constructs in absence of Mg^{2+}

The above-mentioned experiments were performed in absence of Mg^{2+}. The chemical shift perturbations in presence of Mg^{2+} could further help resolve assignments. Moreover, pH titrations and NMR relaxation dispersion studies on these site labeled samples could provide insights into the dynamics at the catalytic sites without having to solve the full assignment of the NMR spectra.

5.3.6 Comparison with One Piece (Full-Length) Twister

The twister samples used above two-piece samples with the ribozyme and the substrate strand separate. However, the natural sequence is a hairpin-loop containing both ribozyme and enzyme strands. In the two-piece constructs the base pairing close the junction or terminal ends can be very

unstable in absence of Mg^{2+}, as seen in Figure 5.1. Therefore, the natural abundance samples of full-length construct were also synthesized using solid phase synthesis. Figure 5.8 shows the imino proton chemical shift overlays of the two-piece construct and the full-length construct. As, expected more imino proton peaks were observed for the full length construct indicating that the helices are more stable for in the full-length construct. However, upon addition of Mg^{2+} the precipitation of the RNA precluded further analysis in presence of Mg^{2+}. Mg^{2+} is known to form aggregates with larger RNA molecules when hairpins have certain sequences that can form intermolecular base pairs. Therefore, choice of alternative sequences at the loop L3 is suggested for Mg^{2+} based studies, for example a UUCG loop.

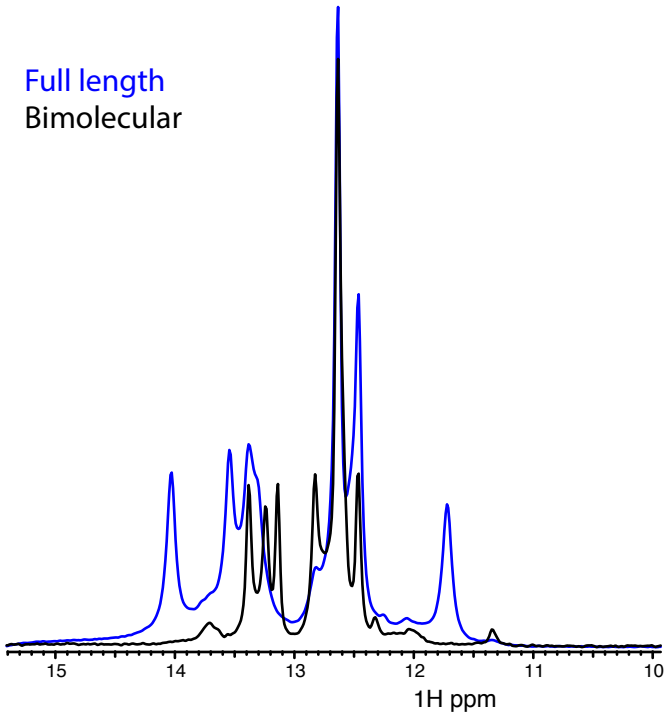

Figure 5.8 Comparison of imino proton spectra of full-length vs. bimolecular construct of twister in absence of Mg^{2+}

5.3.7 Comparison of Different Helix-3 Mutants of Twister

The imino proton spectrum of the full-length construct was also compared with the full-length versions of Helix-3 mutants described in Chapter 4 in order to test whether the key elements of the secondary structure and tertiary folding is similar among the different mutants. As shown in Figure 5.9, the overall chemical shift signatures of the imino protons are very similar, with more number of peaks

observed for longer mutants as expected. However, it was difficult to observe sufficient NOE cross peaks precluding the NOE walk of the exchangeable protons.

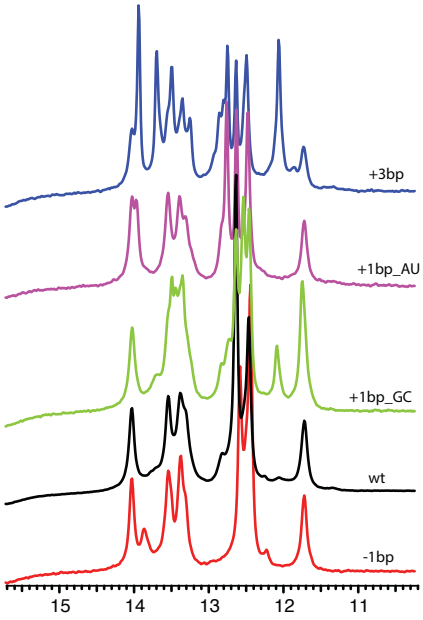

Figure 5.9 Comparison of imino proton spectra of full-length H3 twister mutants in absence of Mg^{2+}

5.4 Conclusions

Formation of folded structure of a bimolecular twister construct in presence of sufficient concentrations of Mg^{2+} was evidenced from imino proton spectra and comparison of aromatic spectra with LARMOR^{D} predicted spectra. It can be thus be concluded that Mg^{2+} clearly plays a structural role i.e. catalytically competent structures are significantly stabilized in presence of Mg^{2+}. The debated direct role of Mg^{2+} in catalysis is yet to be illustrated for which NMR studies on RNA site-specifically labeled at the catalytic site could prove useful. Although unambiguous assignment of residues was not possible with natural abundance samples because of significant spectral overlap, site (atom) specific isotope labels on the RNA synthesized using solid phase synthesis enabled assignment of the carbon chemical shifts of the key residues in the catalytic sites. These will be used to study the dynamics at the catalytic site of twister in presence and absence of Mg^{2+}. Additionally, comparison with the imino proton spectra of the full-length (one piece) twister suggests that the secondary structure base pairs in hybridized form of bimolecular construct are less stable. Lastly, it was also shown that elongation of helix3 of twister does

not significantly affect the overall secondary structure and thus are predicted to be catalytically active given that they are able to form catalytically active tertiary structures.

5.5 References

1. Weinberg, Z.; Kim, P. B.; Chen, T. H.; Li, S.; Harris, K. A.; Lunse, C. E.; Breaker, R. R. New Classes of Self-Cleaving Ribozymes Revealed by Comparative Genomics Analysis. *Nat. Chem. Biol.* 2015, *11*, 606-610.
2. Cochrane, J. C.; Strobel, S. A. Catalytic Strategies of Self-Cleaving Ribozymes. *Acc. Chem. Res.* 2008, *41*, 1027-1035.
3. Roth, A.; Weinberg, Z.; Chen, A. G.; Kim, P. B.; Ames, T. D.; Breaker, R. R. A Widespread Self-Cleaving Ribozyme Class Is Revealed by Bioinformatics. *Nat. Chem. Biol.* 2014, *10*, 56-60.
4. Perreault, J.; Weinberg, Z.; Roth, A.; Popescu, O.; Chartrand, P.; Ferbeyre, G.; Breaker, R. R. Identification of Hammerhead Ribozymes in All Domains of Life Reveals Novel Structural Variations. *PLOS Comput. Biol.* 2011, *7*, e1002031.
5. Webb, C. H.; Luptak, A. HDV-Like Self-Cleaving Ribozymes. *RNA Biol.* 2011, *8*, 719-727.
6. Wilson, T. J.; Liu, Y. J.; Lilley, D. M. J. Ribozymes and the Mechanisms That Underlie RNA Catalysis. *Front. Chem. Sci. Eng.* 2016, *10*, 178-185.
7. Lilley, D. M. Structure, Folding and Mechanisms of Ribozymes. *Curr. Opin. Struct. Biol.* 2005, *15*, 313-323.
8. Strobel, E. J.; Watters, K. E.; Loughrey, D.; Lucks, J. B. RNA Systems Biology: Uniting Functional Discoveries and Structural Tools to Understand Global Roles of Rnas. *Curr. Opin. Biotechnol.* 2016, *39*, 182-191.
9. Martick, M.; Scott, W. G. Tertiary Contacts Distant from the Active Site Prime a Ribozyme for Catalysis. *Cell* 2006, *126*, 309-320.
10. Rupert, P. B.; Ferre-D'Amare, A. R. Crystal Structure of a Hairpin Ribozyme-Inhibitor Complex with Implications for Catalysis. *Nature* 2001, *410*, 780-786.
11. Rupert, P. B.; Massey, A. P.; Sigurdsson, S. T.; Ferre-D'Amare, A. R. Transition State Stabilization by a Catalytic RNA. *Science* 2002, *298*, 1421-1424.
12. Klein, D. J.; Wilkinson, S. R.; Been, M. D.; Ferre-D'Amare, A. R. Requirement of Helix P2.2 and Nucleotide G1 for Positioning the Cleavage Site and Cofactor of the Glms Ribozyme. *J. Mol. Biol.* 2007, *373*, 178-189.
13. Cochrane, J. C.; Lipchock, S. V.; Strobel, S. A. Structural Investigation of the Glms Ribozyme Bound to Its Catalytic Cofactor. *Chem. Biol.* 2007, *14*, 97-105.
14. Ren, A.; Kosutic, M.; Rajashankar, K. R.; Frener, M.; Santner, T.; Westhof, E.; Micura, R.; Patel, D. J. In-Line Alignment and Mg^{2+} Coordination at the Cleavage Site of the Env22 Twister Ribozyme. *Nat. Commun.* 2014, *5*, 5534.
15. Eiler, D.; Wang, J.; Steitz, T. A. Structural Basis for the Fast Self-Cleavage Reaction Catalyzed by the Twister Ribozyme. *Proc. Natl. Acad. Sci. USA* 2014, *111*, 13028-13033.

16. Liu, Y.; Wilson, T. J.; McPhee, S. A.; Lilley, D. M. Crystal Structure and Mechanistic Investigation of the Twister Ribozyme. *Nat. Chem. Biol.* 2014, *10*, 739-744.
17. Izatt, R. M.; Christensen, J. J.; Rytting, J. H. Sites and Thermodynamic Quantities Associated with Proton and Metal Ion Interaction with Ribonucleic Acid, Deoxyribonucleic Acid, and Their Constituent Bases, Nucleosides, and Nucleotides. *Chem. Rev.* 1971, *71*, 439-481.
18. Velikyan, I.; Acharya, S.; Trifonova, A.; Foldesi, A.; Chattopadhyaya, J. The Pk(a)'S of 2'-Hydroxyl Group in Nucleosides and Nucleotides. *J. Am. Chem. Soc.* 2001, *123*, 2893-2894.
19. Singh, V.; Fedeles, B. I.; Essigmann, J. M. Role of Tautomerism in RNA Biochemistry. *RNA* 2015, *21*, 1-13.
20. Kuzmin, Y. I.; Da Costa, C. P.; Fedor, M. J. Role of an Active Site Guanine in Hairpin Ribozyme Catalysis Probed by Exogenous Nucleobase Rescue. *J. Mol. Biol.* 2004, *340*, 233-251.
21. Viladoms, J.; Scott, L. G.; Fedor, M. J. An Active-Site Guanine Participates in Glms Ribozyme Catalysis in Its Protonated State. *J. Am. Chem. Soc.* 2011, *133*, 18388-18396.
22. Nakano, S.; Chadalavada, D. M.; Bevilacqua, P. C. General Acid-Base Catalysis in the Mechanism of a Hepatitis Delta Virus Ribozyme. *Science* 2000, *287*, 1493-1497.
23. Das, S. R.; Piccirilli, J. A. General Acid Catalysis by the Hepatitis Delta Virus Ribozyme. *Nat. Chem. Biol.* 2005, *1*, 45-52.
24. Ke, A.; Zhou, K.; Ding, F.; Cate, J. H. D.; Doudna, J. A. A Conformational Switch Controls Hepatitis Delta Virus Ribozyme Catalysis. *Nature* 2004, *429*, 201-205.
25. Wilson, T. J.; Li, N. S.; Lu, J.; Frederiksen, J. K.; Piccirilli, J. A.; Lilley, D. M. Nucleobase-Mediated General Acid-Base Catalysis in the Varkud Satellite Ribozyme. *Proc. Natl. Acad. Sci. USA* 2010, *107*, 11751-11756.
26. Suslov, N. B.; DasGupta, S.; Huang, H.; Fuller, J. R.; Lilley, D. M.; Rice, P. A.; Piccirilli, J. A. Crystal Structure of the Varkud Satellite Ribozyme. *Nat. Chem. Biol.* 2015, *11*, 840-846.
27. Kosutic, M.; Neuner, S.; Ren, A.; Flur, S.; Wunderlich, C.; Mairhofer, E.; Vusurovic, N.; Seikowski, J.; Breuker, K.; Hobartner, C.; Patel, D. J.; Kreutz, C.; Micura, R. A Mini-Twister Variant and Impact of Residues/Cations on the Phosphodiester Cleavage of This Ribozyme Class. *Angew. Chem. Int. Ed. Engl.* 2015, *54*, 15128-15133.
28. Tang, C. L.; Alexov, E.; Pyle, A. M.; Honig, B. Calculation of Pkas in RNA: On the Structural Origins and Functional Roles of Protonated Nucleotides. *J. Mol. Biol.* 2007, *366*, 1475-1496.
29. Cai, Z.; Tinoco, I., Jr. Solution Structure of Loop a from the Hairpin Ribozyme from Tobacco Ringspot Virus Satellite. *Biochemistry* 1996, *35*, 6026-6036.
30. Kimsey, I. J.; Petzold, K.; Sathyamoorthy, B.; Stein, Z. W.; Al-Hashimi, H. M. Visualizing Transient Watson-Crick-Like Mispairs in DNA and RNA Duplexes. *Nature* 2015, *519*, 315-320.
31. Wilson, T. J.; Liu, Y.; Domnick, C.; Kath-Schorr, S.; Lilley, D. M. The Novel Chemical Mechanism of the Twister Ribozyme. *J. Am. Chem. Soc.* 2016, *138*, 6151-6162.
32. Gaines, C. S.; York, D. M. Ribozyme Catalysis with a Twist: Active State of the Twister Ribozyme in Solution Predicted from Molecular Simulation. *J. Am. Chem. Soc.* 2016, *138*, 3058-3065.

33. Ucisik, M. N.; Bevilacqua, P. C.; Hammes-Schiffer, S. Molecular Dynamics Study of Twister Ribozyme: Role of Mg^{2+} Ions and the Hydrogen-Bonding Network in the Active Site. *Biochemistry* 2016, *55*, 3834-3846.
34. Sathyamoorthy, B.; Lee, J.; Kimsey, I.; Ganser, L. R.; Al-Hashimi, H. Development and Application of Aromatic ^{13}C-^{1}H SOFAST-HMQC NMR Experiment for Nucleic Acids. *J Biomol. NMR* 2014, *60*, 77-83.
35. Schanda, P.; Brutscher, B. Very Fast Two-Dimensional NMR Spectroscopy for Real-Time Investigation of Dynamic Events in Proteins on the Time Scale of Seconds. *J. Am. Chem. Soc.* 2005, *127*, 8014-8015.
36. Frank, A. T.; Law, S. M.; Brooks, C. L., 3rd. A Simple and Fast Approach for Predicting ^{1}H and ^{13}C Chemical Shifts: Toward Chemical Shift-Guided Simulations of RNA. *J. Phys. Chem. B* 2014, *118*, 12168-12175.

CHAPTER 6 CONCLUSIONS AND FUTURE OUTLOOK

The work presented in this thesis is aimed at developing a deeper and more sophisticated understanding of polyplex formation, structure, and dynamics so that systematic design principles to maximize the efficiency of polyplexes for therapeutic nucleic acid delivery can eventually replace the currently favored "look-and-see" approach. The unifying theme of the presented chapters is the use of an array of experimental techniques, several of which have previously not been applied to such systems, to obtain a basic view of polyplexes *in situ*, and to explore how our evolving picture of polyplexes can be ushered into *in vivo* and cell based experiments.

Initial work was focused on visualizing the polyplex assembly of nanoscopic structures. Regarding the influence of polyplex formation on the internal structure and dynamics of RNA cargo, NMR analysis of the structural features of a small RNA hairpin upon polyplex formation under RNA charge excess conditions showed that there was no significant changes in the RNA secondary structure (only small perturbations to conformationally flexible "loops" and "bulges" were observed). Fast internal dynamics on the ps-ns timescales was unaltered by complex formation. However, polyplex formation introduces complex structure and dynamics that go well beyond the internal structure and dynamics of the cargo RNA. The first class involves structures formed between one POCP and multiple RNA molecules. Through NMR and fluorescence quenching experiments it was found that the RNA is in constant exchange between "free" and "bound" forms. This intermolecular dynamic is crucial for the use of these structures for nucleic acid delivery, as the bound forms prevent degradation of the RNA from nucleases present in the body, while the release of the free form is required for delivery into the cell.

The second class is the formation of larger structures arising from the interaction between multiple polymers and multiple RNA molecules. A hierarchical-like assembly was found between smaller assemblies on the order of tens of nanometers, which are considered to be the functional population,

with larger assemblies on the order of hundreds of nanometers. Exchange dynamics between these populations is expected to occur on timescales significantly slower than the timescale for exchange between free and bound RNA, though this fluxionality is needed for the supply of functionally active small assemblies. Furthermore, the degree of complexation and the intermolecular exchange was strongly dependent on the POPC structure. More surprisingly, degree of complexation was dependent on the secondary structure of the nucleic acid, even when the number of nucleotides (and hence the total number of phosphate charges) was the same between two nucleic acids.

Next, we turned to an aspect that has received little attention from the community despite having a clear impact on the behavior of the cargo RNA, which is the chemical makeup of the microenvironment of the polyplex. Leveraging local labeling with a solvatochromic and prototropic fluorescent dye, fluorescence spectroscopy was used to directly observe three distinct microenvironments surrounding a small hairpin RNA polyplexes with three different POCPs. Significant observed differences in local pH (and expected differences in pKa and counterion composition) from bulk solution suggest that a full understanding of the structure, exchange dynamics, and catalytic function of bound RNA must take into account the unique chemical environments in which they are exposed to when assembled. This suggests that the polymer used for complexation must be viewed as active participants in governing the RNA behavior, which can potentially be used to fine-tune catalytic performance of bound RNA. This is in stark contrast to the traditional picture of the polymer component of polyplexes as serving a merely passive role to bind and release the RNA.

Working off this previous conclusion, we explored how polyplexes can influence catalytic performance of several mutants of a RNA belonging to the nucleolytic ribozyme class, twister. Using gel electrophoresis, we monitored the catalytic rate and product yield of the different twister mutants free in solution and in the presence of POCPs. Consistent with our previous results, we found that twister ribozymes can anneal and form proper 3D contacts required for catalysis while bound in polyplexes. Furthermore, we observed that the presence of POCP could significantly influence observed catalytic rates and product yield. Polyplexes of POCPs that were observed to favor exchange of bound RNA

showed enhanced activity, supporting our earlier predictions of the role of intermolecular exchange for the availability of the RNA for function. More strikingly, the role of POCP in influencing the catalytic rates was found to be strongly dependent on subtle changes to the RNA sequence and secondary structure. For example, wild-type twister sequence showed an order of magnitude enhancement in observed rates in presence of POCP, while the scenario was reversed when the RNA was extended by a single base pair at the junction. When the RNA was further elongation such that the observed rates decreased compared to the one base pair mutant, presence of POCP enhanced the rates compared to absence of POCP. In general, it was observed that POCP enhanced rates of only the mutants that had rates lower than or equal to the wildtype. This suggested that the rate limiting step arising due to the elongation mutation was overcome by presence of POCP. However, it remains to be elucidated what the rate limiting step is for all the mutants in absence of POCP. Future studies would involve accessing the rate limiting steps using standard mechanistic analysis of kinetic mechanisms. For example, single turnover experiments with saturating concentrations of the ribozyme strands would give rates representative of the chemical cleavage, as product release would not be rate limiting under single turnover conditions. If the observed rates in single turnover conditions with and without POCP is similar then it suggest that POCP is not directly involved in the chemical cleavage step. However, since the twister cleavage reaction is very fast, either the pH or Mg^{2+} concentrations will have to be lowered in order to have suboptimal conditions for a slower reaction. Temperature dependent measurements of observed rates could also reveal whether POCP enhances complex formation between ribozyme and substrate strand as the catalytic rates are expected to be least effective under temperatures close to the melting temperature of the duplex. Longer the helix, higher the theoretical melting temperatures in absence of POCP, therefore increase in observed rates in presence of POCP at temperatures higher than the melting temperature will suggest that the rates of association of ribozyme substrate is enhanced in presence of POCP. These experiments can help elucidate further why the different mutants respond differently with respect to the observed rates of catalysis.

It was also observed that the product yield after long enough time (approaching thermodynamic equilibrium), was always higher in presence of POCP suggesting that POCP may stabilize the structure of the RNA. This stabilization could be either due to stabilization of secondary structure or tertiary structure. TOPRNA simulations predicted that longer the helix, less probable the helical mutants are to fold into correct 3D structure. It is possible that the enhanced product yield is due to destabilization of misfolded states and stabilization of catalytically active properly folded states in presence of POCP. To test the conformational heterogeneity of the ribozyme-substrate complex for the different mutants, non-denaturing gel electrophoresis experiments can be performed. If the different conformers are not in very fast exchange, non-denaturing gel electrophoresis could resolve the conformational heterogeneity.

Finally, we studied twister RNA by itself using NMR to elucidate the secondary structure and tertiary contacts important for catalysis. As the twister class of ribozymes was discovered recently, only one NMR study has been published to date. Unlike in most known nucleolytic ribozymes, for this particular ribozyme it has been suggested that Mg^{2+} not only stabilizes the tertiary structure but also has a direct role in the catalytic mechanism. From our studies, tertiary folded structure of a bimolecular twister construct in presence of sufficient concentrations of Mg^{2+} was evident from imino proton spectra, as well as comparison of experimental and predicted aromatic spectra. While we were not able to get the complete NMR assignment for non-isotopically labeled RNA, site/atom-specific labeling enabled assignment of chemical shifts of key residues at the catalytic site. This will help in carrying out further NMR experiments aimed at measuring structure and dynamics at the catalytic site both in the ribozyme by itself as well as in presence of POCPs.

Additionally, helical elongation mutants that showed significantly different catalytic activity, both in presence and absence of polymer, did not show significant changes in the secondary structure. This suggests that the differences in activity could be due to differences in the tertiary structure or local dynamics. There are still open questions regarding how nucleobases at the catalytic sites facilitate the acid-base chemistry needed for catalysis. Future work will undertake NMR experiments in conjunction with site-specific labeling techniques to understand the precise role of nucleobases in mediating

acid/base catalysis, whether Mg^{2+} plays a direct role in catalysis, and what ways the subtle mutations at the non-conserved sites play a role. Though no major structural changes have been observed in the helical regions of a simple hairpin RNA via NMR, there is evidence that the more flexible residues at loop and bulge regions can be perturbed in presence of POCPs. It is reasonable to think that such perturbations may impact ribozyme catalysis because the reaction requires a precise geometry at the catalytic site facilitated by long-range interactions of flexible loop and bulge residues. Furthermore, the reactions are highly dependent on nucleobase pKa values, which are often significantly shifted when the nucleobases are present in these complex structural contexts compared to free or unstructured forms. As we have evidenced by fluorescence spectroscopy, local pH/pKa values in polyplexes significantly differ from the bulk solution. To this end, fluorescence experiments using fluorescent solvatochromic nucleobase analogues like 2-amino purine substituted near the catalytic sites can be employed. Whether, local pH/pKa changes at ribozyme catalytic sites in presence of POCPs can be detected using NMR remains to be investigated.

To summarize, when beginning this work the prevailing view of polyplexes was one where the interactions were governed through simple electrostatics, the question of whether the resulting structures were dynamic was being actively debated, and the polymer was viewed as a simple, passive carrier molecule. The prevailing picture today is that polyplexes form highly assembled, hierarchical, and dynamic structures that are in constant flux. To predict such structures requires an intimate knowledge of not only charge density of the two polymers, but also of flexibility, topology, and structural details of the components. As we push towards designing "smart" polymers for polyplexes, we are beginning to appreciate the active role that the polymer can perform in modulating the polyplex microenvironment (pH, chemical composition), intermolecular exchange, and possibly the structure and dynamics of flexible residues at structurally complex contexts. The evolving view of polyplexes as sophisticated, "living" assemblies demonstrates not only the progress that has been made, but also the work that remains to be done.

APPENDIX A

Appendix A: Supplementary material for section 2.1

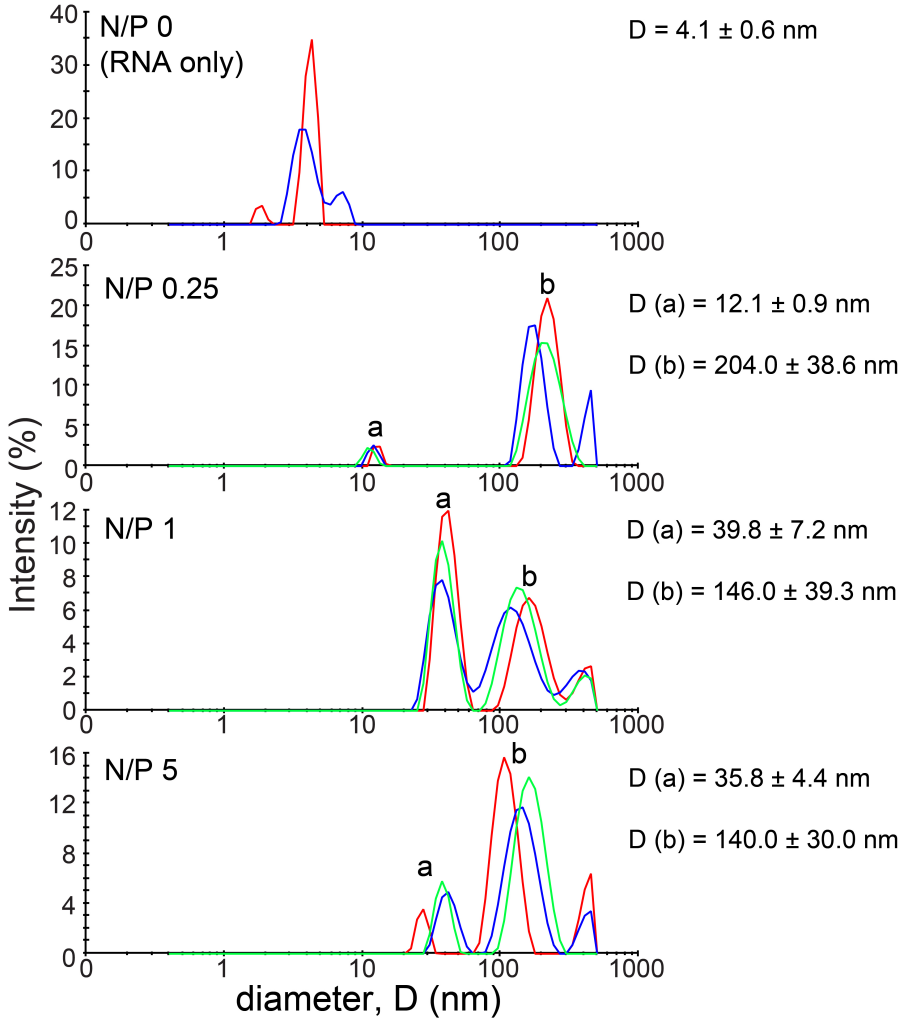

S I. DLS measurements of polyplex samples at different N:P ratios 0 to 5 at NMR concentrations (200 μM TAR). The data has been presented as intensity average diameter. Overlay of three peaks in the same graph indicates triplicate measurements; only duplicate measurements were obtained for N:P 0.

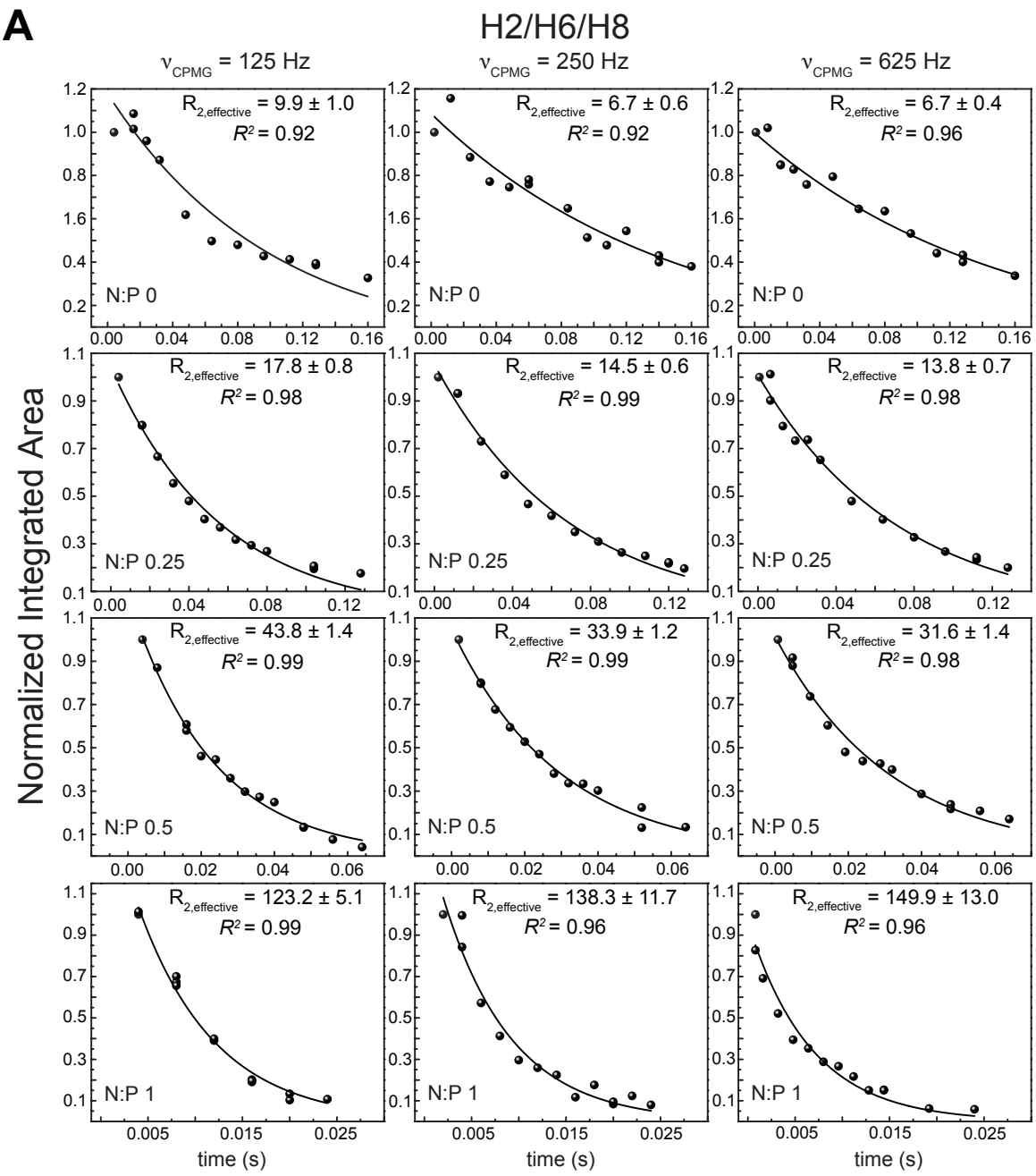
A
H2/H6/H8
νCPMG = 125 Hz
νCPMG = 250 Hz
νCPMG = 625 Hz
Normalized Integrated Area
R2,effective = 9.9 ± 1.0
R2 = 0.92
N:P 0
R2,effective = 6.7 ± 0.6
R2 = 0.92
N:P 0
R2,effective = 6.7 ± 0.4
R2 = 0.96
N:P 0
R2,effective = 17.8 ± 0.8
R2 = 0.98
N:P 0.25
R2,effective = 14.5 ± 0.6
R2 = 0.99
N:P 0.25
R2,effective = 13.8 ± 0.7
R2 = 0.98
N:P 0.25
R2,effective = 43.8 ± 1.4
R2 = 0.99
N:P 0.5
R2,effective = 33.9 ± 1.2
R2 = 0.99
N:P 0.5
R2,effective = 31.6 ± 1.4
R2 = 0.98
N:P 0.5
R2,effective = 123.2 ± 5.1
R2 = 0.99
N:P 1
R2,effective = 138.3 ± 11.7
R2 = 0.96
N:P 1
R2,effective = 149.9 ± 13.0
R2 = 0.96
N:P 1
time (s)
time (s)
time (s)

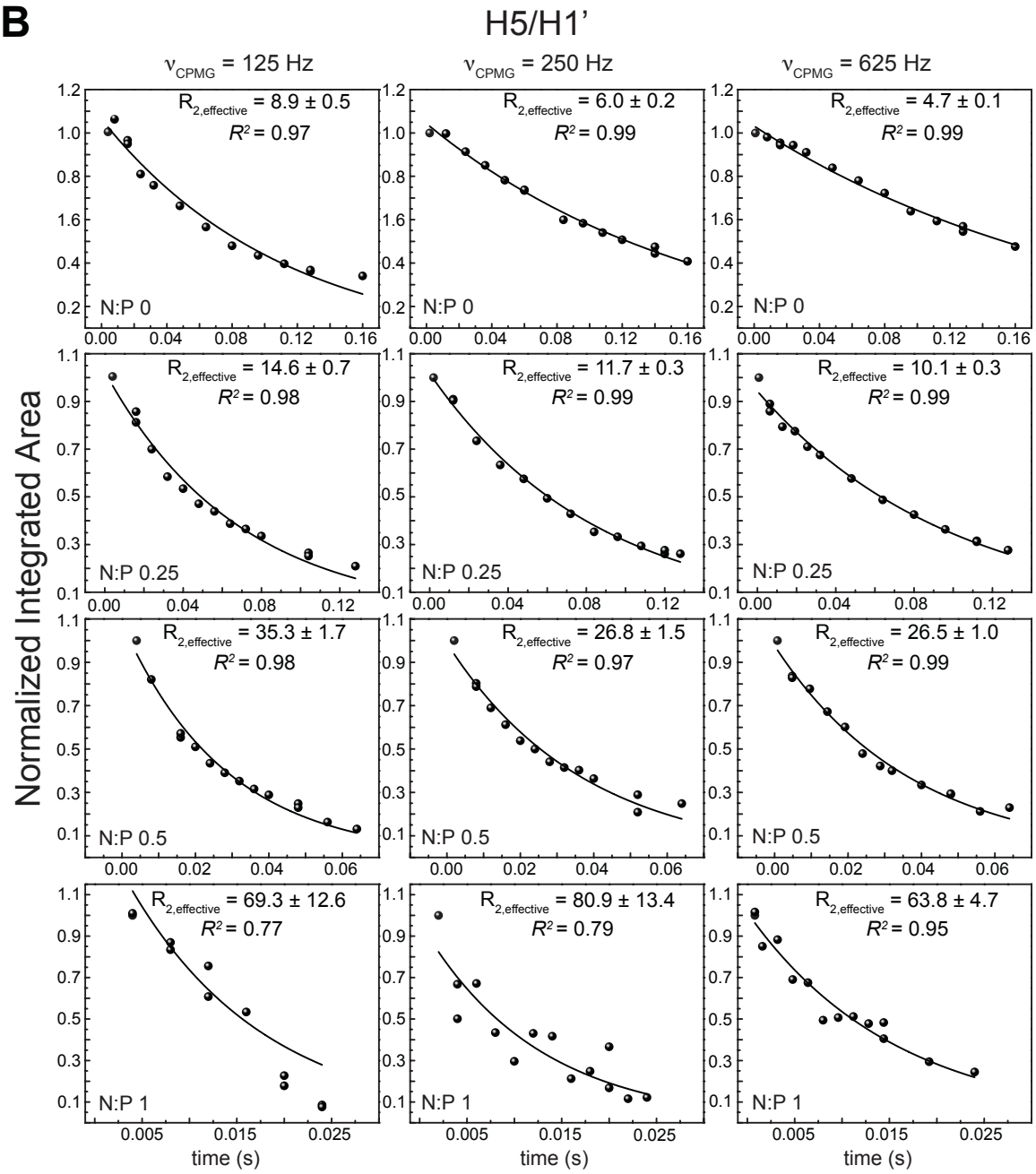

S II. Monoexponential fits of integrated area obtained using 1D ^{1}H CPMG experiment for (A) H2/H6/H8 protons (B) H5/H1' protons to obtain $R_{2,effective}$ for N:P ratios 0, 0.25, 0.5, and 1.

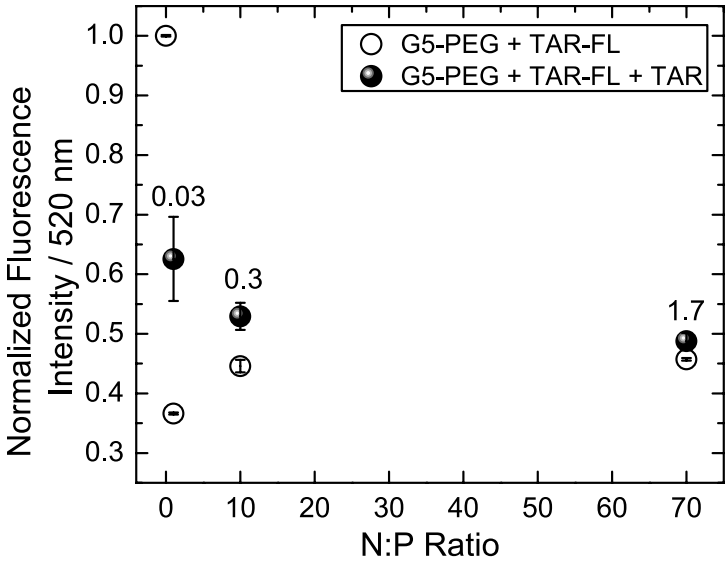

S III. Fluorescence quenching based competitive displacement assay demonstrating release of TAR-FL from polyplexes with G5-PEG within 2 minutes of adding untagged TAR. Open circles indicate fluorescence of polyplex mixture at different N:P ratios before adding untagged RNA. Filled circles indicate fluorescence of the polyplex mixtures after adding untagged 0.3 μL of 200 μM TAR, with the resulting N:P ratios indicated on top of the data points. The total concentration of TAR-FL in all N:P ratios is 50 nM. Buffer conditions used were 50mM Tris-HCl, 50mM KCl, 0.01% Trition-X, pH 7.4.

APPENDIX B

Appendix B: Supplementary material for section 3.2

T I. Bulk solution pH of G5/TAR-FL polyplex solutions

N:P	ug/mL ratio	pH
0.00	0.00	7.54
0.07	0.06	7.54
0.11	0.09	7.53
0.18	0.15	7.54
0.28	0.23	7.54
0.45	0.37	7.54
0.71	0.58	7.54
1.13	0.92	7.54
1.79	1.46	7.53
2.83	2.32	7.54
4.49	3.67	7.53
7.11	5.82	7.54
11.27	9.22	7.53
17.86	14.62	7.54
28.31	23.16	7.53
44.87	36.71	7.54

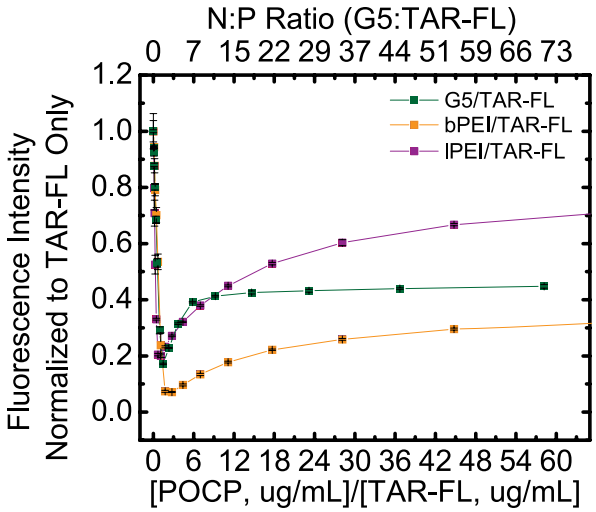

S I. Comparison of fluorescence quenching of TAR-FL upon polyplex formation with different POCP as a function of POCP to TAR-FL concentration ratios.